CANADIAN THESES ON MICROFICHE

THÈSES CANADIENNES SUR MICROFICHE

National Library of Canada
Collections Development Branch

Canadian Theses on
Microfiche Service

Ottawa, Canada
K1A 0N4

Bibliothèque nationale du Canada
Direction du développement des collections

Service des thèses canadiennes
sur microfiche

NOTICE

The quality of this microfiche is heavily dependent upon the quality of the original thesis submitted for microfilming. Every effort has been made to ensure the highest quality of reproduction possible.

If pages are missing, contact the university which granted the degree.

Some pages may have indistinct print especially if the original pages were typed with a poor typewriter ribbon or if the university sent us an inferior photocopy.

Previously copyrighted materials (journal articles, published tests, etc.) are not filmed.

Reproduction in full or in part of this film is governed by the Canadian Copyright Act, R.S.C. 1970, c. C-30. Please read the authorization forms which accompany this thesis.

AVIS

La qualité de cette microfiche dépend grandement de la qualité de la thèse soumise au microfilmage. Nous avons tout fait pour assurer une qualité supérieure de reproduction.

S'il manque des pages, veuillez communiquer avec l'université qui a conféré le grade.

La qualité d'impression de certaines pages peut laisser à désirer, surtout si les pages originales ont été dactylographiées à l'aide d'un ruban usé ou si l'université nous a fait parvenir une photocopie de qualité inférieure.

Les documents qui font déjà l'objet d'un droit d'auteur (articles de revue, examens publiés, etc.) ne sont pas microfilmés.

La reproduction, même partielle, de ce microfilm est soumise à la Loi canadienne sur le droit d'auteur, SRC 1970, c. C-30. Veuillez prendre connaissance des formules d'autorisation qui accompagnent cette thèse.

THIS DISSERTATION
HAS BEEN MICROFILMED
EXACTLY AS RECEIVED

LA THÈSE A ÉTÉ
MICROFILMÉE TELLE QUE
NOUS L'AVONS REÇUE

Canada

NL 339 (r. 86/09)

SIMULATION REQUIREMENTS ON MODELLING THE AEROELASTIC RESPONSES OF STRUCTURES

by

RAYMOND TAI-MAN AO-IEONG

A thesis
presented to the University of Ottawa
in fulfillment of the
thesis requirement for the degree of
Master of Applied Science
in
Civil Engineering

ABSTRACT

In this study, the effects of the Scruton number, a dimentionless product of the mass and damping parameters, on the wind-induced responses of structures were examined. It has been believed that this number can be used as a scaling parameter for tests of sectional models in wind tunnel. The meaning of this particular parameter in wind tunnel testing is described in the first chapter. Chapter II gives a summary of similarity requirements in wind tunnel testing and brief discussion of each dimensionless parameter. In Chapter III, a brief review of the model scaling parameters in conjunction with the study of aerodynamic stability of bridges is presented. The following chapter describes the experimental study. Three different geometrical shapes of structures were selected in order that various types of wind-induced dynamic behaviours would be experimentally produced.

It was found that Scruton number can be used as a scaling parameter for the case of wind-induced vortex excitations. However, for the case of self-excited instabilities and buffeting response, Scruton number cannot be used as a single scaling parameter.

ACKNOWLEDGEMENTS

The author would like to express his gratitude to his supervisor, Dr. Hiroshi Tanaka, Associate Professor in Civil Engineering, the University of Ottawa, for his continuous guidance as well as ever-lasting encouragement throughout this study.

He also wishes to express appreciation to Mr. Bill Watson and Mr. Claude Lavigne for their assistance in setting up the experiment. Sincere thanks are due to Mr. Jackson Chan for correcting the manuscripts.

Finally, the author gratefully acknowledges his family for their spiritual and financial support.

May our gracious God continue to bless them.

TABLE OF CONTENTS

Appendix

LIST OF TABLES

LIST OF FIGURES

List of Symbols

b = width of model

c = damping coefficient

C_D = drag force coefficient

C_L = lift force coefficient

C_M = pitching moment coefficient

d = height of model

F = lateral force

g = gravitational acceleration

I = mass moment of inertia per unit length

k = stiffness

m = mass per unit length

M = pitching moment

N = natural frequency

Sc = Scruton number

t = time

V = mean velocity

Vr = reduced velocity

z = vertical displacement

θ = angular displacement

α = angle of attack

ω = circular natural frequency

δ = logarithmic decrement

ξ = damping ratio

ρ = density of air

Subscripts

B = vertical bending

T = torsion

m = model

p = prototype

Chapter I

INTRODUCTION

1.1 BACKGROUND AND OBJECTIVE OF THE STUDY

Wind-induced forces acting on structures depend upon the characteristics of the oncoming wind flow and the geometry and mechanical properties of the structure. In the past half century, there was a development of analytical tools which enabled engineers to estimate, to some extent, various types of wind-induced structural responses. However, wind-induced phenomena cannot be fully explained yet by analytical tools alone because of the complexity in aerodynamic properties of the structures involved and also because of the random nature of wind. In the absence of workable analytical models or of previous experience with similar structures and environment, the effects of wind, therefore, still have to be determined experimentally. In fact, it is still a normal practice to undertake wind tunnel testing for design of intermediate and long-span bridges or tall towers and buildings. This method enables the designer to investigate the aerodynamic behaviour of structures at the design stage and to avoid any future problems by modifying the proposed

structure. Generally, the cost of the aerodynamic investigation is really a very minor fraction of the construction cost of the full-scale structure. Bearing in mind the significance of the possible aerodynamic responses on the final design, undue restriction of the investigation on cost grounds should be avoided.

In order that test results on reduced-scale models be applicable to the prototype, it is necessary, in principle, to satisfy certain model laws or similarity requirements. A discussion of similitude is presented in the next chapter, and it will be seen that compliance with all the similarity criteria required by theory is impractical. However, this may not seriously affect the results from wind tunnel tests provided that the relaxation of the requirements be properly considered. The influence of each parameter upon the behaviour of a structure, therefore, has to be carefully examined by both analytical and experimental procedures.

Well-established dimensionless scaling parameters are essential in wind tunnel modelling of the bridge dynamics. In Chapter III, a brief review of the model scaling parameters used in modelling different bridges is presented. Variables such as wind velocity, bridge width, mass of structure, damping ratio, air density, etc., are grouped together to form dimensionless scaling parameters by applying the

principles of dimensional analysis. It will be seen that, basically, similar parameters have been used throughout the past four decades for the testing of bridges by various researchers.

However, there is one parameter, used by Scruton in England for his investigation of the Severn Bridge (1), which reveals a concept somewhat different from the other research works. Generally speaking, both mass and damping ratio of a structure exhibit similar influence on the aerodynamic behaviour of the structure. For example, increasing the mass of a structure may result in reducing its wind-induced response. A similar result can be expected when the damping ratio is increased. Scruton considered that, for tests of sectional models in isolated vibration mode, vertical or torsional, the product of mass and damping ratio of a structure can be used as one independent dimensionless scaling parameter (1). It will be explained in Chapter V that Scruton's conclusion was based on a simplified theoretical approach for the case of vortex-induced oscillations. In his experiments, however, Scruton examined the effects of structural damping only and the effect of change in mass was never investigated experimentally (2).

If Scruton's conclusion were right, it would not be necessary to model the mass or damping of the prototype ac-

cording to scaling criteria so long as the product of mass and damping ratio is the same for both model and prototype. A higher value for the mass parameter of the model can be compensated by a lower damping ratio, and vice versa. This approach is very useful in designing models since exact values of the mass parameter and damping ratio of a prototype may not be easily obtained. Moreover, due to the lack of reliable information on the actual structural damping of bridges, only a vague estimate is possible for the latter parameter. The sensitivity of the response to a change in the mass parameter or damping ratio, separately, is also required to be examined.

The purpose of this study is to examine the relation, if any, between the mass and damping parameters in wind-induced responses of structures, as well as the sensitivity of such responses to these two parameters. In order to produce various wind-induced dynamic behaviours, three different geometric shapes are selected to form the cross-section of the models. A brief summary of the mechanisms of wind-induced oscillations is given in the next section. With the mass of the model kept constant, the responses under various damping conditions are obtained and the effect of the damping ratio can thus be examined. Similarly, the effect of the mass parameter can also be examined by varying mass parameters with constant damping. These two sets of results, when

plotted against the Scruton number,[1] will exhibit the relationship between mass and damping more clearly.

1.2 AERODYNAMIC BEHAVIOUR OF BLUFF BODIES

Wind-induced oscillations of structures such as bridges are often classified as follows: (1) vortex-induced oscillation in vertical or torsional mode, (2) flutter, (3) instability in vertical or torsional mode, and (4) buffeting induced by wind gust. These four types of behaviours are briefly explained in this section for future discussion.

1. Vortex-induced oscillations

   A bluff structure, such as bridge deck, when placed in a flow, sheds vortices in its wake alternatively from its top and bottom edges. The vortices give rise to fluctuating forces, the frequency of which is proportional to the flow speed. When the shedding frequency comes close to the natural frequency of the system, vertical or torsional oscillations can build up a resonance. This phenomenon has been known as the "vortex-induced oscillation" and has often quite significant consequences at relatively low wind speeds. The detail of this mechanism will

[1] Scruton number, $2m\delta/\rho bd$, is a dimensionless product of the mass ratio, $2m/\rho bd$, and logarithmic decrement, δ, named after C. Scruton in 1983.

be discussed in Section 5.1.

2. Flutter

Flutter is a kind of instability which occurred when the two degrees of freedom of the structures, vertical and torsional, are coupled together in a wind flow. Generally speaking, flutter occurs at higher wind speeds than those of vortex excitation and the motion quickly builds up to a very large amplitude, sufficient to cause structural failure. This phenomenon has been causing significant trouble to aeroplane wings ever since the early days of flight. It is known to occur for streamlined structures such as aerofoils. However, even in civil engineering structures, a similar behaviour has been reported (3). Flutter must be avoided completely by raising the critical onset velocity to a value beyond the range of expected wind speed.

3. Vertical Instability and Torsional Instability

These are single-degree-of-freedom self-excited oscillations which are induced by the aerodynamic negative damping. In the case of vertical instability, often called galloping, the lift force is the controlling factor, while the torsional instability, or stall flutter, is excited by the pitching moment. A well-known example of vertical instability is the

galloping of power transmission line with ice. The famous Den Hartog's theory was introduced some 50 years ago (4). Stall flutter has been often referred to in the case of turbine blade failure. Unlike the "classical" flutter mentioned above, this phenomenon is caused by the flow separation from the wing and hence could occur in any structure with bluff cross-sections. The failure of the Tacoma Narrows Bridge could probably be classified under this category.

4. Buffeting

Buffeting is a kind of random vibration by an excitation over a wide range of frequencies. Vibration is induced by the fluctuating components of the wind velocity. Buffeting can cause both vertical and torsional motions of structures.

In the present study, vortex-induced oscillations in vertical and torsional modes, instability in vertical and torsional modes in smooth flow, and buffeting in vertical motion induced by turbulence are examined.

Chapter II

SIMILARITY REQUIREMENTS IN WIND TUNNEL TESTING

It is usually impossible to determine all the aerodynamic behaviours of a structure by theories or analytical procedures alone. The use of model study has primary importance in this respect. However, a reliable prediction from model testing is largely based on how well a prototype structure is simulated geometrically, kinematically and dynamically by a scaled model. The laws of similitude make it possible to predict the performance of the prototype from test results.

There are three basic types of similitude which must be considered between prototype and model phenomena (5).

1. Geometric Similarity:

   The model and its prototype must be identical in geometrical shape but differ only in size. If the scale ratio is denoted by λ_L (L_m/L_p), it follows that areas vary λ_L^2 and volume as λ_L^3. Moreover, the boundaries of flow fields of the model and prototype must also be geometrically identical. Anything that affects the flow field of the prototype must be taken into consideration in modelling.

2. Kinematic Similarity:

In addition to geometric similarity, the similarity of the ratio of the velocities (λ_V) and accelerations (λ_a) at all corresponding points in the flow field must be considered. The magnitude of these scaling factors in relation to λ_L can be determined by dynamic similarity.

3. Dynamic Similarity:

The forces acting on corresponding fluid masses are related by ratios similar to those above. These are classified as dynamic similarities. Since the forces acting on the fluid elements will thus control the motion of these elements, it follows that dynamic similarity will yield similarity of flow patterns. Consequently, the flow patterns will be the same in the model as in the prototype if geometric similarity is satisfied and if the relative forces acting on the fluid are the same in the model as in the prototype.

The forces that may affect a flow field are forces due to pressure, F_P ; inertia, F_I; gravity field, F_G; viscosity, F_V; elasticity, F_E; surface tension of liquid, F_T and Coriolis accelerations, F_C. These forces may be expressed in simplest terms as follows:

$$F_P = (\Delta p)A = (\Delta p)L^2$$

$$F_I = Ma = \rho L^3(\frac{V^2}{L}) = \rho V^2 L^2$$

$$F_G = Mg = \rho L^3 g$$

$$F_V = \mu(\frac{dv}{dy})A = \mu(\frac{V}{L})L^2 = \mu VL$$

$$F_E = EA = EL^2 \qquad (2.1)$$

$$F_T = \sigma L$$

$$F_C = M\Omega V = \rho L^3 \Omega V$$

In order to obtain dynamic similarity, all corresponding force ratios must be the same in the model and prototype. These relations can be expressed as follows:

$$(\frac{F_I}{F_P})_p = (\frac{F_I}{F_P})_m = (\frac{\rho V^2}{\Delta p})_p = (\frac{\rho V^2}{\Delta p})_m \qquad \text{Euler number, } E = V\sqrt{\frac{\rho}{2\Delta p}}$$

$$(\frac{F_I}{F_V})_p = (\frac{F_I}{F_V})_m = (\frac{VL\rho}{\mu})_p = (\frac{VL\rho}{\mu})_m \qquad \text{Reynolds number, } R = \frac{VL}{\nu}$$

$$(\frac{F_I}{F_G})_p = (\frac{F_I}{F_G})_m = (\frac{V^2}{Lg})_p = (\frac{V^2}{Lg})_m \qquad \text{Froude number, } F = \frac{V}{\sqrt{Lg}}$$

$$(\frac{F_I}{F_E})_p = (\frac{F_I}{F_E})_m = (\frac{\rho V^2}{E})_p = (\frac{\rho V^2}{E})_m \qquad \text{Mach number, } M = V\sqrt{\frac{\rho}{E}} \qquad (2.2)$$

$$(\frac{F_I}{F_T})_p = (\frac{F_I}{F_T})_m = (\frac{\rho LV^2}{\sigma})_p = (\frac{\rho LV^2}{\sigma})_m \qquad \text{Weber number, } W = \frac{V}{\sqrt{\sigma/\rho L}}$$

$$(\frac{F_I}{F_C})_p = (\frac{F_I}{F_C})_m = (\frac{V}{L\Omega})_p = (\frac{V}{L\Omega})_m \qquad \text{Rossby number, } R_o = \frac{V}{\Omega L}$$

It will be noted that only five of these equations are independent, thus, if any five of them are simultaneously satisfied, dynamic similarity will be ensured. Fortunately, in most engineering problems five simultaneous equations are not necessary, since some of the forces stated above (1) may not act, (2) may be of negligible magnitude, or (3) may oppose other forces in such a way that the effects of both are cancelled.

All the dimensionless parameters stated above are flow properties. Other parameters which are related to the fluid properties are Prandtl (P_r) and Schmidt numbers (S_c). Moreover, parameters related to the interaction between the flow and structure are reduced velocity and the ratio of the air density to the density of the structure. The damping parameter must also be modelled in order that the dissipative energy due to structural damping is properly accounted for.

Because of the complexity of the fluid phenomena, it is worthwhile to discuss the significance of the dimensionless ratios stated above in order to enable one to simplify a problem by the elimination of the irrelevant, negligible, or compensating forces.

Reynolds number:

Reynolds number becomes a significant factor when the frictional force due to viscosity plays an important role. Typical example is the flow of a fluid through a completely filled conduit or when the flow speed is slow. Reynolds number similarity will be discussed in detail later.

Froude number:

This is the ratio of inertia force to gravity force. Systems involving gravity and inertia force include: surface wave action, flow of water in open channels, aerodynamic behaviour of cable-supported structures such as suspension bridges and other cases where gravity is a dominant factor. Buoyancy effect can be considered as the negative gravity in this similarity requirement and "densimetric Froude number" is considered for such cases.

Mach number:

Where the compressibility of fluid is important, it is necessary to consider the ratio of the fluid velocity to that of a sound wave in the same medium. This ratio is known as the Mach number.

Weber number:

In some cases, the effect of surface tension may be important, but in many cases it is negligible. The square root of the ratio of inertia force to the surface tension is known as the Weber number.

Euler number:

A dimensionless quantity related to the ratio of the inertia force to the pressure.

Rossby number:

The Rossby number is the ratio of the local accelerations to the Coriolis accelerations.

Prandtl number:

The Prandtl number is the ratio of the momentum diffusivity, or kinematic viscosity to the thermal diffusivity.

Schmidt number:

The Schmidt number is the ratio of the momentum diffusivity to the mass diffusivity.

Fortunately, for most of the model tests in wind tunnels, the satisfaction of all force ratios is not necessary. For air, the Prandtl number does not vary much with temperature. When air is used as the medium for modelling, the Prandtl number in the model and prototype will be nearly the same (6). Moreover, the Schmidt number will be nearly the same in the model as in the prototype if air is used as the medium for modelling (6). The effect of Rossby number can also be ignored unless local wind acceleration is of significant magnitude compared with the Coriolis acceleration, which is unlikely for ordinary wind tunnel testing of structures. If dynamic similarity exists, it follows that the pressure coefficient will also be the same in the model and

prototype. If the order of wind velocities involved in either model or prototype is such that the compressibility of the air may be neglected, and if surface tension is irrelevant, the remaining parameters needed to be satisfied are the Froude number and the Reynolds number.

From the foregoing discussion, if the Reynolds number of a model and its prototype are the same, the velocity scale ratio λ_V must be equal to the model-to-full-scale ratio of ν/L. However, if the Froude number similitude needs to be satisfied, the velocity scale ratio λ_V must be equal to the model-to-full-scale ratio of $\sqrt{gL}$.

From above:

$$\lambda_V = \{\frac{\nu}{L}\}_m \Big/ \{\frac{\nu}{L}\}_p \qquad (2.3)$$

$$\lambda_V = \{\sqrt{gL}\}_m \Big/ \{\sqrt{gL}\}_p \qquad (2.4)$$

Taking 'g' to be the same for the model as for the prototype, and solving these equations yields $(\lambda_L)^{3/2} = \nu_m/\nu_p$. This indicates that the relationship between the viscosities of the fluids can be established once the model scale has been selected, or vice versa. This means that (1) a fluid of appropriate viscosity can be found for the model test, or (2) if the same fluid is used for model and prototype, the model must be as large as the prototype. Since in most of

wind tunnel testings, the same fluid (air) as the prototype is used for the model test, and full-scale modelling is obviously impractical, engineers are forced to choose one of the two equations, Eqs. (2.3) or (2.4), if both fluid viscosity and gravitational acceleration are to be considered.

As a practice, by experience, Reynolds number is neglected in most of wind tunnel testings due to the belief that the viscous forces are small and relatively unimportant compared to the inertia forces in air. However, this assumption must be carefully examined. As is well known (7), when the solid boundary of flow field has curvature, such as in the case of a flow around a circular cylinder, with the Reynolds number ranging from $3x10^4$ to $3x10^5$ based on the cylinder diameter, there is a drastic change of the flow pattern around the body. The most apparent change is the reduction of the wake width immediately behind the cylinder caused by the shift of flow separation points. There is a corresponding reduction of the drag coefficient, C_D, and an increase in the frequency of formation of the vortices in the wake. It is important, therefore, that, in modelling a structure with circular cross-sections, these effects are properly taken into consideration. A similar consideration is required for any other structures with curved surface geometry. Compensation of the difference in C_D is necessary if prototype Reynolds number is above its critical value and

yet the model value is below critical. The value of the critical Reynolds number is also dependent on the surface roughness of the cylinder and the turbulence level in the approaching air flow.

There are other Reynolds number effects. In the case of the flow over rectangular cylinders, for example, the separation points do not shift with the Reynolds number due to the existence of sharp corners. However, broad wake after separation from the upstream corner may reattach to the surface of the body and consequently, depending on the aspect ratio of the rectangle, the wake may become narrower compared to the case without reattachment (7). This results in a reduction of the value of C_D and a higher value of the dimensionless vortex frequency, the Strouhal number, S. The length-to-width ratio of a rectangle at which this change occurs depends on the Reynolds number, the corner radius and the airstream turbulence level.

As mentioned above, the generally inadequate duplication of full-scale Reynolds number may cause discrepancies between test results and full-scale measurement. However, the condition of oncoming wind turbulence and the model surface roughness may cause this discrepancy too. In problems involving random excitation of the structure due to wind gust, it is necessary to simulate the velocity spectra cor-

rectly. It is pointed out by Townsend (8) that the structures of turbulent flows are very nearly similar for all Reynolds numbers which are large enough to allow turbulent flow. As mentioned previously, it is impractical to satisfy the Reynolds number similitude in usual wind tunnel testings. As such, the above fact is significant when models are tested in turbulent flow. However, the Reynolds number does play a part in the existence of the inertia subrange of the energy spectrum. As the Reynolds number increases, the large-wave-number end of the distribution will be extended so that the total dissipation of turbulence energy remains unchanged. On the other hand, when the Reynolds number is small, the ratio of the size of the dissipating eddies to that of the energy-containing eddies becomes larger and consequently, the shape of the energy spectrum becomes highly dependent on viscosity. The results of this is inaccurate simulation of turbulence structure due to narrower inertia subrange.

In the foregoing discussion, it is mentioned that it is difficult to satisfy the Reynolds number requirement. However, it is also mentioned that, to a certain extent, the Reynolds number does play an important role in the flow pattern. In reality, as it can be seen in the next chapter, the Reynolds number requirement has been neglected in most of wind tunnel testings because of the assumption that the flow

around bodies of sharp-cornered shapes were insensitive to the Reynolds number effects.

Chapter III

REVIEW OF THE PAST STUDIES

3.1 BRIEF HISTORY OF STUDY OF AERODYNAMIC STABILITY OF BRIDGES

Wind effect on bridges is not a new subject in the history of wind engineering. In fact, the history of modern suspension bridges since the end of the 18th century registers constant struggle of engineers against wind. There have been many famous incidents in which major bridges were seriously damaged, or even completely blown down by wind. However, systematic studies on the wind-resistant designs of bridges, especially using wind tunnel facilities, do not enjoy such a long history. Not long before the Tacoma disaster occurred in November 1940, long-span suspension bridges such as the George Washington Bridge, the Bronx-Whitestone Bridge in New York City, and the Golden Gate Bridge in San Francisco were completed and oscillations of these bridges were reported (9). However, not until 1950, ten years after the collapse of the Tacoma Narrows Bridge, were model tests of the above-mentioned bridges carried out. At the wind tunnel of the University of Washington, both sectional and full

model tests of the Tacoma Narrows Bridge were carried out by Farquharson, et al (15). The above-mentioned bridges were also tested using sectional models at this laboratory. In designing the sectional models, the same similarity criteria as the ones used for the Tacoma Narrows Bridge were followed. The new Tacoma Narrrows Bridge was completed at the end of 1950 after the series of wind tunnel testings. Also, some reinforcements to the other bridges mentioned above had been introduced based on the wind tunnel test results.

During the years 1946 to 1951, the investigation of aerodynamic stability of the proposed Severn Bridge was carried out at the National Physical Laboratory of England by Scruton, et al (1). Both the full and sectional models were tested and all the results showed very good agreement between the two test methods. The section decided at this time was actually used for the Forth Road Bridge, the first long-span suspension bridges in the U.K. since World War II. Later the Severn Bridge project was revived and the NPL again undertook the wind tunnel investigation. The adopted section for this testing was a streamlined box girder.

There were many other wind tunnel studies on aerodynamic stability of bridges. Vincent's studies on the Golden Gate Bridge, as well as other bridges at NBS, are well known. Selberg of Norway, Rocard of France, Kloppel of Ger-

many, Hirai of Japan were the people who founded this field from the 1940s through the 1960s. In Canada, the Low Speed Aerodynamics Laboratory at the National Aeronautical Establishment, NRCC, led by Wardlaw, and the Boundary Layer Wind Tunnel Laboratory, the University of Western Ontario, headed by Davenport, have been most productive working in this field. Typical testings carried out at the NAE are those for the Pasco-Kennewick Intercity Bridge, the St. Johns River Bridge, the Longs Creek Bridge, the Annacis Island Bridge, the Lions' Gate Bridge, and the Quincy Bridge, etc. Western's BLWT has tested the Golden Gate Bridge, the Bronx-Whitestone Bridge, the Thomas Mckay Bridge, the Weirton-Steubenville Bridge, and the Sunshine Skyline Bridge, etc.

The concept of wind turbulence was introduced to wind tunnel studies in the early 1960's. However, it is still not a common practice to test bridge models in turbulent flow. Not much research work has been done to compare results from two different flow conditions. Recent studies on the Lions' Gate Bridge in Vancouver and the Annacis Island Bridge over the Fraser River at New Westminster included testings in both smooth and turbulent flow. However, as far as the similitude requirement for the model construction is concerned, similar parameters were considered in all the testings.

3.2 REVIEW OF TYPICAL WIND TUNNEL STUDIES

Three particular model tests are reviewed here to examine the similitude requirement to wind tunnel test bridges. These are the studies on the Tacoma Narrows Bridge, the Severn Bridge, and the Palmerston Bridge. They were selected because of the reasons given below. The testing of the Tacoma Narrows Bridge initiated development of the aerodynamic study of bridges as a scientific discipline. In that respect, it is important to review the similitude requirement of this classical study. Both the full and sectional models were investigated in the wind tunnel. In designing the sectional model of the Severn Bridge, a new approach was introduced by Scruton, who suggested that the mass parameter and the damping ratio could be combined as a single parameter in modelling. This was a new concept in modelling. In testing the model of the Palmerston Bridge, the concept of generalized mass for the interpretation of test results for full-scale prediction was introduced.

1. Tacoma Narrows Bridge

After the failure of the Tacoma Narrows Bridge in 1940, both sectional and full models of the bridge were constructed for the full dynamic testing. The experiment was carried out at the University of Wash-

ington, and at the California Institute of Technology. The project was managed by F.B. Farquharson, G. Vincent and T. von Karman. In this series of wind tunnel tests, the Reynolds number similarity was ignored. "With the experience in the general field of hydraulics and aerodynamics," said Farquharson (9), "..... and in particular the case of blunt bodies involving sharp corners, the effect of viscosity is negligible." This assumption has been well-accepted since then and there are many experimental evidences which prove Farquharson's view. With this assumption, the Froude number constitutes the total similitude requirement. Possible problems by negligence of Reynolds number similarity are as discussed in the previous section. It should be noted here that the wind tunnel tests of these days employed only smooth flow without any simulation of natural wind turbulence.

The model scales, with respect to the Froude number similarity, are listed in Table 1 (9).

However, there was one practical difficulty: if the model were to be an exact replica, it would be necessary to use materials having lower moduli of elasticity, E, than the prototype materials in proportion to the geometric scale ratio λ_L. Even if such

material does exist, it may not possess the other necessary properties such as workability and sufficiently low damping characteristics. Alternatively, the scaled stiffnesses can be made correctly by combining E and I into one parameter for bending stiffness EI and G and J for torsional stiffness GJ. In modelling cables, the cross-sectional area, A, can be modified so that axial stiffness EA can be used as a single parameter. In constructing the full model of the original Tacoma Narrows Bridge, a linear scale factor of 1:50 was adopted. Due to the unavailibility of suitable materials in modelling the girder, an equivalent structure which provides proper elastic properties was used.

As the structural damping of the prototype bridge is not known, the damping requirement for the model can only be determined approximately. It was concluded that the frictional damping should be reduced to the lowest possible value. Great care was taken in the design of the model to insure that this level of friction could be maintained over a long period of time. Such a model with the lowest possible damping would further afford opportunities to study the effect of increase in damping.

On Nov. 7, 1940, according to the eyewitness' account of the failure of the Bridge, a single amplitude of up to 45^0 was observed prior to the failure. The corresponding wind speed and frequency observed were said to be 42 mph and 14 cpm, respectively. With the width of the bridge equal to 39 ft, the failure of the bridge probably occurred at a reduced wind speed, $V/N_T b$, of 6.8. Interpretations for this wind speed are many. First of all, it is not clear where and how the wind speed could be determined. No information was available about the exact wind direction. It is not even known if this "critical" wind speed corresponds to the onset of instability or the final stage of collapse of the bridge. Consequently the comparison of this field observation with the laboratory test results is somewhat obscure. However, the following comments can be made in this regard: The critical $V/N_T b$ for the onset of instability obtained from full bridge model test was 2.34 with structural damping of 0.54%. With two values of structural damping, 0.17% and 0.41%, the $V/N_T b$ obtained from the section-model test were 2.07 and 2.50, respectively. Due to mechanical limitations, these tests were terminated when the single amplitude of the models reached approximately 12^0. Nevertheless, the growth of vibration amplitude was found to be rather gradu-

al. The wind speed reading corresponding to the maximum amplitude of 12^0 was almost twice as high compared with the onset critical speed. Due to the lack of accurate field measurements, particularly in estimating the structural damping of the bridge and wind speed reading, no definite comparison can be made with the test results.

2. Severn Bridge

During the period of 1946-1951, both sectional models and full models in the linear scales of 1/32 and 1/100, respectively, were made to investigate the aerodynamic stability of the proposed Severn Bridge at NPL (1). R.A. Frazer and C. Scruton were in charge.

In designing the full model, all the model scale requirements were exactly the same as those used in modelling the Tacoma Narrows Bridge. The Reynolds number requirement was again disregarded for the same reason (9). Reference, on this question, was also made regarding the "satisfactory" correlation between the full-scale measurement and the results from the tests of the model of the Tacoma Narrows Bridge (9). As discussed in the previous section, it should be

noted that this remark about the "satisfactory" correlation is questionable. The similitude requirements were summarized by Scruton in the following way.

$$\text{a)} \quad I/\rho b^4 \;,\; m/\rho b^2$$

$$\text{b)} \quad k_T/(\rho V^2 b^2) \;,\; k_B/(\rho V^2)$$

$$\text{c)} \quad gb/V^2 \qquad (3.1)$$

$$\text{d)} \quad \delta_T \;,\; \delta_B$$

where I = mass moment of inertia per unit length,

m = mass per unit length,

k_T = elastic stiffness corresponding to I,

k_B = elastic stiffness corresponding to m,

ρ = air density,

b = width of bridge,

V = wind speed,

δ_T = logarithmic decrement for vertical oscillation due to structural damping,

and δ_B = logarithmic decrement for torsional oscillation due to structural damping.

However, conditions of similarity with sectional models are somewhat different. The inertial coefficients of sectional models must include total contributions from both the suspended structure and the cables. The stiffnesses for the model are provided by artificial springs to give the required frequencies of oscillation and the model itself was constructed as a rigid body, unlike the correctly proportioned gravitational and elastic stiffness of full models. Since the gravitational forces do not affect the model dynamics for the case of sectional models, the parameter (c) above was therefore omitted. The appropriate parameters for the sectional model were then expressed as follows:

$$\begin{aligned} &\text{a)} \quad I/\rho b^4 \ , \ m/\rho b^2 \\ &\text{b)} \quad V/N_T b \ , \ V/N_B b \\ &\text{c)} \quad \delta_T \ , \ \delta_B \end{aligned} \tag{3.2}$$

where N_T = natural frequency in torsion,
and N_B = natural frequency in bending.

In this case, m and I represent the total contributions due to the suspended structure and the cables of the actural bridge. Since the Froude number similarity is not required anymore, unlike the full model scaling, the velocity scale can be decided by the relation to the frequencies. The only relevant parameter is now given by (b) above. It was also concluded by Scruton in another paper (10) that if the response frequency at resonance is approximately equal to the natural frequency, and with the motion only in isolated single mode of vibration, strict inertial scaling is not essential and that the critical values of Vr depend only on the geometric shape of the structure and on the products of parameters (a) and (c) above. This theory will be introduced later again in Section 5.1. In conclusion, only the following two parameters were used:

$$\begin{aligned} &a). \quad I\delta_T/\rho b^4 \quad , \quad m\delta_B/\rho b^2 \\ &b) \quad V/N_T b \quad , \quad V/N_B b \end{aligned} \tag{3.3}$$

The bridge tested here was later adopted for the Forth Road Bridge. There has been no report of full-scale observation of wind-induced response of the bridge since then and no comparison can be made with the test results.

3. Palmerston Bridge

A 1:60 scale sectional model of the new Palmerston Bridge, Pugwash, Nova Scotia was wind-tunnel tested in smooth and turbulent wind at NAE/NRCC (11).

In designing the model, the following non-dimensional parameters, which must have the same values for the model as for the full-scale bridge, were considered. The philosophy here is identical to the case of Severn Bridge, except that the mass-damping parameter, or Scruton number, was not employed.

$$\frac{I}{\rho b^4}\ ,\ \frac{m}{\rho b^2}\ ,\ \frac{V}{N_B b}\ ,\ \frac{N_T}{N_B}\ ,\ \xi_B\ ,\ \xi_T \qquad (3.4)$$

where I = generalized moment of inertia per unit length,

m = generalized mass per unit length

ρ = air density,

b = width of the deck,

V = wind speed,

N_T = torsional frequency,

N_B = vertical bending frequency,

and ξ_B, ξ_T = zero wind damping ratios in vertical bending and torsion, respectively.

It was assumed again that, for bluff, sharp-edged structures, the influence of the Reynolds number tends to be very small and was therefore neglected. The other model scales were the same as those discussed in the previous section. The particular importance of this project is that this was the first wind tunnel test of a bridge that introduced the concept of generalized mass. Strictly speaking, the total generalized inertias per unit length, I_G and M_G, should be considered for the testing of sectional models because they include weighted contributions from all parts of the bridge participating in the motion including cables and towers. It has been shown that, in some cases, the true mass per unit length of the bridge may be some 50% higher than the total generalized mass which ev included contributions from cables and towers (12). Therefore, when true mass per unit length is used in modelling, the results obtained may underestimate the full-scale effects. The formulation of generalized mass is shown in Appendix C.

In modelling the Palmerston Bridge, the vertical mode shape was defined in such a way that the generalized mass per unit length is the same as the true

mass per unit length. For the interpretation of test results to full-scale prediction of the peak amplitude, Eq. C7 in Appendix C was used. However, this approach is based on the assumption that the exciting force is independent of the amplitude, as explained in Appendix C. When the exciting force is a function of both amplitude and time, the generalized force given in Eq. C4 should be used.

Chapter IV

EXPERIMENT

4.1 PURPOSE

The purpose of this experiment is to investigate the effects of the mass and damping parameters on the wind-induced responses of structures. Various geometrical shapes of structures were selected to examine various types of wind-induced dynamic behaviours.

4.2 FACILITIES

The tests were carried out at the 2'x3' open circuit wind tunnel of the University of Ottawa. The available wind speed range is up to 50 m/s. The general layout of model installation in the wind tunnel is illustrated in Fig. 1.

4.3 EQUIPMENT

The following equipments were used for the experiment:

Strain Gauge Conditioner, VISHAY instruments Model 2110

Voltmeter, TSI Model 1076

Sum-and-difference Amplifier, TSI Model 1063

Dual Power Supply, Bum-Brown Model 552

Chart Recorder, Gould 220

Inclined Manometer, R. Fuess, G 1611 together with a standard NPL type Pitot-tube

Arrangement of the equipment is depicted in Fig. 2.

4.4 SET-UP FOR THE EXPERIMENT

Three different geometric shapes of models were selected to examine various wind-induced dynamic behaviours.

Model No. 1 (H section) was designed to establish vortex-induced oscillations in vertical and torsional modes and self-excited torsional instability.

Model No. 2 (1x2 box section) was designed to establish self-excited vertical instability.

Model No. 3 (flat plate) was designed to establish buffeting response.

The models were made of balsa wood and all were 61 cm in length. The geometry of the models is given in Fig. 3.

As is diagrammatically explained in Fig. 4, a short aluminium bar was extended to the outside of the wind tunnel wall from each model. This bar is connected to two horizontal aluminium bars along the wind direction outside the wind tunnel and then the whole system is supported by four elastic springs per side. The location of these springs can be adjusted so that the natural frequency for torsion of the system can be easily changed.

4.5 PROCEDURE

The vertical frequency of the model is controlled by the spring stiffness while the torsional frequency can be controlled by both the spring stiffnesses and the spacing between a pair of springs. The mass, as well as the mass moment of inertia, can be increased without changing the aerodynamic characteristics of the model by attaching weights on the bar outside the wind tunnel. The structural damping of the model can also be adjusted by using various liquids in

dash-pots, the viscous dampingg system (see Fig. 4). A free vibration test of the model was performed before each run to obtain the structural damping and natural frequencies of the model. All testings were carried out in smooth wind flow with the exception of Model No. 3, which was tested in turbulence produced by a coarse grid installed upstream of the test section. The root-mean-square (RMS) response of the model was detected through the strain gauge system connected in series to the model-supporting springs. The response of the model was recorded on a voltmeter. The detail of the measuring system is explained in the next section.

A typical run of the tests consists of the following steps:

1. Adjust the various parameters to make sure that the desired type of wind-induced responses would be observed with the model.
2. Obtain the damping and natural frequency of the system.
3. Increase the wind speed, from zero, in increments of approximately 0.1 m/s.
4. Obtain the RMS displacement of the model at each wind speed from a voltmeter.
5. Repeat the above procedure with the change of either mass (or damping) while keeping the damping (or mass) constant.

4.6 MEASUREMENT

A Pitot tube for the measurement of reference wind speed was located above the model. The difference between the Pitot static and Pitot dynamic pressure was then measured using the manometer. Mean wind speed was then determined from the manometer reading. In testing the models, the transverse and rotational motions of the models were detected from the vertical deflection of two leaf springs which were clamped from the support at one end and connected to the model supporting spring system at another. The springs were hooked on the leaf springs, on which strain gauges were attached. The detail of the system is shown in Fig. 4. Individual vertical motion of the springs will induce bending moment along the leaf springs and give corresponding strains at the location of the gauges. Torsional displacement was obtained from the difference between two signals. This was done through the sum-and-difference amplifier. The damping of the model in still air was measured from the free vibration trace by exciting the model manually. The decay in the oscillations was recorded by the chart recorder. The logarithmic decrement method was used. A sample oscillation decay trace and the calibration for the response measurement are described in Appendix D.

Chapter V

SUMMARY AND DISCUSSION OF EXPERIMENTAL DATA

5.1 VORTEX EXCITATION

The equation of motion for a single-degree-of-freedom vertical motion is

$$m\ddot{y} + c\dot{y} + ky = F(y, \dot{y}, \ddot{y}; t) \qquad (5.I)$$

where m = mass per unit length,

c = damping coefficient,

k = stiffness,

F = external force per unit length,

and y = displacement.

As was briefly explained in Section 1.2, the simplest explanation of the mechanism of vortex excitation is the resonance of the structural frequency to the frequency of vortex shedding in its wake. This is because when the vortices separate from the section at a certain frequency, an alternating lift force will be produced on the body with the same frequency. Therefore, for the analysis of vortex excitation, let us first of all consider, following Scruton, the simple harmonic excitation function as follows:

$$F(t) = \frac{\rho V^2}{2} C_L d \sin(2\pi nt) \tag{5.2}$$

where C_L = coefficient of alternating lift force,

$\frac{1}{2}\rho V^2$ = dynamic pressure,

d = height of the structure projected on the plane taken normal to the mean flow,

and n = excitation frequency.

Eq. (5.1) thus becomes

$$m\ddot{y} + c\dot{y} + ky = \frac{\rho V^2}{2} C_L d \sin(2\pi nt) \tag{5.3}$$

The amplitude of the steady-state motion is

$$y(r,\xi) = \frac{F}{k\sqrt{(1-r^2)^2 + (2r\xi)^2}} \tag{5.4}$$

where $r=n/N$, $N = \frac{1}{2\pi}\sqrt{\frac{k}{m}}$, $\xi = \frac{c}{2\sqrt{mk}} = \frac{\delta}{2\pi}$

and δ is defined as the natural logarithm of the ratio of any two successive peak amplitudes in free vibration.

When the frequency of excitation coincides with the natural frequency, i.e., r=1, Eq. (5.4) gives the peak amplitude

$$y_p = \frac{d}{4\pi} \frac{Vr^2 C_L}{(2m\delta/\rho d^2)} \tag{5.5}$$

where Vr = reduced wind speed, V/Nd or V/Nb, corresponding to the peak amplitude

and $\frac{2m\delta}{\rho d^2}$ = dimensionless parameter, or so-called Scruton number.

Similarly, for torsional oscillation, a pitching moment per unit length on the system can be expressed as

$$M(t) = \frac{\rho V^2}{2} C_M d^2 \sin(2\pi nt) \tag{5.6}$$

where C_M = coefficient of alternating pitching moment.

Similar to the previous case, it can cause the maximum displacement at the resonance, and its amplitude y_p, at the edge of the deck is as follows:

$$y_p = \frac{b}{8\pi} \frac{Vr^2 C_M}{(2I\delta/\rho d^4)} \tag{5.7}$$

where b = width of the deck.

The dimensionless parameter $2I\delta/\rho d^4$ of Eq. (5.7) corresponds to the Scruton number but this time for the torsional motion. This number is called the "Scruton number in torsion" throughout this thesis.

According to Eq. (5.5), the peak amplitude resulting from harmonic loading varies inversely with the Scruton number. When Eq. (5.5) is applied to the prediction of the response due to vortex excitation, the following assumptions were made (10). The variation of C_L with amplitude is fairly weak over the range of interest. The motion is always isolated and harmonic. The frequency of oscillation corresponding to the critical wind speed is approximately equal to the natural frequency.

However, as is mentioned by Scruton (2), the use of forcing functions as given by Eqs. (5.2) and (5.6) would be valid only for the "resonance" condition Vr=1/S where S is the Strouhal number. Outside the resonance range of Vr, this expression is evidently not consistent with the observations of oscillatory behaviour in wind. It can be observed, from Figs. 5 and 6, that the range of the wind speed at which the vortex response was observed decreases with increasing structural damping. In all cases, the vibration amplitude shows pseudo-parabolic humps as a response curve against wind velocity rather than having sharp response which is

typical for the case of the ordinary resonance. Also, for the case of ordinary simple harmonic excitation, the bandwidth of the response curve should increase with increasing structural damping. This is different from the wind-induced response characteristics we are dealing with now. Another important point is the following: it is also known that, except at large damping, the frequency of the vibration and the frequency of vortex shedding within the wind speed corresponding to the structural response stay constant at the natural frequency of the structure. But when the wind velocity gets lower or higher than this range and when the structural response does not exist, the frequency of the vortex shedding varies in proportion to the wind velocity. The phenomenon is known as "lock-in" because the flow characteristics of the wake are locked-in, or governed, by the dynamic motion of the body upstream. It implies that, once the vibration starts, the behaviour is considered to be a coupled motion between the body and its surrounding fluid; i.e., the wake formation is dominated by the body motion and thus the induced motion of the body by the wake have mutual interaction with the formation of shedding. It is also pointed out by Yamaguchi, et al. (13) that the relationship between the resonant amplitude and the Scruton number differs from the property of the linear forced vibration given above, which predicts inversely proportional relationship to each other. These evidences lead to the conclusion that the

lift coefficient is probably considerably affected by the resonant amplitude.

From the above discussion, it is believed that vortex excitation is not a simple harmonic forced vibration but has an aspect of self-excited vibration. Since self-excited vibration is caused by forces produced by the displacements of the system, the excitation force should be considered dependent of time as well as amplitude. However, for simplicity and convenience, Eq. (5.5) and (5.7) can be used in predicting the resonant amplitude. For the precise prediction of structural response, more work is needed in this area.

5.1.1 Vertical Response

The H-section model was used to investigate the vertical vortex-induced response. The experiment was divided into two parts. Part 1: with the mass of the model kept constant at 0.282 kg, the structural damping was increased from 0.32% to 2.20% of critical. Part 2: with the structural damping kept constant at 0.65% of critical, the mass was increased from 0.282 kg to 0.990 kg.

Figs. 5 and 6 show the RMS response plotted against the reduced wind speed for parts 1 and 2, respectively. It can

be seen that the range of the wind speed at which the response was observed and the maximum amplitudes are decreased by increasing either the structural damping, or the mass, but the wind speed corresponding to the maximum response is not significantly influenced.

Figs. 7 and 8 show the maximum amplitude plotted against the damping ratio (ξ) and the mass ratio ($m/\rho b^2$) respectively. The results are summarised in Fig. 9, in which both the maximum RMS response amplitude and the wind speed range of instability are given as functions of the Scruton number. It is noted that the maximum amplitude oscillations occurred in the range of $V/N_B b$ =2.15 to 2.53 and it decreases with increasing Scruton number. The maximum amplitude falls rapidly to a low value with the increase of the Scruton number to up to 5 or so and then decreases only slowly with further increases. For values of $V/N_B b$ outside the instability region shown in Fig. 9, the section was positively damped. With all the experimental data plotted on the same curve, Fig. 9 clearly shows that the maximum amplitudes can be described as a function of the Scruton number alone.

Fig. 10 shows the comparison of the maximum response amplitude results from various sources, including those shown in Fig. 9. Other results are from Refs. 2, 14, 15 and

16. In Ref. 2, a rigid cylinder was tested under various damping conditions by Scruton. In Ref. 14, circular cylinders were tested under various damping conditions and an empirical formula to predict the maximum amplitude was obtained by Iwan. In Ref. 15, a sectional model, H-section with the aspect ratio of 1 to 5, similar to the original Tacoma Narrows Bridge, was tested under various damping conditions by von Karman. In Ref. 16, the values of $Vr^2 C_L$ obtained from the testing of various types of box girders were summarized into an empirical equation as follows:

$$Vr^2 C_L = 5.8(\frac{b}{d}) \qquad (5.8)$$

where Vr = reduced wind speed as defined previously,

and C_L = lift coefficient.

For plotting Fig. 10, this empirical expression is substituted into Eq. (5..15) given in section 5.1, to determine the relationship between the Scruton number and corresponding response magnitude.

It is noted that the maximum amplitude obtained from the empirical formula by Iwan yields results very similar to those obtained experimentally by Scruton for a circular cylinder. However, there are some discrepancies between the experimental results of von Karman and those of the present

experiment for a Tacoma-like H-section. The reason of this discrepancy is not immediately clear. However, this may be attributed to the fact that the flow condition of the von Karman's experiment was somewhat different from the present testing condition. It is possible to have some three-dimensionality of the flow for the case of testing at the California Institute of Technology with the open jet wind tunnel employed. The reason of discrepancy between results obtained from Smith's empirical formula, and those from of von Karman and the present experiment is even more obscure. It may be attributed to the fact that the lift coefficient in Eq. (5.8) is not only a function of the cross-sectional shape of the model but is also a function of the response amplitude. It is interesting to note that the results by Smith, which includes various bluff sections, are not far away from the results of the present study. The experimental results of the present study are summarized in Table 2.

5.1.2 Torsional Response

The H-section was also used to investigate the vortex-induced torsional response. The procedure is similar to that of vertical response. Part 1: with the mass moment of inertia kept constant at 31.37×10^{-4} kg.m^2, the structural damping was increased from 0.22% to 1.60% of critical. Part

2: with the structural damping kept constant at 0.65% of critical, the mass moment of inertia was increased from 31.37×10^{-4} kg.m^2 to 50.36×10^{-4} kg.m^2. The centre of rotation of the model was fixed throughout this part of testing in order to prevent any coupling with the vertical motion, as it is explained in Appendix D.

Figs. 11 and 12 show the RMS response plotted against the reduced wind speed for parts 1 and 2, respectively. Similar to the case of vertical vortex excitation, Figs. 11 and 12 indicate that the extent of the wind speed range and the maximum amplitudes are decreased by increasing either the structural damping or the mass moment, but the wind speed to give the maximum response is not significantly affected by this increase. It is also indicated, in Fig. 12, that the torsional response resulted from vortex excitation is very sensitive to damping compared with the case of vertical vibration mode. When the damping factor was raised from 1.22% to 1.60%, the response was not observed any more.

Figs. 13 and 14 show the maximum amplitude plotted against the damping ratio (ξ) and the mass ratio ($I/\rho b^4$) respectively. The curve of maximum amplitude as a function of Scruton number in torsion is shown in Fig. 15. It can be seen that the maximum amplitude reduces with increasing Scruton number. However, unlike the vertical response, a

linear relationship is found between the maximum amplitude and Scruton number.

Fig. 16 compares results from Fig. 15 with those from Ref. 16. In Ref. 16, the value of $Vr^2 C_M$ obtained from the testing of various types of box girders was summarized into an empirical equation as follows:

$$Vr^2 C_M = 5.8\left(\frac{b}{d}\right) \tag{5.9}$$

where Vr = reduced wind speed as defined previously,

and C_M = moment coefficient.

For plotting Fig. 16, this empirical expression is substituted into Eq. (5.7) given in Section 5.1 to determine the relationship between the Scruton number and corresponding response magnitude.

According to Eq. (5.7), the maximum amplitude should vary inversely with the Scruton number. However, the results of the present study show somewhat different functional relationship, as shown in Fig. 16. Relatively few data are available in the open literature concerning the torsional vortex excitation and the results shown here represent the limited information available to the author at the present time. Although results from the present experiment do not show inverse proportionality of the maximum amplitude

with the Scruton number as predicted by the theory, it does show that the maximum amplitude depends on the Scruton number as a single important parameter. The experimental results of the present study are summarized in Table 3.

5.2 SELF-EXCITED INSTABILITY

5.2.1 Torsional Instability

The equation for the torsional response (17) is

$$I\ddot{\theta} + 2I\xi\omega\dot{\theta} + k\theta = \frac{\rho V^2}{2} d^2 C_M \qquad (5.10)$$

where I = mass moment of inertia per unit length,

θ = angular displacement,

ξ = damping ratio in torsion,

ω = circular frequency in torsion,

k = torsional stiffness,

$\frac{1}{2}\rho V^2$ = dynamic pressure,

d = length of lateral side of the model,

and C_M = pitching moment coefficient.

Angles are taken as positive when the leading edge of the body is up against the wind. Eq. (5.10) can be linearized for small rotations to determine the onset of torsional instability, using the quasi-static theory as follows:

$$I\ddot{\theta} + 2I\xi\omega\dot{\theta} + k\theta = \frac{\rho V^2}{2} d^2 \left(\frac{\partial C_M}{\partial \alpha}\right)_{\alpha=0} \left(\theta - \frac{b\dot{\theta}}{2V}\right) \qquad (5.11)$$

where α = angle of attack,

and b = width of the deck.

The minimum critical velocity for the onset of torsional instability is reached when the total damping becomes zero; i.e.,

$$\frac{V}{N_T d} = -4\left(\frac{2I\delta}{\rho d^3 b}\right) \Big/ \left(\frac{\partial C_M}{\partial \alpha}\right)_{\alpha=0} \qquad (5.12)$$

This expression implies that the critical reduced wind speed for the onset of torsional instability should be proportional to the Scruton number in torsion.

The H-section model was used to investigate the torsional response. In the first part of this experiment, the mass moment of inertia was kept constant at 31.37×10^{-4} kg.m^2 while the structural damping was changed from 1.59% to 12.73% of critical. The structural damping was then kept constant at 3.60% and the mass moment of inertia was increased from 17.85×10^{-4} kg.m^2 to 89.95×10^{-4} kg.m^2. The centre of rotation of the model was fixed throughout this part of the testing in order to prevent any vertical motion, as is explained in Appendix D.

Figs. 17 and 18 show the RMS response plotted against the reduced wind speed for parts 1 and 2, respectively. The results consistently show that, at the critical speed at which the total damping is zero, the amplitude increases rapidly with further increase in wind speed. Due to mechanical limitations, the experiment had to be terminated when the displacement of the model reached approximately ± 5 deg.

Figs. 19 and 20 show the critical reduced wind speed plotted against the damping ratio (ξ) and the mass ratio ($I/\rho b^4$) respectively. Fig. 21 shows the critical reduced wind speed plotted against the Scruton number in torsion. It can be seen that the increase of structural damping or mass moment of inertia raises the critical speeds for the onset of torsional instability, but the rapid growth of amplitude is not suppressed in any case once the wind speed exceeds the critical value. Unlike vortex excitation, the curve obtained from varying the structural damping does not coincide with the one obtained from varying the mass moment of inertia. When the Scruton number is below 30, the critical reduced wind speed is more sensitive to structural damping than to mass moment of inertia. However, this trend reverses when the Scruton number is above 30. It was also observed that the critical reduced wind speed is almost linearly related to both the structural damping and mass moment of inertia, except at low damping and high mass moment of

inertia. From the above observation, it can be said that the critical wind speeds depend on both the damping factor and mass ratio, both being independent parameters. A good agreement is also found with the testing by von Karman (15) as shown in Fig. 21. In his report, a sectional model of the original Tacoma Narrows Bridge, H-section with the aspect ratio 1 to 5, was tested under various damping conditions. The experimental results of the present study are summarized in Table 4.

5.2.2 Vertical Instability (Galloping).

The fundamental assumption of conventional galloping analysis is that the fluid force is quasi-steady in nature; i.e., the fluid force on the structure is determined solely by the instanstaneous relative velocity and the angle of attack of the flow to the structure.

The equation of motion can be given as follows (17) :

$$m\ddot{y} + 2m\xi\omega\dot{y} + ky = \frac{\rho V^2}{2} d\, C_y \qquad (5.13)$$

where m = mass per unit length,

y = vertical displacement, upward positive,

ξ = structural damping in bending,

ω = circular frequency in bending,

k = bending stiffness,

$\frac{1}{2}\rho V^2$ = dynamic pressure,

d = length of lateral side of the model,

and $C_y = (V_{rel}/V)^2 (C_L \cos\alpha + C_D \sin\alpha)$.

Eq. (5.13) can be linearized for small angle of attack, α, to determine the onset of vertical instability; i.e.,

$$\ddot{y} + 2\xi\omega\dot{y} + \omega^2 y = -\frac{\rho V^2}{2m} d \left(\frac{\partial C_y}{\partial \alpha}\right)_{\alpha=0} \frac{\dot{y}}{V} \qquad (5.14)$$

The minimum flow velocity for the onset of instability is reached when the total damping becomes zero; i.e.

$$\frac{V}{N_B d} = -2\left(\frac{2m\delta}{\rho d^2}\right) \Big/ \left(\frac{\partial C_L}{\partial \alpha} + C_D\right)_{\alpha=0} \qquad (5.15)$$

This expression implies that the critical reduced wind speed for the onset of vertical instability should be proportional to the Scruton number.

The 1x2 box section model was used to investigate the vertical response. In the first part of this experiment, the mass of the model was kept constant at 0.321 kg while the structural damping was increased from 0.57% to 2.07% of critical. The mass was then increased to 0.937 kg while the structural damping was again changed from 0.57% to 1.57%.

Figs. 22 and 23 show the RMS response plotted against reduced wind speed for parts 1 and 2, respectively. It can be seen that, unlike the torsional instability of the H-section model, the velocity at which the amplitude rises rapidly is largely independent of either mass or structural damping of the model. In both cases, the critical reduced wind speed ($V/N_B b$) is approximately 6. However, the response amplitude above this velocity decreases with increasing structural damping. Regardless of the mass parameter, when structural damping is higher than approximately 0.8%, the response drops with increasing wind speed after exceeding a peak. The response remains almost constant with further increase in wind speed. For the case of the higher mass parameter, no rise in amplitude was observed when the structural damping was above 0.72%. The mass parameter ($m/\rho bd$) used in this experiment was either 107 or 313. Figs. 24 and 25 show the results of the similar tests obtained by Novak (18) and Yamada (19), respectively. The mass parameters used by these researchers were 64 and 280, respectively. The range of structural damping used in their study was from 0.20% to 4.40%. It is clearly seen that the reduced wind velocity at which the amplitude rises rapidly depends neither on the mass parameter nor the structural damping. The strong vibration starts developing at reduced velocities close to the expected vortex resonance velocity ($V/N_B d$)=12.3. Novak (18) explained that this phenomenon appears to result from the

composite action of galloping instability and vortex shedding because the theoretical onset velocity for galloping, with lowest damping (0.37%), would be $(V/N_B d)=5.2$. With the higher damping of 4.40%, the galloping onset might be expected around $(V/N_B d)=61$, well above the theoretical vortex resonance. Therefore the corresponding curve shown in Fig. 24 resembles the vortex-excited response peak quite well. However, this explanation cannot explain the result obtained from the present experiment for the case of higher mass parameter with low structural damping.

The galloping onset velocity for the above case as obtained from Eq. (5.15) is approximately 38. This is well above the theoretical vortex resonance. However, from Fig. 23, there is no indication of vortex shedding at $V/N_B b$ of near 6. The above observation is somewhat different from Novak's experiment. This difference may be explained as follows.

It was also mentioned by Novak (18) that for a 1x2 box section in smooth flow, the lateral force coefficient features a curvature change, as shown in Fig. 26, and galloping can exist at velocities lower than the onset velocity given by Eq. (5.15), if the appropriate magnitude of initial disturbance is provided. When Fig. 24 is compared with Figs. 22 and 23, the sudden rise in amplitude at $V/N_B d=12$ in No-

vak's figure may be initiated by vortex shedding and followed by galloping. In both cases, the rapid rise in amplitude, with a slight increase in wind speed, describes a "boundary of instability". To the left of the "boundary" is the stability region, and to the right, the instability region. For the case of higher damping, the onset velocity calculated is far beyond the wind speed range used in the present experiment and therefore, galloping may exist at higher wind speed.

The solution obtained as Eq. (5.15) is based on the assumption that the aerodynamic forces are linear, i.e., both the energy input by the flow and the energy dissipated by damping increase linearly with amplitude. However, the energy input by the flow has a finite limit, because the fluid forces on the structure cannot increase indefinitely with amplitude. A non-linear quasi-steady approach, in which the force coefficient C_y is expressed as a power series, is derived by Novak (18) to cover this point.

It has been established that the quasi-steady theory can be applied to the prediction of the galloping oscillations as long as the wind speed range corresponding to instability is well separated from the region of vortex resonance. For the case of the 1x2 box section, the quasi-steady approach cannot explain all the phenomena observed. The peculiar phenomena of 1x2 box section may be

closely related to the fact that this section exhibits two Strouhal numbers (19). As shown in Fig. 27, after Yamada (19), for aspect ratio between 2 to 3, there exists a transition range where the separated flow from the upstream corners may reattach to the surface of the body and this results in a lower value of C_D and a higher value of the Strouhal number.

From the above discussion, it can be concluded that the Scruton number cannot be used as a single parameter in predicting the onset velocity of the instability of the 1X2 box section.

5.3 BUFFETING

Random response of the model can be calculated by statistical method using spectral analysis, with the appropriate physical and aerodynamic properties of the model in conjunction with functions which satisfy the corresponding flow conditions. Basically, the buffeting response is decided by the aerodynamic forces, the aerodynamic admittance function, the frequency response function of the system, the joint acceptance function, and the power spectral density of gust. A flat plate model was used to investigate the buffeting response induced by homogeneous turbulence which was created

by square-mesh coarse grid located at the upstream of the wind tunnel test section. Theoretical estimate of the response is obtained using the computer. A full description of the analytical procedure is given elsewhere (20). The computer program was constructed based on this procedure (21) but was modified for the present calculation. The program is listed in Appendix E.

In the first part of this experiment, the mass of the model was kept constant at 0.765 kg while the structural damping was increased from 0.10% to 2.31% of critical in two steps. The structural damping was then kept constant at 0.50% and the mass was increased from 0.397 kg to 0.949 kg in two steps. In order to maintain the same frequency ratio, N_T/N_B, masses were added at a distance equivalent to the radius of gyration from the centre of the model.

Figs. 28 and 29 show the RMS vertical response plotted against the reduced wind speed. Generally, the response increases gradually with increasing wind speed for all cases. Figs. 30 and 31 show the effect of structural damping and mass parameter, respectively, on the response of the model at constant reduced wind speed. It can be seen that an increase in either parameter will result in reducing the amplitude and it varies almost linearly with structural damping whereas the change is strongly nonlinear with mass

parameter. Fig. 32 shows the variation of amplitude with both damping and mass in terms of the Scruton number. It is clearly seen that the amplitude depends on both the structural damping and mass parameter which are essentially independent parameters except at high Scruton number and low reduced wind speed. Fig. 32 also shows that the response amplitude is not so much affected by structural damping as by the mass. There is a drastic rise in amplitude when the mass is decreased at relatively low values of damping and high reduced wind speed.

The main parameters which affect the buffeting response are the turbulence intensity, the structural damping, the frequency ratio and the mass parameter. With all the parameters, except the structural damping and mass parameters, at values similar to the present experiment, the theoretical response is obtained from the computer analysis. The amplitude is plotted against the Scruton number in Fig. 33. The response is seen to be similar to the one described previously. The frequency ratio used in the present experiment is approximately 1.0. Since the theoretical analysis gives unstable solution with the frequency ratio of 1, an arbitrary value of 1.5 is used for the sample calculation. The experimental results of the present study are summarized in Table 5.

Chapter VI

CONCLUDING REMARKS

The wind-induced dynamic responses of different models under different mass and damping conditions were studied. The results from the present study can be summarized as follows:

1. For the case of vortex-induced oscillation, in both vertical and torsional motions, an increase in either the mass or the structural damping of the structure will result in a weaker system response. The product of the mass parameter and damping ratio, the Scruton number, can be used as a single dimensionless parameter in predicting the maximum amplitude. However, the maximum amplitude is not necessarily inversely proportional to the Scruton number. A slightly different functional relationship was observed for the case of torsional vortex excitation. More research is needed in this area due to the limited information available presently.

2. An increase in either the mass moment of inertia or the structural damping will result in raising the onset speed of the torsional instability. The Scruton

number in torsion cannot be used as a single parameter for this case. Increase of mass moment of inertia is more effective in raising the onset speed than increasing the structural damping.

3. The galloping response of the 1x2 box section decreases with increasing structural damping. The response is less sensitive to the change of mass parameter. Unlike the torsional instability of the H-section, the velocity at which the amplitude rises rapidly is almost independent of the change of either mass or damping. It was discovered in the course of present study that this particular cross-section has rather peculiar response characteristics which should be considered as a mixture of vortex induced response and galloping instability. There is an indication that this peculiarity may not be seen for other box sections. For the study of mass and damping effects on galloping, other sections such as 1x1 and 1x4 box, or 1x2 box section in slightly turbulent flow should be attempted for further study.

4. The buffeting response of flat plate model in turbulent flow showed that an increase in either mass or damping will reduce the magnitude of response. The response is less sensitive to damping than to the change in mass. The Scruton number cannot be used as

a single parameter in predicting the buffeting response.

REFERENCES

1. Scruton, C., and Frazer, R.A., "A Summarized Account of the Severn Bridge Aerodynamic Investigation", NPL/Aero/222, National Physical Laboratory, Teddington, England, Feb., 1952, pp. 26.

2. Scruton, C., "On the Wind-Excited Oscillations of Stacks, Tower, and Masts", Wind Effects on Buildings and Structures, Proceedings of the Conference, National Physical Laboratory, Teddington, England, Vol. 11, 1963, pp. 798-832.

3. Farquharson, F.B., Smith, F.C., and Vincent, G.S., "Aerodynamic Stability of Suspension Bridges with Special Reference to the Tacoma Narrows Bridge", No. 116, University of Washington Engineering Experiment Station Bulletin, June, 1954, Part V.

4. Den Hartog, J.P., "Mechanical Vibrations," 4th ed., McGraw-Hill, New York, N.Y., 1956.

5. Daugherty, R., and Franzini, J., "Fluid Mechanics with Engineering Applications," 7th ed., McGraw-Hill Book Company, New York, N.Y., 1977, pp. 174-190.

6. Snyder, W., "Similarity Criteria for The Application of Fluid Models to the study of Air Pollution Meteorology," Boundary Layer Meteorology, Vol. 3, 1972.

7. Wardlaw, R.L., "Sectional versus Full Model Wind Tunnel Testing of Bridge Road Decks", presented at 1978 FCP Research Review Conference, U.S. Federal Highway Administration.

8. Townsend, A.A., "The Structure of Turbulent Shear Flow", 2nd ed., Cambridge University Press, Great Britain, 1976, pp. 53-56.

9. Farquharson, F.B., Smith, F.C., and Vincent, G.S., "Aerodynamic Stability of Suspension Bridge with Special Reference to the Tacoma Narrows Bridge", No. 116, University of Washington Engineering Experiment Station Bulletin, 1950, Part 1.

10. Scruton, C. and Wyatt, T.A., "A Brief Survey of the Aerodynamic Stability Problems of Bridges," Bridge Aerodynamics, TTL, London, 1981.

11. Irwin, H.P.A.H., Duffy, K., and Savage, M.G., "Wind Tunnel Investigation of the Palmerston Bridge, Pugwash, Nova Scotia", NAE Report LTR-LA-244, National Research Council of Canada, July 1980.

12. Wardlaw, R.L., Tanaka, H., and Savage, M.G., "Wind Tunnel Investigation of the Mississippi River Bridge Concrete Alternative, Quincy, Illinois," NAE Report LTR-LA-265, National Research Council of Canada, Feb., 1984.

13. Yamaguchi, T., Shiraki, K., and Umemura, S., "Vibration caused by Karman Vortex on Bridge Members and its Countermeasures," Proc. Third International Conference on Wind Effect on Buildings and Structures, Tokyo, 1971, pp. 747-756.

14. Iwan, W.D., "The Vortex Induced Oscillation of Elastic Structural Elements," Journal of Eng. Industry, Vol. 97, 1975, pp. 1378-1382.

15. Farquharson, F.B., Smith, F.C., and Vincent, G.S., "Aerodynamic Stability of Suspension Bridge with Special Reference to the Tacoma Narrows Bridge", No. 116, University of Washington Engineering Experiment Station Bulletin, June, 1952, Part III.

16. Smith, E.W. and Wyatt, T.A., "Development of the Draft Rules for Aerodynamic Stability," Bridge Aerodynamics, TTL, London, 1981.

17. Blevins, R.D., "Flow-Induced Vibration", Van Nostrand Reinhold, New York, N.Y., 1977, pp. 55-87.

18. Novak, M., "Galloping and Vortex Induced Oscillations of Structures," Proceedings of the third International Conference on Wind Effects on Buildings and Structures, Held in Tokyo, Japan, Sept., 1971, Paper IV-16, pp. 11.

19. Yamada, Hitoshi "Identification and Estimation of Vortex-Induced Response of Shallow Bluff Bodies," Ph. D. Thesis, University of Tokyo, Dec., 1983.

20. Tanaka, H. and Davenport, A.G., "Response of Taut Strip Model in Turbulent Wind," Proc. ASCE (108) EMI, 1982

21. Kan, T., "Comparison of 2-Dimensional and 3-Dimensional Testing in Bridge Aerodynamics," M.A. Sc. Thesis, University of Ottawa, 1983.

Appendix A

TABLES

TABLE 1

COMPUTATIONS OF IDEAL SCALES [9]

	FUNCTION	SYMBOL	DIMENSIONS	IDEAL SCALE
1	Length	L, S	L	$L_p/L_m = n$
2	Area	A	L^2	$A_p/A_m = n^2$
3	Volume	V	L^3	$V_p/V_m = n^3$
4	Moment of Inertia (r^2A)	I, J	L^4	$I_p/I_m = n^4$
5	Acceleration ($a=S/t^2$)	a, g	L/T^2	$a_p/a_m = 1$
6	Time ($t= L/a$)	T, t	T	$T_p/T_m = \sqrt{n/1} = \sqrt{n}$
7	Velocity ($V=S/t$)	V, v	L/T	$V_p/V_m = n/\sqrt{n} = \sqrt{n}$
8	Frequency	N	1/T	$N_p/N_m = 1/\sqrt{n}$
9	Density (mass/unit vol.)	ρ	M/L^3	$\rho_p/\rho_m = 1$
10	Mass (ρ x V)	m	M	$m_p/m_m = 1 \times n^3 = n^3$
11	Weight (mg)	W	ML/T^2	$W_p/W_m = n^3 \times 1 = n^3$
12	Force (ma)	F	ML/T^2	$F_p/F_m = n^3 \times 1 = n^3$
13	Bending Moment (F x L)	M	ML^2/T^2	$M_p/M_m = n^3 \times n = n^4$
14	Mass Moment of Inertia (r^2M)	I	L^2M	$I_p/I_m = n^2 \times n^3 = n^5$
15	Unit Strain	ε	—	$\varepsilon_p/\varepsilon_m = n/n = 1$
16	Unit Stress (F/A)	s	M/LT^2	$s_p/s_m = n^3/n^2 = n$
17	Elastic Modulus ($\frac{F/A}{L/L}$)	E, G	M/LT^2	$E_p/E_m = n^3/n^2 = n$
18	Bending Deflection ($\frac{FL^3}{EI}$)	Δ	L	$\Delta_p/\Delta_m = \frac{n^3 \times n^3}{n \times n^4} = n$
19	Direct Stress Distortion ($\frac{FL}{EA}$)	Δ	L	$\Delta_p/\Delta_m = \frac{n^3 \times n}{n \times n^2} = n$
20	Torsional Deflection ($\frac{FL^2}{GJ}$)	θ	—	$\theta_p/\theta_m = \frac{n^3 \times n^2}{n \times n^4} = 1$

TABLE 2

Summary of the results of vertical vortex excitation

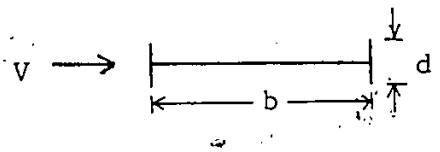

ρ = 1.2 kg/m^3

b = 228.6 mm

d = 45.7 mm

Structural Damping	Mass Parameter	Scruton Number	Peak Amplitude	Reduced Speed at Peak Amplitude
ξ (%)	$m/\rho b^2$	Sc	z/b ($\times 10^{-3}$)	Vr
0.32	7.53	1.51	15.53	2.53
0.40	"	1.89	14.52	2.48
2.20	"	10.41	7.83	2.27
0.65	"	3.08	10.67	2.41
"	12.45	5.08	8.97	2.29
"	19.82	8.10	8.09	2.15
"	26.45	10.80	7.53	2.15

TABLE 3

Summary of the results of torsional vortex excitation

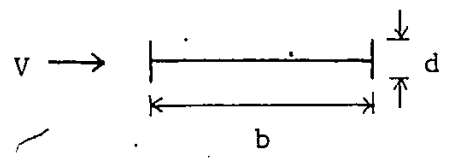

ρ = 1.2 kg/m^3

b = 228.6 mm

d = 45.7 mm

Structural Damping	Mass Parameter	Scruton Number	Peak Amplitude	Reduced Speed at Peak Amplitude
ξ (%)	$I/\rho b^4$	Sc	$(\theta)_{max}$ (deg.)	Vr
0.22	1.60	1.11	0.74	1.29
0.31	"	1.56	0.68	1.26
1.22	"	6.15	0.23	1.16
1.60	"	8.06	0.02	1.12
0.65	"	3.27	0.53	1.22
"	2.09	4.27	0.42	1.16
"	2.57	5.26	0.31	1.15

TABLE 4

Summary of the results of torsional instability

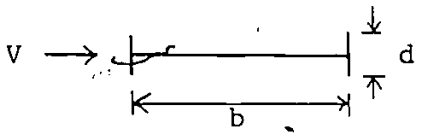

ρ = 1.2 kg/m^3

b = 228.6 mm

d = 45.7 mm

Structural Damping	Mass Parameter	Scruton Number	Critical Speed
ξ (%)	$I/\rho b^4$	Sc	$(Vr)_{cr}$
1.59	1.60	8.01	2.05
3.30	"	16.63	3.76
6.92	"	34.86	5.19
12.73	"	64.14	7.12
3.60	0.91	10.32	1.69
"	3.52	39.81	6.57
"	4.60	52.01	9.42

TABLE 5

Summary of the results of buffeting response

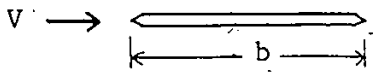

ρ = 1.2 kg/m^3

b = 197.0 mm

$m/\rho b^2$ = 27.52 ξ = 0.50 %

ξ (%)	0.10	0.50	1.54
Sc	0.35	1.73	5.33

$m/\rho b^2$	14.28	27.52	34.07
Sc	0.90	1.73	2.15

Vr	(z/b) x10^{-3}		
1	0.35	0.32	0.17
2	0.72	0.68	0.38
3	1.10	1.02	0.64
4	1.45	1.32	0.96
5	1.66	1.58	1.12
6	1.83	1.74	1.24
7	1.98	1.94	1.37
8	2.19	2.01	1.48
9	2.47	2.14	1.62
10	2.75	2.34	1.84

Vr	(z/b) x10^{-3}		
1	0.41	0.32	0.31
2	0.90	0.68	0.58
3	1.54	1.02	0.84
4	2.10	1.32	1.13
5	2.43	1.58	1.38
6	2.53	1.74	1.57
7	2.64	1.94	1.70
8	2.84	2.01	1.84
9	3.15	2.14	1.96
10	3.50	2.34	2.07

TABLE 6

EXPERIMENTAL RESPONSE OF MODEL NO. 1 IN SMOOTH FLOW

mass per unit length $m = 0.472$ kg/m
structural damping $\xi = 0.32$ %
width of the model $b = 0.229$ m
natural frequency $N_B = 5.7$ Hz

WIND VELOCITY [V]	REDUCED VELOCITY [$V/N_B b$]	FLEXURAL RESPONSE [z/b]
0.00	0.00	0.00
0.86	0.66	0.00022
0.95	0.73	0.00039
1.03	0.79	0.00109
1.31	1.01	0.00066
1.49	1.14	0.00087
1.74	1.34	0.00122
1.92	1.47	0.00197
2.10	1.61	0.00267
2.25	1.73	0.00503
2.43	1.86	0.00731
2.57	1.97	0.00936
2.68	2.06	0.01076
2.92	2.24	0.01304
3.07	2.35	0.01430
3.21	2.46	0.01518
3.30	2.53	0.01553
3.33	2.56	0.01549
3.45	2.66	0.01457
3.64	2.79	0.00595
3.72	2.85	0.00608
3.86	2.96	0.00608

TABLE 7

EXPERIMENTAL RESPONSE OF MODEL NO. 1 IN SMOOTH FLOW

mass per unit length $m = 0.472$ kg/m
structural damping $\xi = 0.40$ %
width of the model $b = 0.229$ m
natural frequency $N_B = 6.0$ Hz

WIND VELOCITY [V]	REDUCED VELOCITY $[V/N_B b]$	FLEXURAL RESPONSE [z/b]
0.00	0.00	0.00
1.03	0.75	0.00022
1.49	1.08	0.00057
1.64	1.20	0.00079
2.02	1.47	0.00083
2.18	1.59	0.00101
2.31	1.68	0.00114
2.38	1.73	0.00455
2.53	1.84	0.00639
2.65	1.93	0.00783
2.86	2.08	0.01063
2.96	2.16	0.01150
3.00	2.19	0.01207
3.15	2.29	0.01330
3.26	2.38	0.01409
3.40	2.48	0.01452
3.54	2.58	0.01321
3.58	2.61	0.01050

TABLE 8

EXPERIMENTAL RESPONSE OF MODEL NO. 1 IN SMOOTH FLOW

mass per unit length $m = 0.472$ kg/m
structural damping $\xi = 2.20$ %
width of the model $b = 0.229$ m
natural frequency $N_B = 5.0$ Hz

WIND VELOCITY [V]	REDUCED VELOCITY [$V/N_B b$]	FLEXURAL RESPONSE [z/b]
0.00	0.00	0.00
0.70	0.61	0.00022
1.34	1.17	0.00026
1.72	1.50	0.00039
1.85	1.62	0.00048
1.94	1.70	0.00149
2.10	1.84	0.00490
2.43	2.12	0.00770
2.49	2.18	0.00770
2.59	2.27	0.00783
2.68	2.35	0.00608
2.86	2.50	0.00232
3.03	2.65	0.00149
3.26	2.85	0.00127

TABLE 9

EXPERIMENTAL RESPONSE OF MODEL NO. 1 IN SMOOTH FLOW

mass per unit length $m = 0.472$ kg/m
structural damping $\xi = 0.65$ %
width of the model $b = 0.229$ m
natural frequency $N_B = 6.67$ Hz

WIND VELOCITY [V]	REDUCED VELOCITY $[V/N_B b]$	FLEXURAL RESPONSE [z/b]
0.00	0.00	0.00
0.90	0.59	0.00022
1.34	0.88	0.00070
1.46	0.96	0.00070
1.69	1.11	0.00096
1.92	1.26	0.00114
2.21	1.45	0.00149
2.41	1.58	0.00219
2.57	1.69	0.00416
2.76	1.81	0.00595
2.89	1.89	0.00700
3.18	2.09	0.00927
3.44	2.26	0.01019
3.47	2.27	0.01028
3.64	2.39	0.01054
3.67	2.41	0.01067
3.78	2.48	0.01045
3.88	2.54	0.01024
4.04	2.65	0.00761
4.20	2.76	0.00433
4.27	2.80	0.00385
4.39	2.88	0.00367
4.48	2.94	0.00372

TABLE 10

EXPERIMENTAL RESPONSE OF MODEL NO. 1 IN SMOOTH FLOW

mass per unit length $m = 0.781$ kg/m
structural damping $\xi = 0.65$ %
width of the model $b = 0.229$ m
natural frequency $N_B = 5.4$ Hz

WIND VELOCITY [V]	REDUCED VELOCITY $[V/N_B b]$	FLEXURAL RESPONSE [z/b]
0.00	0.00	0.00
0.70	0.57	0.00013
1.07	0.87	0.00026
1.54	1.25	0.00044
1.64	1.33	0.00096
1.92	1.55	0.00149
1.98	1.60	0.00157
2.08	1.69	0.00179
2.12	1.72	0.00258
2.18	1.76	0.00363
2.31	1.87	0.00529
2.44	1.98	0.00704
2.51	2.03	0.00770
2.67	2.16	0.00871
2.77	2.25	0.00884
2.83	2.29	0.00897
2.89	2.34	0.00884
3.00	2.43	0.00770
3.08	2.49	0.00271

TABLE 11

EXPERIMENTAL RESPONSE OF MODEL NO. 1 IN SMOOTH FLOW

mass per unit length $m = 1.243$ kg/m
structural damping $\xi = 0.65$ %
width of the model $b = 0.229$ m
natural frequency $N_B = 4.4$ Hz

WIND VELOCITY [V]	REDUCED VELOCITY [$V/N_B b$]	FLEXURAL RESPONSE [z/b]
0.00	0.00	0.00
0.81	0.80	0.00009
1.14	1.14	0.00017
1.28	1.27	0.00031
1.43	1.42	0.00044
1.59	1.58	0.00057
1.67	1.66	0.00070
1.76	1.75	0.00411
1.96	1.95	0.00608
2.04	2.03	0.00752
2.12	2.11	0.00783
2.16	2.15	0.00809
2.25	2.24	0.00787
2.31	2.29	0.00770
2.34	2.33	0.00315

TABLE 12

EXPERIMENTAL RESPONSE OF MODEL NO. 1 IN SMOOTH FLOW

mass per unit length $m = 1.659$ kg/m
structural damping $\xi = 0.65$ %
width of the model $b = 0.229$ m
natural frequency $N_B = 3.4$ Hz

WIND VELOCITY [V]	REDUCED VELOCITY $[V/N_B b]$	FLEXURAL RESPONSE [z/b]
0.00	0.00	0.00
0.76	0.97	0.00013
1.03	1.33	0.00026
1.14	1.47	0.00052
1.28	1.65	0.00105
1.34	1.73	0.00206
1.43	1.84	0.00503
1.49	1.91	0.00599
1.57	2.01	0.00713
1.67	2.15	0.00735
1.72	2.21	0.00669
1.79	2.30	0.00074

TABLE 13

EXPERIMENTAL RESPONSE OF MODEL NO. 1 IN SMOOTH FLOW

mass moment of inertia per unit length	$I = 5.255 \times 10^{-3}$	kg m^2/m
structural damping	$\xi = 0.22$	%
width of the model	$b = 0.229$	m
natural frequency	$N_T = 8.30$	Hz

WIND VELOCITY [V]	REDUCED VELOCITY [$V/N_T b$]	TORSIONAL RESPONSE [θ]
0.00	0.00	0.00
0.64	0.34	0.00
1.03	0.54	0.005
1.21	0.64	0.014
1.34	0.71	0.017
1.54	0.81	0.019
1.62	0.85	0.019
1.72	0.90	0.023
1.90	1.00	0.230
1.96	1.03	0.312
2.08	1.10	0.481
2.27	1.20	0.628
2.36	1.24	0.736
2.44	1.29	0.725
2.60	1.37	0.628
2.70	1.42	0.148

TABLE 14

EXPERIMENTAL RESPONSE OF MODEL NO. 1 IN SMOOTH FLOW

mass moment of inertia per unit length	$I = 5.255 \times 10^{-3}$	kg m^2/m
structural damping	$\xi = 0.31$	%
width of the model	$b = 0.229$	m
natural frequency	$N_T = 8.25$	Hz

WIND VELOCITY [V]	REDUCED VELOCITY $[V/N_T b]$	TORSIONAL RESPONSE [θ]
0.00	0.00	0.00
0.50	0.26	0.003
0.76	0.40	0.005
0.90	0.48	0.007
1.03	0.55	0.007
1.11	0.59	0.008
1.37	0.73	0.012
1.49	0.79	0.014
1.59	0.84	0.015
1.69	0.90	0.016
1.79	0.95	0.032
1.92	1.02	0.199
2.04	1.08	0.363
2.10	1.11	0.470
2.12	1.12	0.510
2.31	1.22	0.672
2.38	1.26	0.677
2.49	1.32	0.498
2.60	1.38	0.209
2.68	1.42	0.104

TABLE 15

EXPERIMENTAL RESPONSE OF MODEL NO. 1 IN SMOOTH FLOW

mass moment of inertia per unit length	$I = 5.255 \times 10^{-3}$	kg m^2/m
structural damping	$\xi = 1.22$	%
width of the model	$b = 0.229$	m
natural frequency	$N_T = 8.33$	Hz

WIND VELOCITY [V]	REDUCED VELOCITY $[V/N_T b]$	TORSIONAL RESPONSE [θ]
0.00	0.00	0.00
0.81	0.42	0.002
1.14	0.60	0.004
1.28	0.67	0.005
1.49	0.78	0.005
1.69	0.89	0.010
1.87	0.98	0.016
1.92	1.01	0.022
2.08	1.09	0.149
2.12	1.11	0.185
2.21	1.16	0.228
2.25	1.18	0.206
2.38	1.25	0.100
2.56	1.34	0.056

TABLE 16

EXPERIMENTAL RESPONSE OF MODEL NO. 1 IN SMOOTH FLOW

mass moment of inertia per unit length	$I = 5.255 \times 10^{-3}$	kg m^2/m
structural damping	$\xi = 1.60$	%
width of the model	$b = 0.229$	m
natural frequency	$N_T = 8.20$	Hz

WIND VELOCITY [V]	REDUCED VELOCITY [$V/N_T b$]	TORSIONAL RESPONSE [θ]
0.00	0.00	0.00
1.18	0.63	0.002
1.28	0.68	0.004
1.54	0.82	0.007
1.79	0.95	0.010
1.94	1.03	0.014
2.00	1.07	0.015
2.21	1.18	0.018
2.38	1.27	0.022
2.51	1.34	0.025
2.64	1.41	0.025

TABLE 17

EXPERIMENTAL RESPONSE OF MODEL NO. 1 IN SMOOTH FLOW

mass moment of inertia per unit length	$I = 5.255 \times 10^{-3}$	kg m^2/m
structural damping	$\xi = 0.65$	%
width of the model	$b = 0.229$	m
natural frequency	$N_T = 8.50$	Hz

WIND VELOCITY [V]	REDUCED VELOCITY [$V/N_T b$]	TORSIONAL RESPONSE [θ]
0.00	0.00	0.00
0.50	0.25	0.004
0.70	0.36	0.005
0.81	0.42	0.005
1.03	0.53	0.008
1.18	0.61	0.009
1.37	0.71	0.013
1.49	0.76	0.016
1.64	0.85	0.018
1.79	0.92	0.023
1.87	0.96	0.031
1.92	0.99	0.037
1.98	1.02	0.133
2.08	1.07	0.328
2.29	1.18	0.519
2.38	1.22	0.530
2.44	1.26	0.476
2.60	1.34	0.242
2.83	1.46	0.063

TABLE 18

EXPERIMENTAL RESPONSE OF MODEL NO. 1 IN SMOOTH FLOW

mass moment of inertia per unit length	$I = 6.847 \times 10^{-3}$	kg m^2/m
structural damping	$\xi = 0.65$	%
width of the model	$b = 0.229$	m
natural frequency	$N_T = 7.50$	Hz

WIND VELOCITY [V]	REDUCED VELOCITY $[V/N_T b]$	TORSIONAL RESPONSE $[\theta]$
0.00	0.00	0.00
0.57	0.33	0.008
0.99	0.58	0.013
1.11	0.65	0.015
1.21	0.71	0.018
1.51	0.88	0.025
1.57	0.91	0.028
1.69	0.99	0.199
1.76	1.03	0.288
1.85	1.08	0.390
1.94	1.13	0.403
1.96	1.14	0.405
1.98	1.16	0.418
2.06	1.20	0.411
2.10	1.23	0.382
2.16	1.26	0.333
2.32	1.35	0.197
2.46	1.43	0.059

TABLE 19

EXPERIMENTAL RESPONSE OF MODEL NO. 1 IN SMOOTH FLOW

mass moment of inertia per unit length	$I = 8.437 \times 10^{-3}$	kg m^2/m
structural damping	$\xi = 0.65$	%
width of the model	$b = 0.229$	m
natural frequency	$N_T = 7.90$	Hz

WIND VELOCITY [V]	REDUCED VELOCITY [$V/N_T b$]	TORSIONAL RESPONSE [θ]
0.00	0.00	0.00
0.86	0.47	0.005
1.14	0.63	0.009
1.49	0.82	0.012
1.59	0.88	0.014
1.64	0.91	0.016
1.72	0.95	0.019
1:87	1.04	0.189
1.92	1.06	0.225
2.08	1.15	0.308
2.14	1.18	0.279
2.34	1.30	0.204
2.39	1.32	0.181
2.57	1.42	0.041

TABLE 20

EXPERIMENTAL RESPONSE OF MODEL NO. 1 IN SMOOTH FLOW

mass moment of inertia per unit length	$I = 5.255 \times 10^{-3}$	kg m^2/m
structural damping	$\xi = 1.59$	%
width of the model	$b = 0.229$	m
natural frequency	$N_T = 4.40$	Hz

WIND VELOCITY [V]	REDUCED VELOCITY [$V/N_T b$]	TORSIONAL RESPONSE [θ]
0.00	0.00	0.00
0.90	0.90	0.013
1.11	1.10	0.104
1.28	1.27	0.142
1.34	1.33	0.063
1.51	1.50	0.053
1.59	1.58	0.043
1.76	1.75	0.046
1.98	1.97	0.067
2.06	2.05	0.097
2.23	2.22	0.519
2.41	2.40	1.280
2.67	2.65	2.086
2.86	2.84	2.640
3.13	3.11	3.672

TABLE 21

EXPERIMENTAL RESPONSE OF MODEL NO. 1 IN SMOOTH FLOW

mass moment of inertia per unit length	$I = 5.255 \times 10^{-3}$	kg m^2/m
structural damping	$\xi = 3.30$	%
width of the model	$b = 0.229$	m
natural frequency	$N_T = 3.75$	Hz

WIND VELOCITY [V]	REDUCED VELOCITY [$V/N_T b$]	TORSIONAL RESPONSE [θ]
0.00	0.00	0.00
0.81	0.94	0.013
1.18	1.38	0.031
1.46	1.70	0.035
1.54	1.80	0.039
1.69	1.97	0.045
1.85	2.16	0.151
2.02	2.36	0.260
2.34	2.73	0.264
2.51	2.93	0.264
2.68	3.13	0.236
2.93	3.42	0.228
2.99	3.48	0.208
3.22	3.76	0.228
3.28	3.83	0.787
3.41	3.97	5.222
3.53	4.11	5.938

TABLE 22

EXPERIMENTAL RESPONSE OF MODEL NO. 1 IN SMOOTH FLOW

mass moment of inertia per unit length	$I = 5.255 \times 10^{-3}$	kg m^2/m
structural damping	$\xi = 6.92$	%
width of the model	$b = 0.229$	m
natural frequency	$N_T = 2.80$	Hz

WIND VELOCITY [V]	REDUCED VELOCITY [$V/N_T b$]	TORSIONAL RESPONSE [θ]
0.00	0.00	0.00
1.43	2.23	0.051
1.92	3.00	0.045
2.21	3.46	0.045
2.57	4.02	0.045
2.83	4.42	0.045
3.17	4.95	0.067
3.26	5.09	0.081
3.44	5.38	0.500
3.50	5.47	0.858
3.62	5.65	1.365
3.99	6.24	2.813

TABLE 23

EXPERIMENTAL RESPONSE OF MODEL NO. 1 IN SMOOTH FLOW

mass moment of inertia per unit length	$I = 5.255 \times 10^{-3}$	kg m^2/m
structural damping	$\xi = 12.73$	%
width of the model	$b = 0.229$	m
natural frequency	$N_T = 2.81$	Hz

WIND VELOCITY [V]	REDUCED VELOCITY $[V/N_T b]$	TORSIONAL RESPONSE $\circ[\theta]$
0.00	0.00	0.00
1.34	2.09	0.040
1.87	2.92	0.034
2.48	3.85	0.040
2.80	4.36	0.046
3.40	5.29	0.080
3.59	5.59	0.197
3.75	5.84	0.206
3.95	6.15	0.300
4.00	6.23	0.389
4.05	6.31	0.291
4.23	6.59	0.375
4.41	6.87	0.403
4.57	7.12	*

TABLE 24

EXPERIMENTAL RESPONSE OF MODEL NO. 1 IN SMOOTH FLOW

mass moment of inertia per unit length	$I = 2.990 \times 10^{-3}$	kg m^2/m
structural damping	$\xi = 3.60$	%
width of the model	$b = 0.229$	m
natural frequency	$N_T = 5.30$	Hz

WIND VELOCITY [V]	REDUCED VELOCITY [$V/N_T b$]	TORSIONAL RESPONSE [θ]
0.00	0.00	0.00
0.99	0.82	0.00
1.31	1.08	0.031
1.54	1.27	0.056
1.92	1.58	0.130
2.00	1.65	0.139
2.04	1.69	0.155
2.20	1.81	0.525
2.27	1.87	1.500
2.48	2.04	2.135
2.84	2.35	3.337

TABLE 25

EXPERIMENTAL RESPONSE OF MODEL NO. 1 IN SMOOTH FLOW

mass moment of inertia per unit length	$I = 11.536 \times 10^{-3}$	kg m^2/m
structural damping	$\xi = 3.60$	%
width of the model	$b = 0.229$	m
natural frequency	$N_T = 3.00$	Hz

WIND VELOCITY [V]	REDUCED VELOCITY [$V/N_T b$]	TORSIONAL RESPONSE [θ]
0.00	0.00	0.00
0.86	1.25	0.022
1.25	1.82	0.033
1.54	2.25	0.069
2.04	2.98	0.085
2.46	3.59	0.099
2.68	3.91	0.114
2.86	4.17	0.103
3.00	4.37	0.106
3.31	4.83	0.141
3.58	5.22	0.153
3.64	5.31	0.160
3.71	5.40	0.186
3.84	5.59	0.141
3.94	5.75	0.139
4.20	6.13	0.157
4.23	6.17	0.159
4.37	6.38	0.183
4.41	6.43	0.197
4.50	6.57	0.255
4.69	6.84	0.474
4.75	6.93	0.629
4.86	7.09	*

TABLE 26

EXPERIMENTAL RESPONSE OF MODEL NO. 1 IN SMOOTH FLOW

mass moment of inertia per unit length	$I = 15.070 \times 10^{-3}$	kg m^2/m
structural damping	$\xi = 3.60$	%
width of the model	$b = 0.229$	m
natural frequency	$N_T = 2.00$	Hz

WIND VELOCITY [V]	REDUCED VELOCITY [$V/N_T b$]	TORSIONAL RESPONSE [θ]
0.00	0.00	0.00
0.81	1.77	0.023
1.11	2.42	0.036
1.54	3.37	0.047
1.85	4.05	0.085
2.10	4.60	0.100
2.56	5.59	0.103
2.82	6.16	0.111
3.16	6.91	0.131
3.44	7.53	0.150
3.73	8.15	0.183
3.94	8.62	0.204
4.26	9.32	0.208
4.34	9.48	0.259
4.46	9.75	0.283
4.67	10.22	0.453
4.89	10.70	1.212
4.99	10.92	*

TABLE 27

EXPERIMENTAL RESPONSE OF MODEL NO. 2 IN SMOOTH FLOW

mass per unit length $m = 0.538$ kg/m
structural damping $\xi =$ [illegible] %
width of the model $b =$ [illegible] m
natural frequency $N_B = 5.45$ Hz

WIND VELOCITY [V]	REDUCED VELOCITY $[V/N_B b]$	FLEXURAL RESPONSE [z/b]
0.00	0.00	0.00
0.90	1.82	0.00088
1.46	2.94	0.00033
1.87	3.78	0.00143
2.02	4.08	0.00176
2.20	4.43	0.00209
2.36	4.75	0.00253
2.54	5.12	0.00363
2.60	5.25	0.00484
2.68	5.41	0.00714
2.96	5.96	0.01560
3.16	6.37	0.02209
3.44	6.94	0.03571
3.78	7.63	0.04956
4.03	8.13	0.05736
4.65	9.38	0.06648
5.23	10.54	0.06648
5.53	11.15	0.06747
6.13	12.35	0.06923
6.82	13.75	0.07264

TABLE 28

EXPERIMENTAL RESPONSE OF MODEL NO. 2 IN SMOOTH FLOW

mass per unit length $m = 0.538$ kg/m
structural damping $\xi = 0.95$ %
width of the model $b = 0.091$ m
natural frequency $N_B = 6.00$ Hz

WIND VELOCITY [V]	REDUCED VELOCITY [$V/N_B b$]	FLEXURAL RESPONSE [z/b]
0.00	0.00	0.00
1.11	2.03	0.00044
1.67	3.05	0.00121
2.10	3.85	0.00176
2.48	4.54	0.00253
2.87	5.26	0.00396
3.11	5.69	0.00736
3.47	6.35	0.01440
3.67	6.73	0.01670
3.89	7.12	0.02055
4.10	7.52	0.02319
4.35	7.98	0.02560
4.63	8.48	0.02659
4.85	8.89	0.02659
5.16	9.45	0.02571
6.10	11.17	0.02220
6.63	12.15	0.02253
7.29	13.35	0.02286

TABLE 29

EXPERIMENTAL RESPONSE OF MODEL NO. 2 IN SMOOTH FLOW

mass per unit length $m = 0.538$ kg/m
structural damping $\xi = 2.07$ %
width of the model $b = 0.091$ m
natural frequency $N_B = 5.42$ Hz

WIND VELOCITY [V]	REDUCED VELOCITY $[V/N_B b]$	FLEXURAL RESPONSE [z/b]
0.00	0.00	0.00
0.95	1.92	0.00055
1.40	2.84	0.00088
1.76	3.57	0.00132
2.00	4.06	0.00176
2.29	4.64	0.00220
2.53	5.12	0.00297
2.60	5.28	0.00352
2.84	5.77	0.00549
3.13	6.35	0.01088
3.23	6.56	0.01242
3.33	6.76	0.01363
3.45	7.00	0.01286
3.63	7.36	0.01231
3.90	7.91	0.00615
4.07	8.26	0.00637
4.33	8.77	0.00736
4.99	10.11	0.00736
5.99	12.15	0.00989
6.73	13.64	0.01055

TABLE 30

EXPERIMENTAL RESPONSE OF MODEL NO. 2 IN SMOOTH FLOW

mass per unit length $m = 1.570$ kg/m
structural damping $\xi = 0.57$ %
width of the model $b = 0.091$ m
natural frequency $N_B = 3.75$ Hz

WIND VELOCITY [V]	REDUCED VELOCITY $[V/N_B b]$	FLEXURAL RESPONSE [z/b]
0.00	0.00	0.00
1.43	4.19	0.00110
1.59	4.67	0.00143
1.90	5.56	0.00231
2.04	5.98	0.00286
2.32	6.81	0.00396
2.43	7.11	0.00484
2.65	7.77	0.00780
2.77	8.12	0.01099
2.90	8.50	0.01440
3.25	9.52	0.04725
3.36	9.84	0.05747
3.66	10.73	0.07538

TABLE 31

EXPERIMENTAL RESPONSE OF MODEL NO. 2 IN SMOOTH FLOW

mass per unit length	$m = 1.570$	kg/m
structural damping	$\xi = 0.72$	%
width of the model	$b = 0.091$	m
natural frequency	$N_B = 3.64$	Hz

WIND VELOCITY [V]	REDUCED VELOCITY [$V/N_B b$]	FLEXURAL RESPONSE [z/b]
0.00	0.00	0.00
0.81	2.44	0.00
0.99	2.99	0.00047
1.37	4.14	0.00065
1.62	4.88	0.00132
1.90	5.73	0.00236
2.20	6.63	0.00372
2.31	6.96	0.00449
2.54	7.67	0.00449
2.64	7.96	0.00411
2.83	8.55	0.00486
3.03	9.14	0.00411
3.32	10.03	0.00411
3.58	10.82	0.00523

TABLE 32

EXPERIMENTAL RESPONSE OF MODEL NO. 2 IN SMOOTH FLOW

mass per unit length $m = 1.570$ kg/m
structural damping $\xi = 1.18$ %
width of the model $b = 0.091$ m
natural frequency $N_B = 3.89$ Hz

WIND VELOCITY [V]	REDUCED VELOCITY [$V/N_B b$]	FLEXURAL RESPONSE [z/b]
0.00	0.00	0.00
1.03	2.91	0.00033
1.43	4.04	0.00132
1.83	5.17	0.00231
2.00	5.65	0.00253
2.20	6.20	0.00330
2.36	6.66	0.00407
2.57	7.27	0.00462
2.82	7.95	0.00418
2.97	8.39	0.00451
3.15	8.88	0.00462
3.33	9.42	0.00462
3.58	10.12	0.00484
3.88	10.96	0.00560
4.20	11.87	0.00516
4.50	12.72	0.00549
4.78	13.49	0.00593
5.47	15.45	0.00648

TABLE 33

EXPERIMENTAL RESPONSE OF MODEL NO. 2 IN SMOOTH FLOW

mass per unit length $m = 1.570$ kg/m
structural damping $\xi = 1.59$ %
width of the model $b = 0.091$ m
natural frequency $N_B = 3.89$ Hz

WIND VELOCITY [V]	REDUCED VELOCITY $[V/N_B b]$	FLEXURAL RESPONSE [z/b]
0.00	0.00	0.00
0.99	2.80	0.00
1.34	3.79	0.00044
1.46	4.12	0.00077
1.76	4.98	0.00165
1.87	5.30	0.00198
2.04	5.77	0.00264
2.25	6.36	0.00286
2.49	7.04	0.00374
2.64	7.45	0.00374
2.76	7.79	0.00363
3.12	8.81	0.00385
3.27	9.24	0.00396
3.51	9.93	0.00418
3.87	10.93	0.00473
4.07	11.51	0.00473
4.39	12.41	0.00484
4.81	13.59	0.00516

TABLE 34

EXPERIMENTAL RESPONSE OF MODEL NO. 3 IN COARSE GRID TURBULENT FLOW

mass per unit length $m = 3.883$ kg/m
structural damping $\xi = 0.10$ %
width of the model $b = 0.197$ m
natural frequency $N_B = 3.75$ Hz

WIND VELOCITY [V]	REDUCED VELOCITY [$V/N_B b$]	FLEXURAL RESPONSE [z/b]
0.00	0.00	0.00
0.81	1.09	0.00038
1.67	2.26	0.00083
2.21	3.00	0.00110
2.97	4.02	0.00146
3.73	5.05	0.00164
4.45	6.02	0.00184
5.29	7.16	0.00201
6.19	8.37	0.00244
6.75	9.14	0.00252
7.39	10.00	0.00275

TABLE 35

EXPERIMENTAL RESPONSE OF MODEL NO. 3 IN COARSE GRID TURBULENT FLOW

mass per unit length $m = 3.883$ kg/m
structural damping $\xi = 1.54$ %
width of the model $b = 0.197$ m
natural frequency $N_B = 3.67$ Hz

WIND VELOCITY [V]	REDUCED VELOCITY [$V/N_B b$]	FLEXURAL RESPONSE [z/b]
0.00	0.00	0.00
1.07	1.48	0.00027
1.67	2.31	0.00045
2.36	3.26	0.00069
3.13	4.33	0.00103
3.75	5.19	0.00109
4.48	6.20	0.00124
5.10	7.05	0.00137
5.75	7.95	0.00148
6.35	8.79	0.00157
7.28	10.07	0.00187
8.06	11.14	0.00207

TABLE 36

EXPERIMENTAL RESPONSE OF MODEL NO. 3 IN COARSE GRID TURBULENT FLOW

mass per unit length $m = 2.015$ kg/m
structural damping $\xi = 0.50$ %
width of the model $b = 0.197$ m
natural frequency $N_B = 4.90$ Hz

WIND VELOCITY [V]	REDUCED VELOCITY $[V/N_B b]$	FLEXURAL RESPONSE [z/b]
0.00	0.00	0.00
1.21	1.26	0.00045
2.14	2.22	0.00102
2.71	2.81	0.00144
3.55	3.68	0.00188
4.22	4.37	0.00229
5.19	5.38	0.00247
5.82	6.03	0.00254
6.44	6.68	0.00262
7.08	7.34	0.00269
7.60	7.87	0.00279
8.14	8.43	0.00296
8.58	8.89	0.00313
9.40	9.73	0.00342

TABLE 37

EXPERIMENTAL RESPONSE OF MODEL NO. 3 IN COARSE GRID TURBULENT FLOW

mass per unit length $m = 3.883$ kg/m
structural damping $\xi = 0.50$ %
width of the model $b = 0.197$ m
natural frequency $N_B = 3.86$ Hz

WIND VELOCITY [V]	REDUCED VELOCITY [$V/N_B b$]	FLEXURAL RESPONSE [z/b]
0.00	0.00	0.00
1.21	1.60	0.00046
2.06	2.71	0.00094
2.65	3.49	0.00124
3.45	4.54	0.00143
4.14	5.45	0.00169
4.65	6.11	0.00186
5.27	6.93	0.00186
5.66	7.44	0.00196
6.20	8.15	0.00201
6.94	9.13	0.00217
7.62	10.02	0.00235
8.14	10.70	0.00247

TABLE 38

EXPERIMENTAL RESPONSE OF MODEL NO. 3 IN COARSE GRID TURBULENT FLOW

mass per unit length $m = 4.817$ kg/m
structural damping $\xi = 0.50$ %
width of the model $b = 0.197$ m
natural frequency $N_B = 3.53$ Hz

WIND VELOCITY [V]	REDUCED VELOCITY [$V/N_B b$]	FLEXURAL RESPONSE [z/b]
0.00	0.00	0.00
0.90	1.30	0.00038
1.90	2.73	0.00076
2.59	3.72	0.00112
3.31	4.76	0.00129
4.24	6.10	0.00159
5.00	7.19	0.00172
5.60	8.06	0.00184
6.25	8.99	0.00196
6.81	9.80	0.00205
7.50	10.78	0.00215
8.28	11.90	0.00244

Appendix B

FIGURES

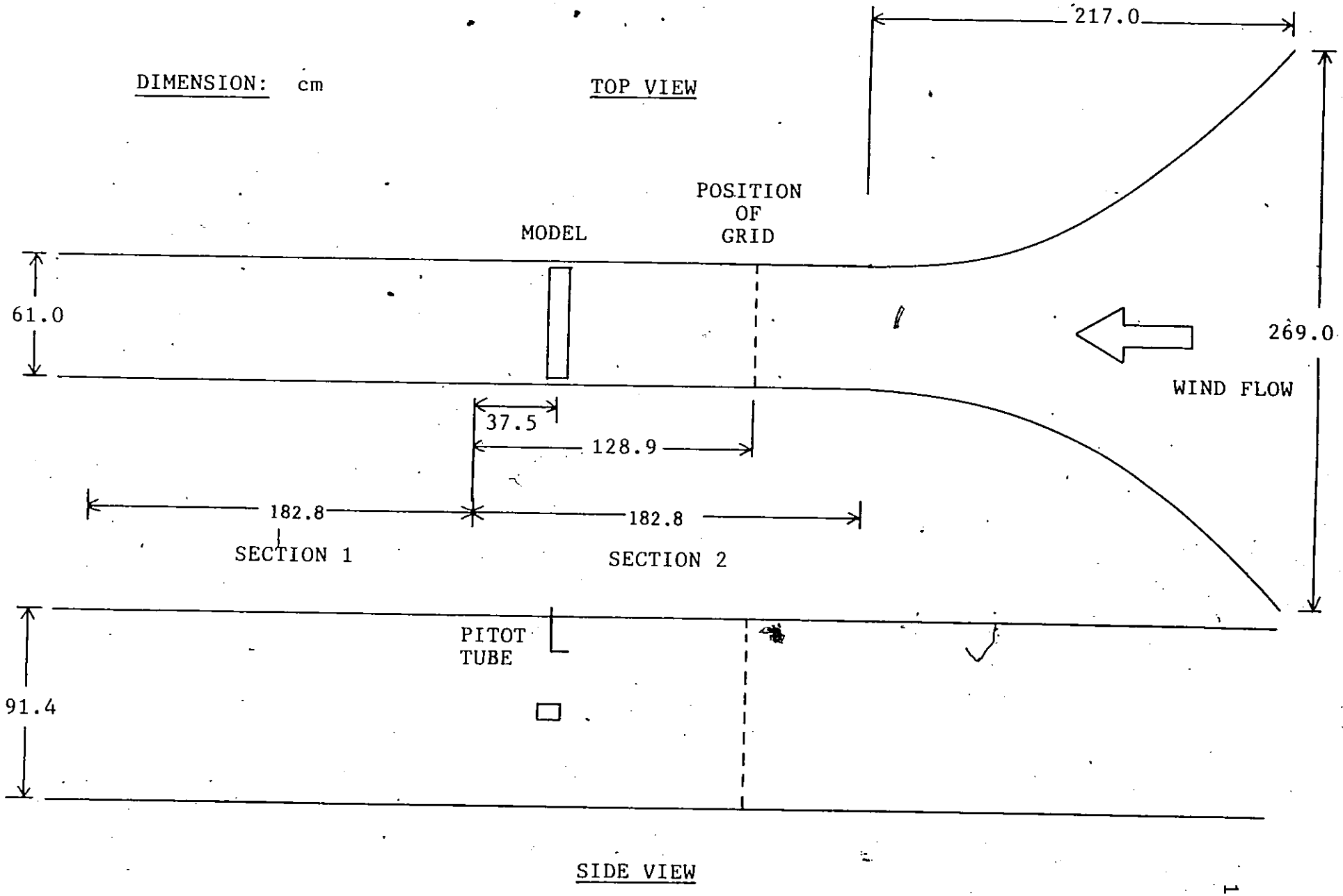

FIG. 1 GENERAL LAYOUT OF THE WIND TUNNEL

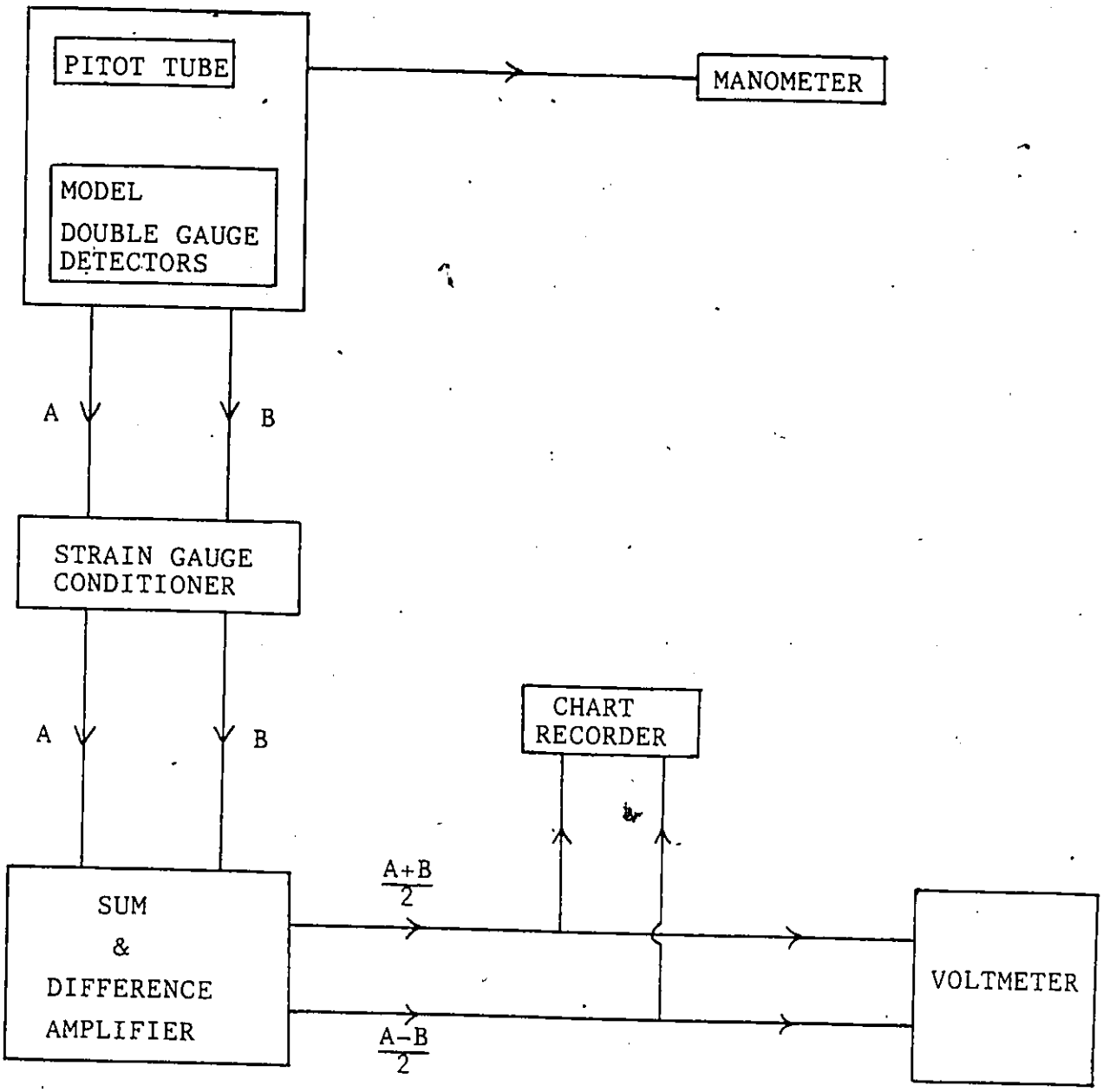

FIG. 2 FLOW CHART OF DOUBLE GAUGE MEASURING SYSTEM

MODEL NO. 1
(H-SECTION)

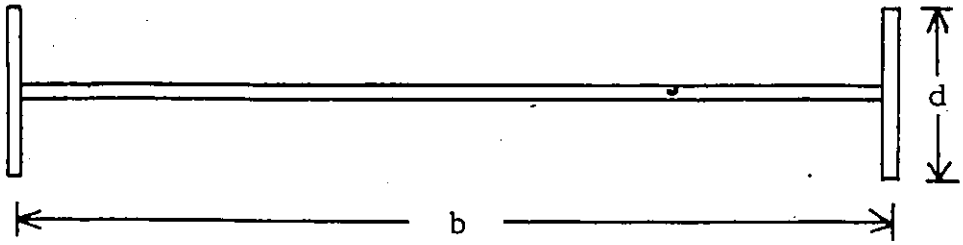

b = 228.60 mm
d = 45.72 mm

MODEL NO. 2
(1x2 BOX SECTION)

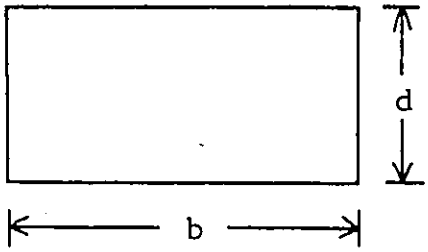

b = 91.44 mm
d = 45.72 mm

MODEL NO. 3
(FLAT PLATE)

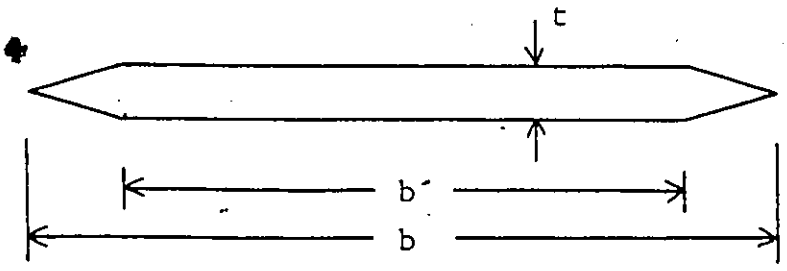

b = 197.00 mm
b' = 150.00 mm
t = 12.70 mm

FIG. 3 MODEL CONFIGURATION

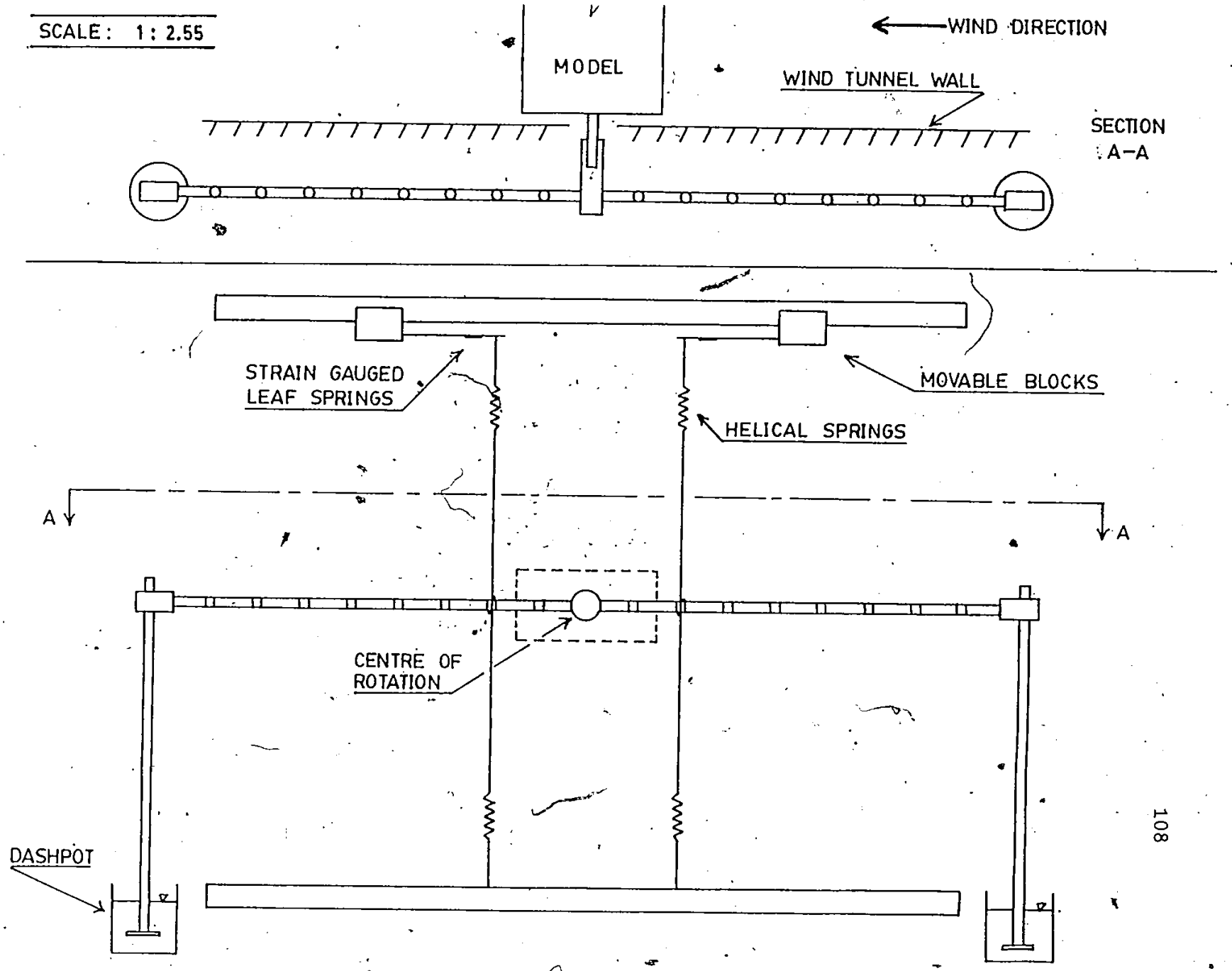

FIG. 4 MODEL SUSPENSION SYSTEM

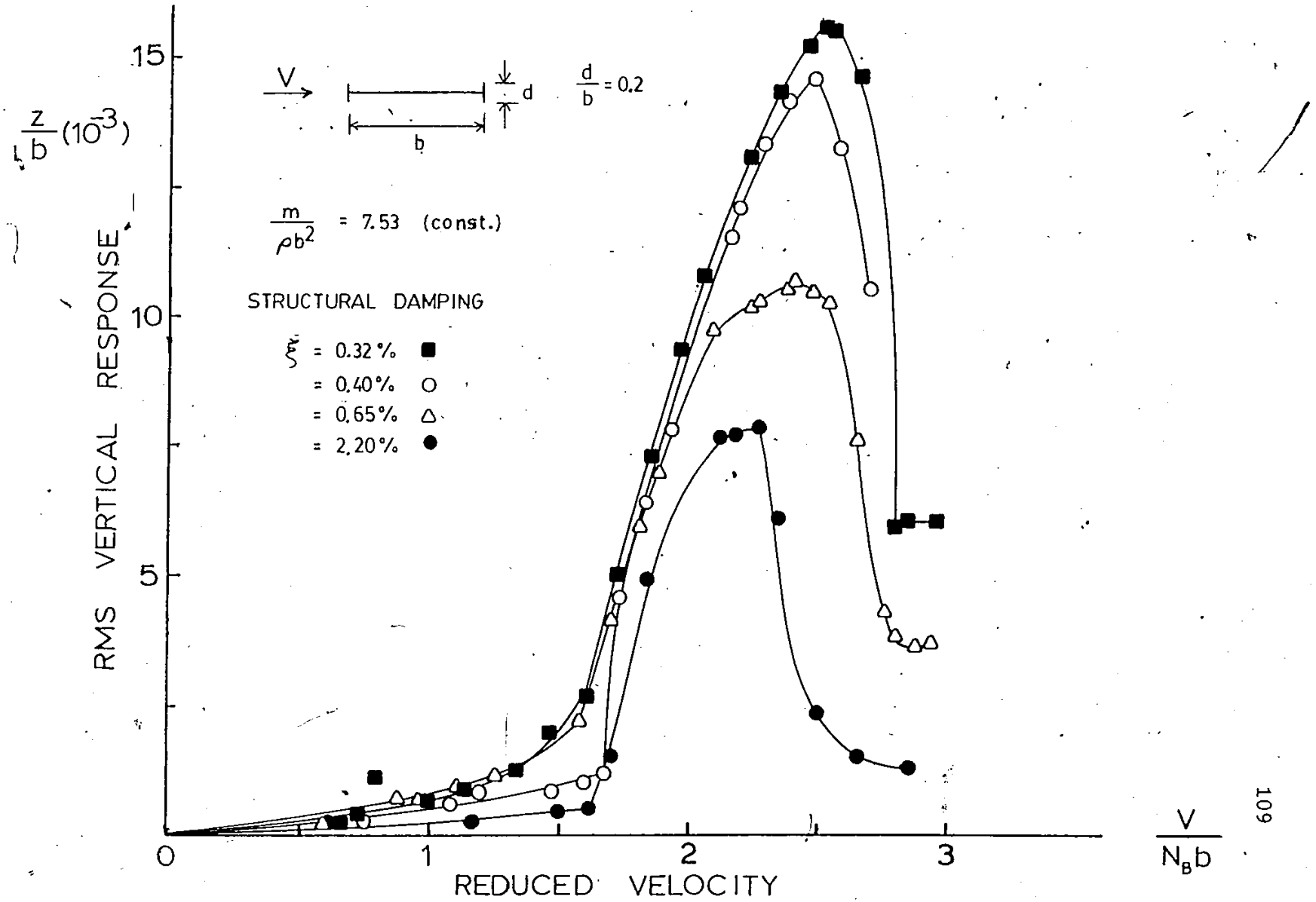

FIG. 5 VORTEX INDUCED VERTICAL RESPONSE WITH VARIABLE STRUCTURAL DAMPING

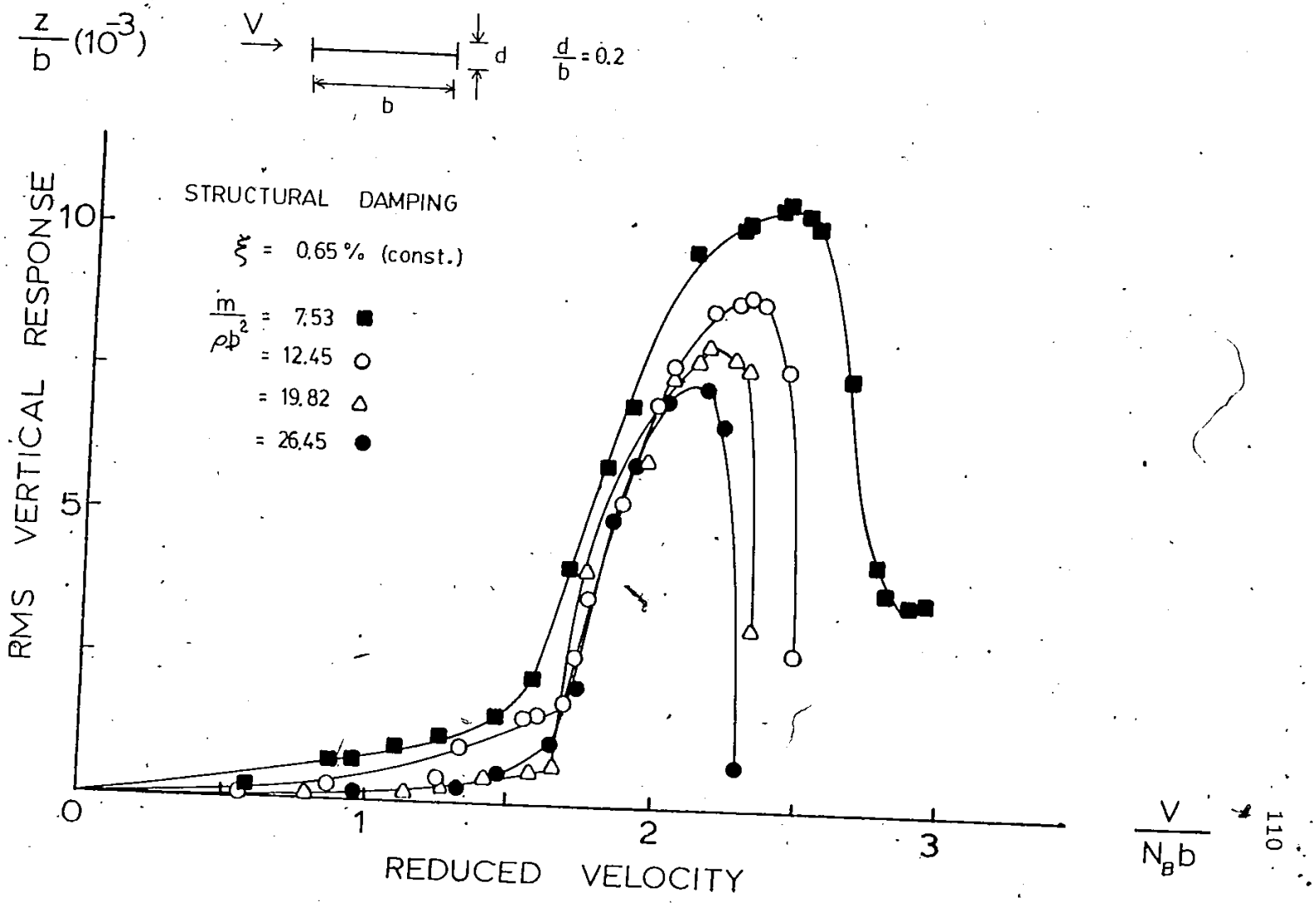

FIG. 6 VORTEX INDUCED VERTICAL RESPONSE WITH VARIABLE MASS PARAMETER

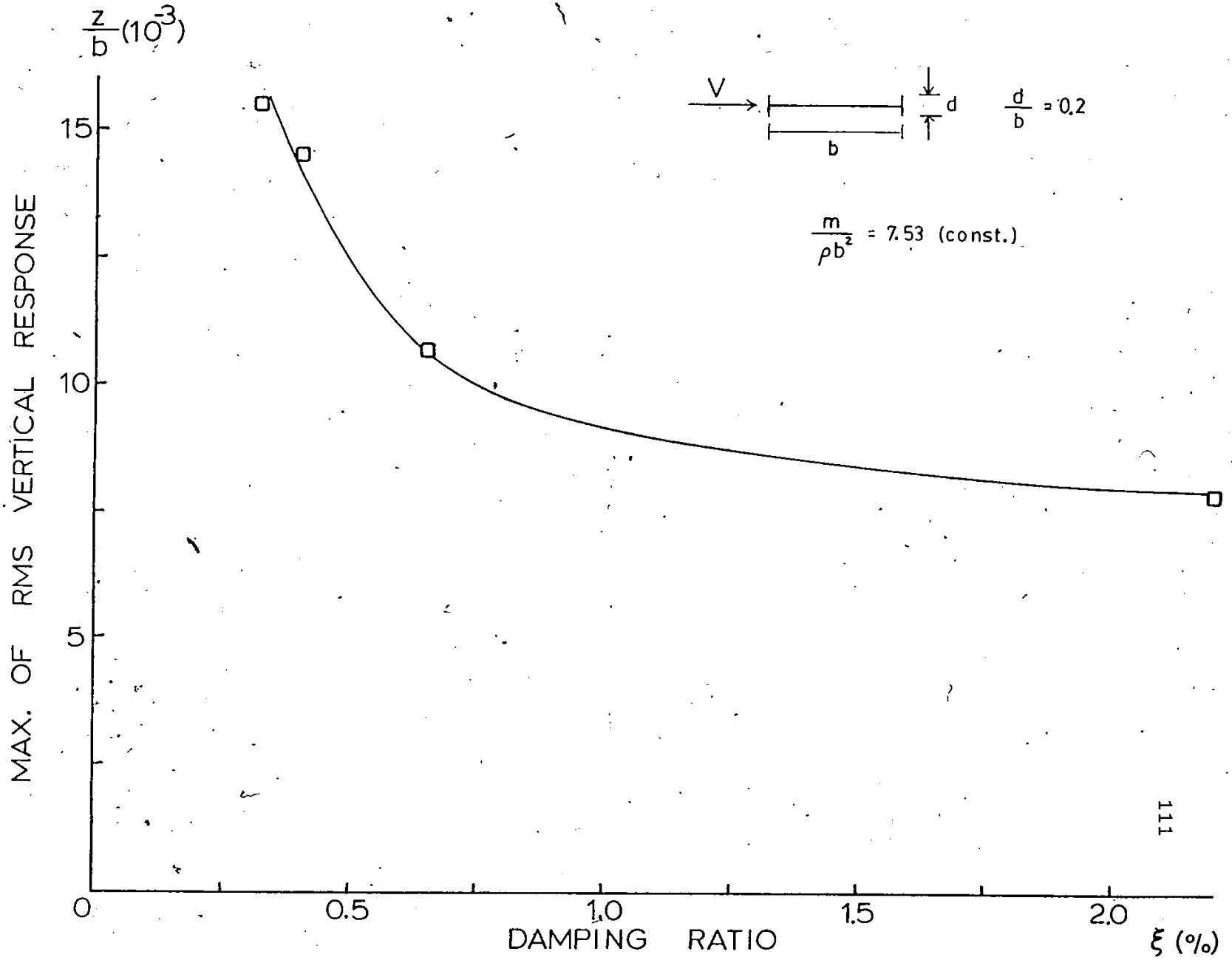

FIG. 7 EFFECT OF STRUCTURAL DAMPING ON VORTEX INDUCED VERTICAL RESPONSE

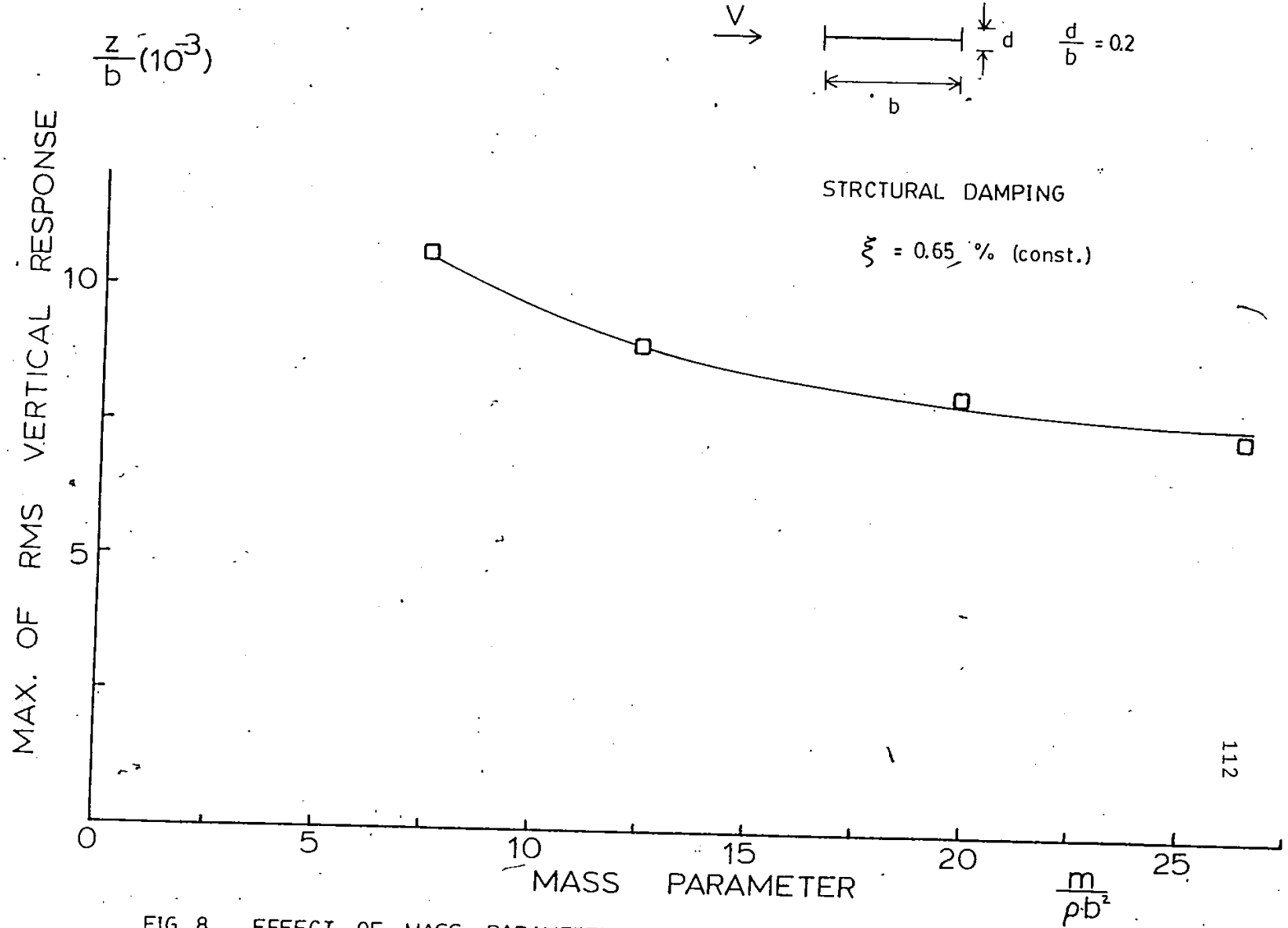

FIG. 8 EFFECT OF MASS PARAMETER ON VORTEX INDUCED VERTICAL RESPONSE

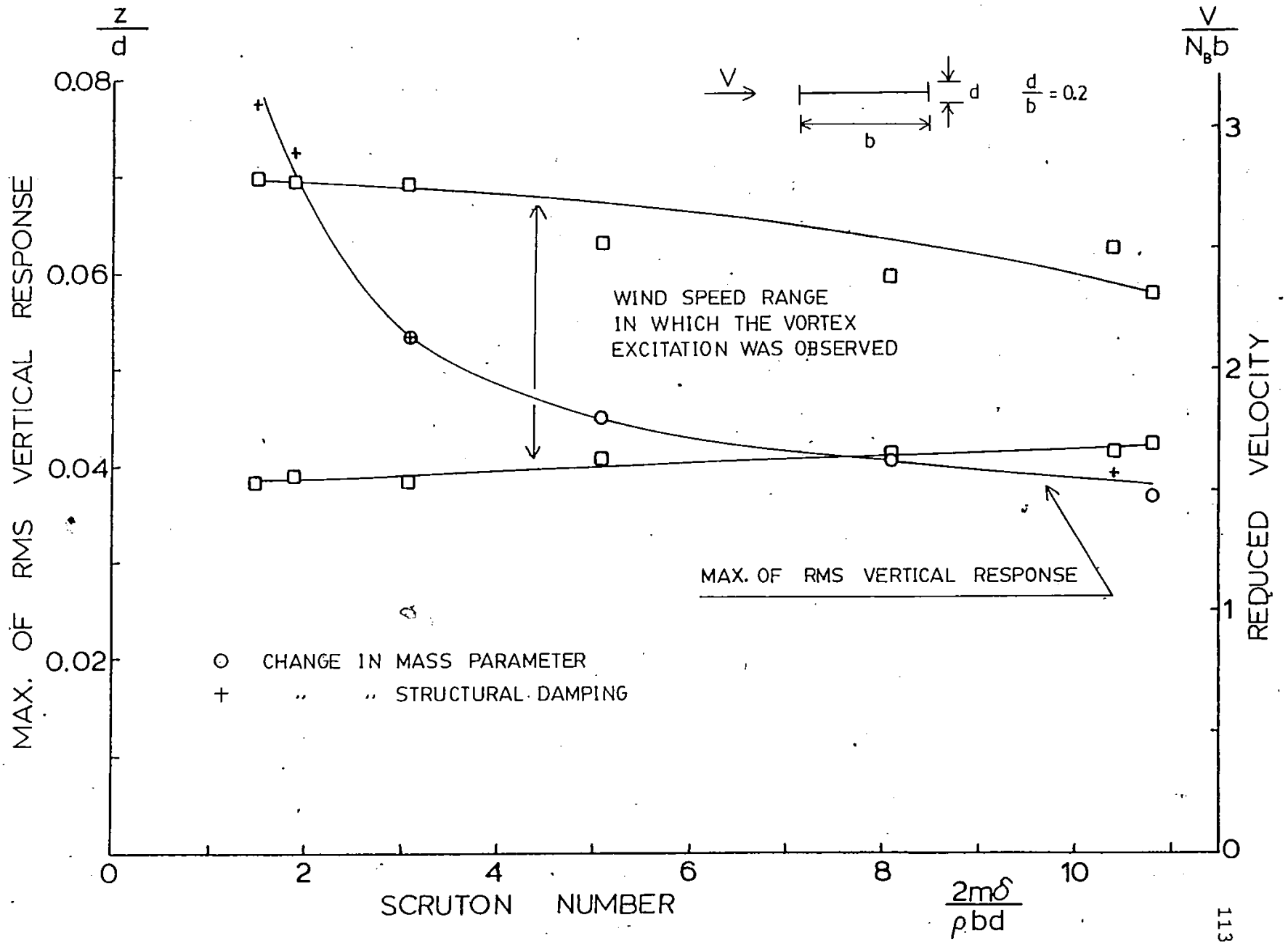

FIG. 9 EFFECT OF SCRUTON NUMBER ON VORTEX INDUCED VERTICAL RESPONSE

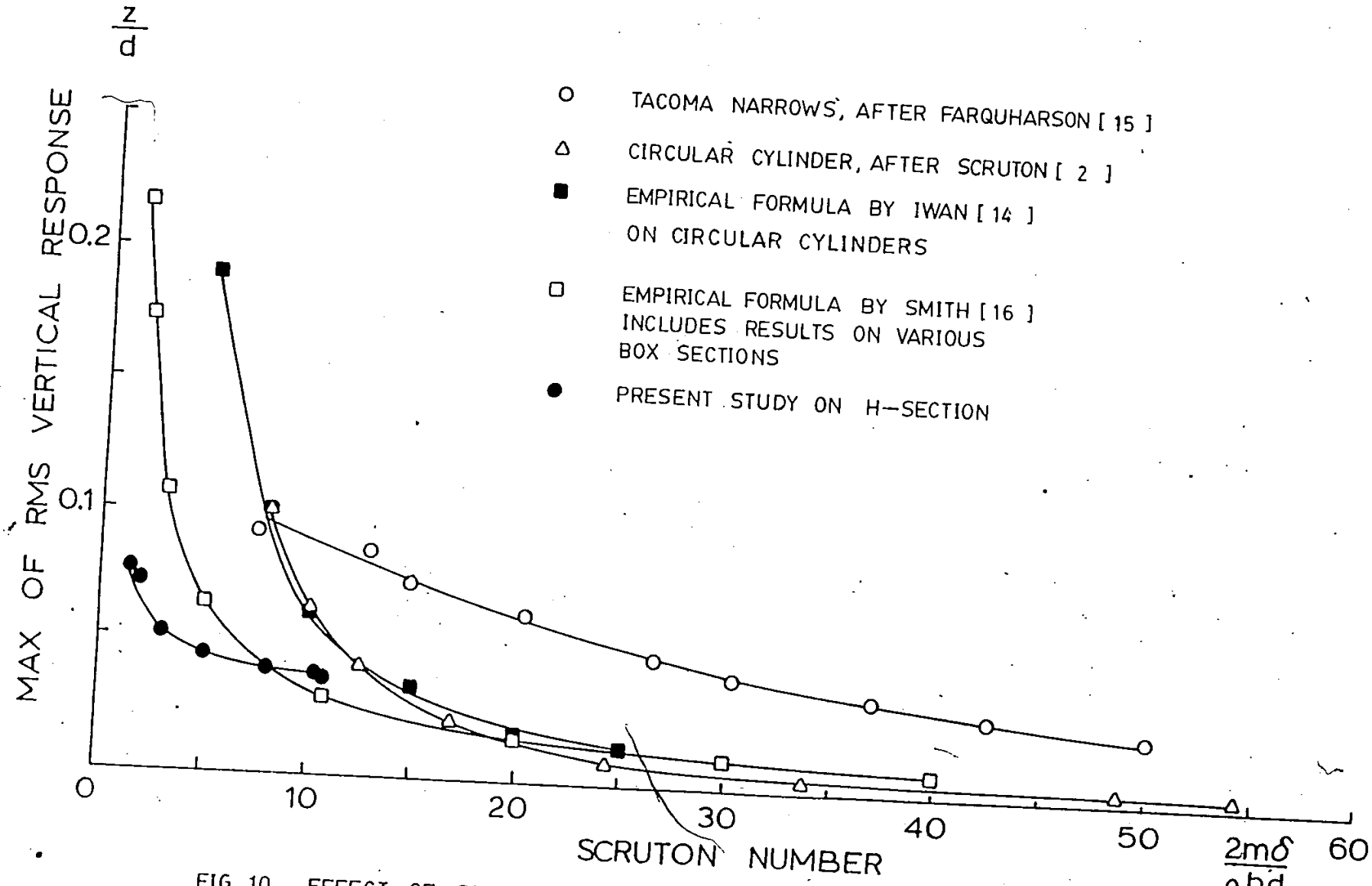

FIG. 10 EFFECT OF SCRUTON NUMBER ON VORTEX INDUCED VERTICAL RESPONSE

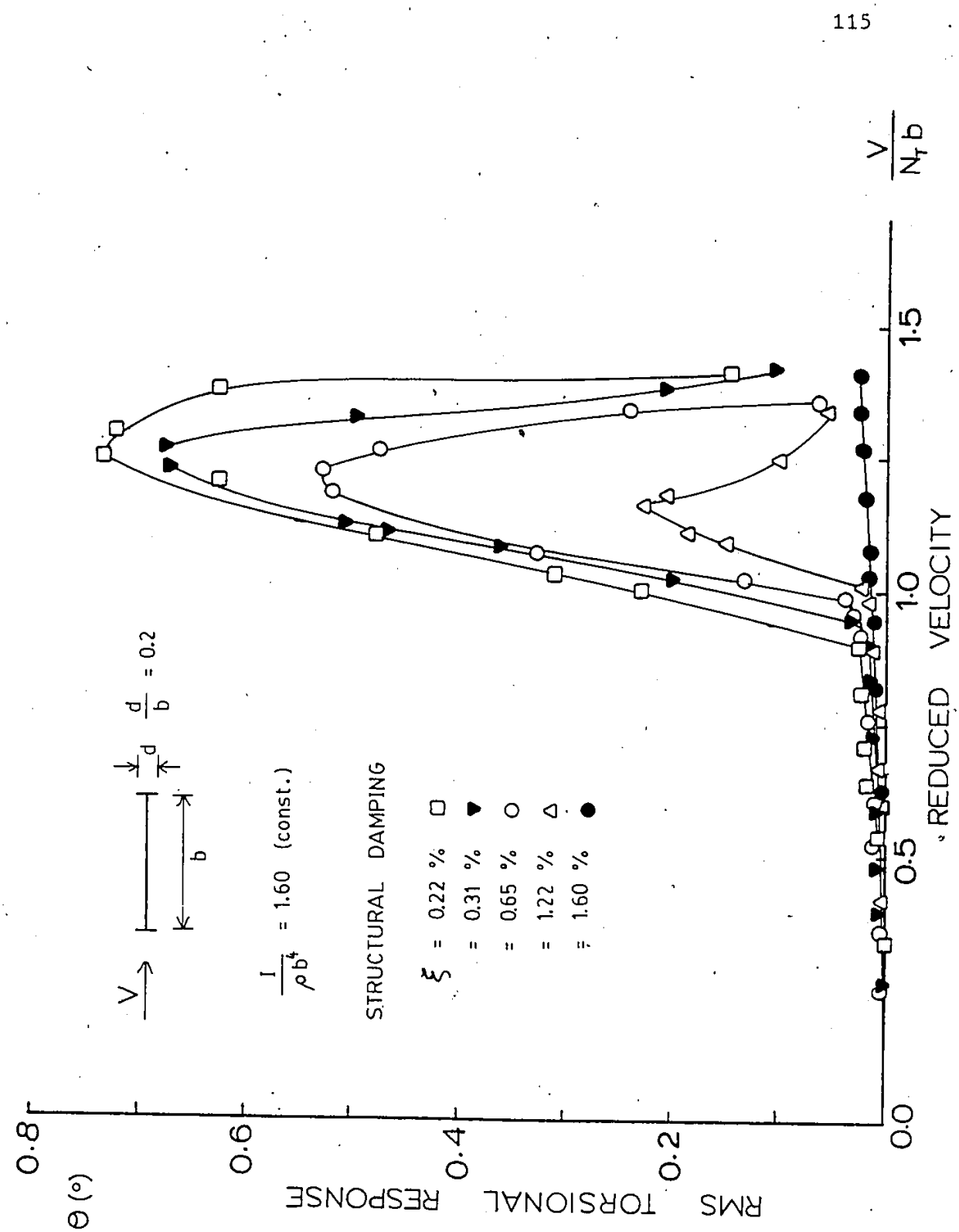

FIG. 11 VORTEX INDUCED TORSIONAL RESPONSE WITH VARIABLE STRUCTURAL DAMPING

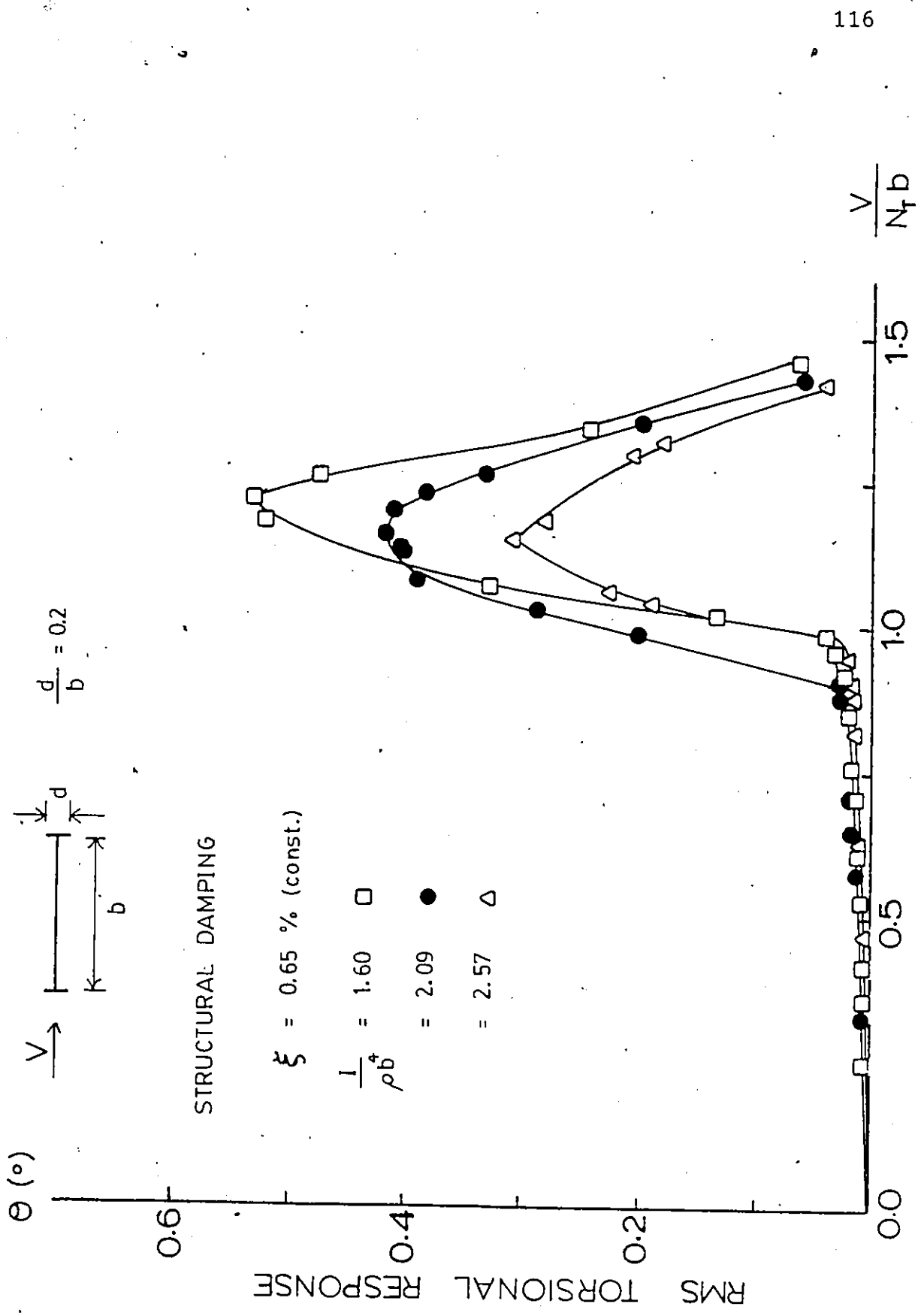

FIG. 12 VORTEX INDUCED TORSIONAL RESPONSE WITH VARIABLE MASS PARAMETER

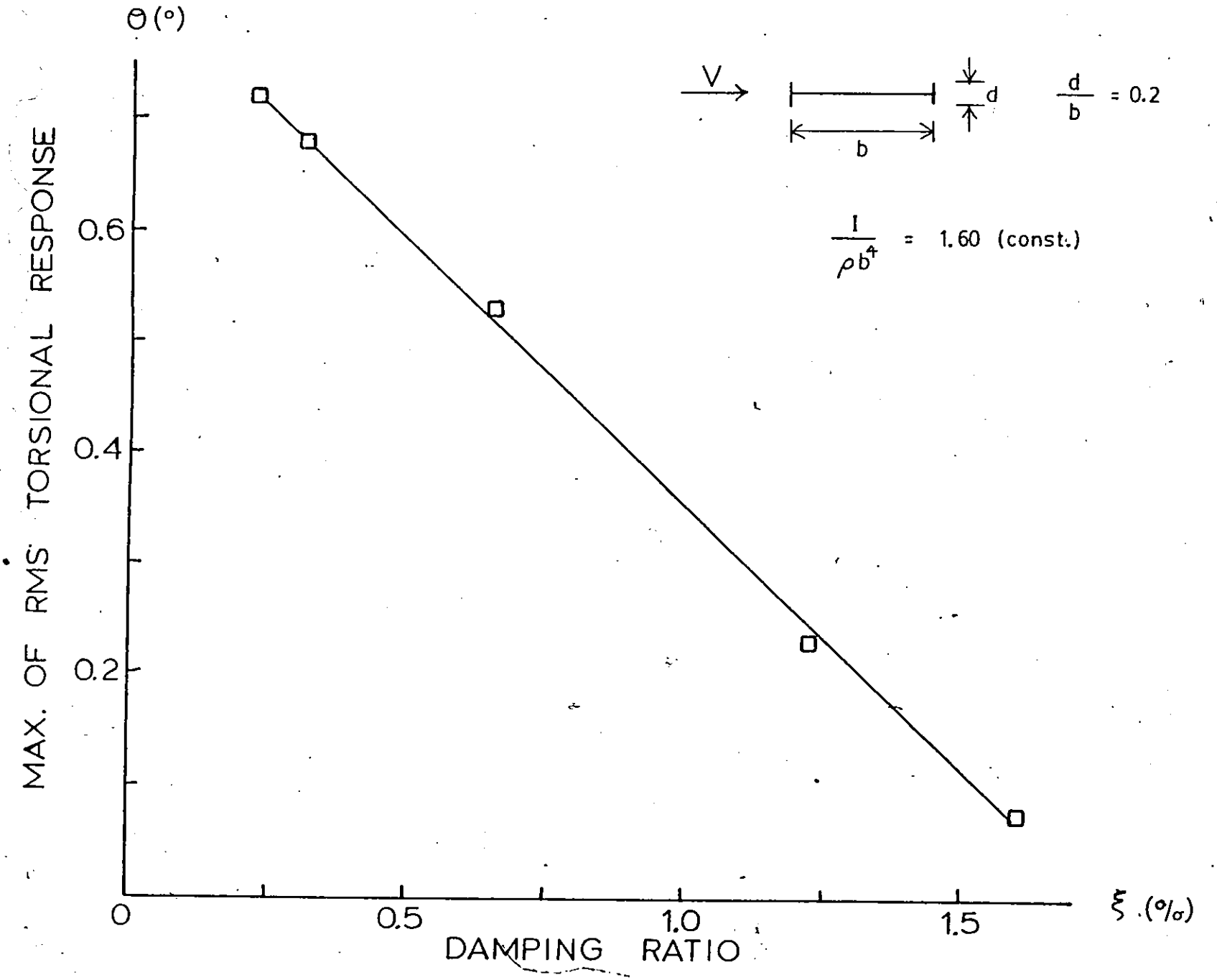

FIG. 13 EFFECT OF STRUCTURAL DAMPING ON VORTEX INDUCED TORSIONAL RESPONSE

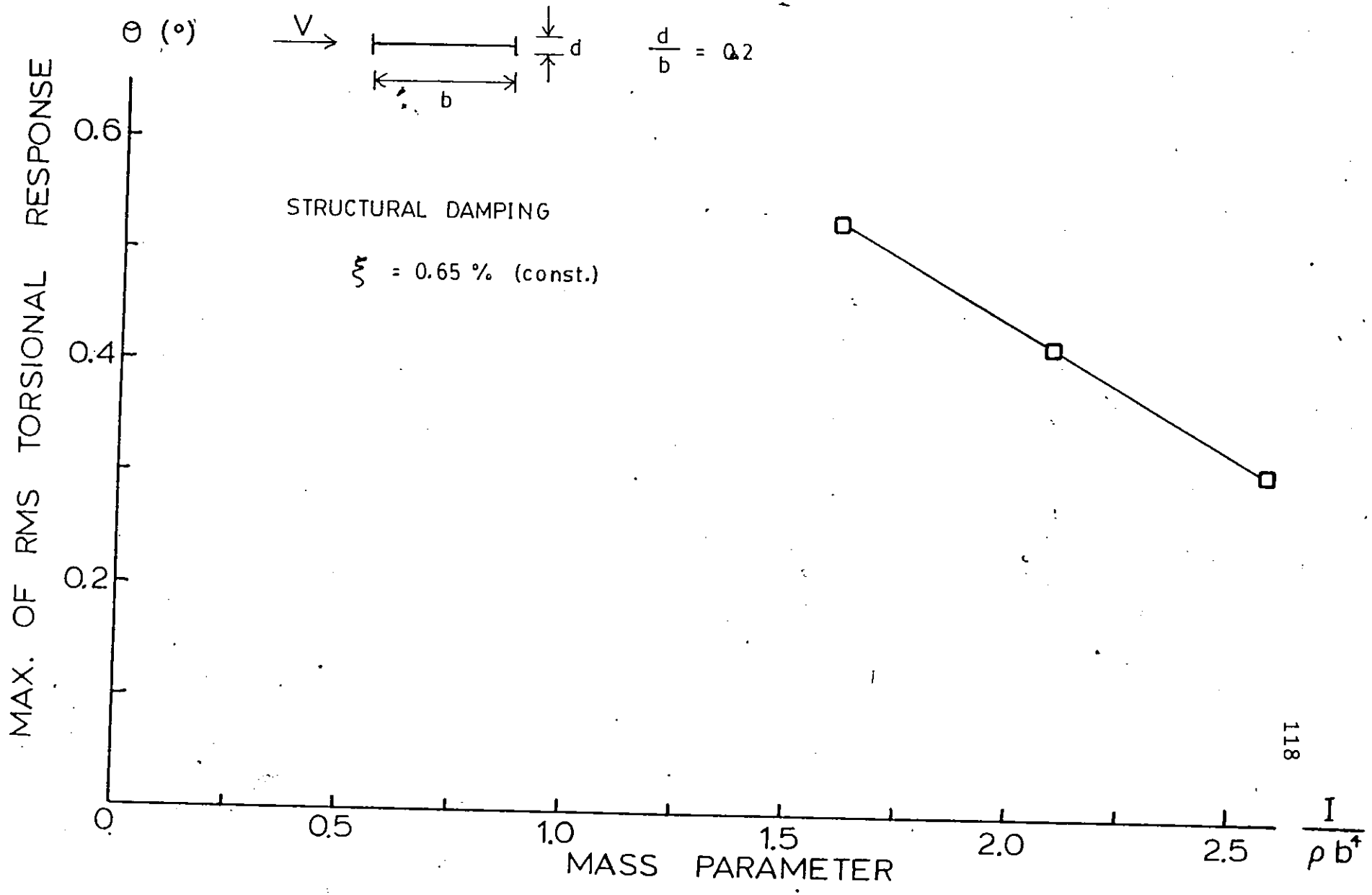

FIG. 14 EFFECT OF MASS PARAMETER ON VORTEX INDUCED TORSIONAL RESPONSE

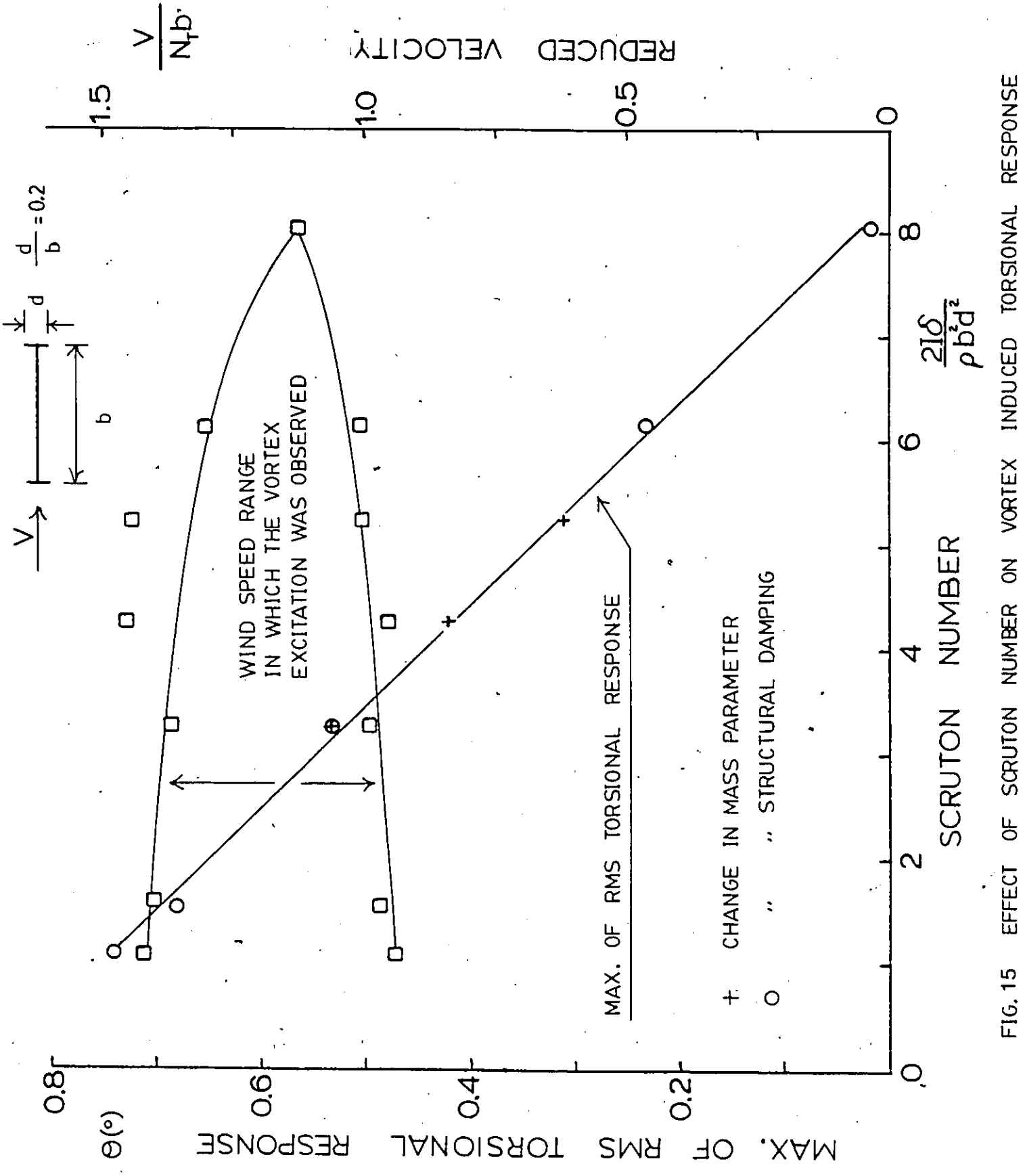

FIG. 15 EFFECT OF SCRUTON NUMBER ON VORTEX INDUCED TORSIONAL RESPONSE

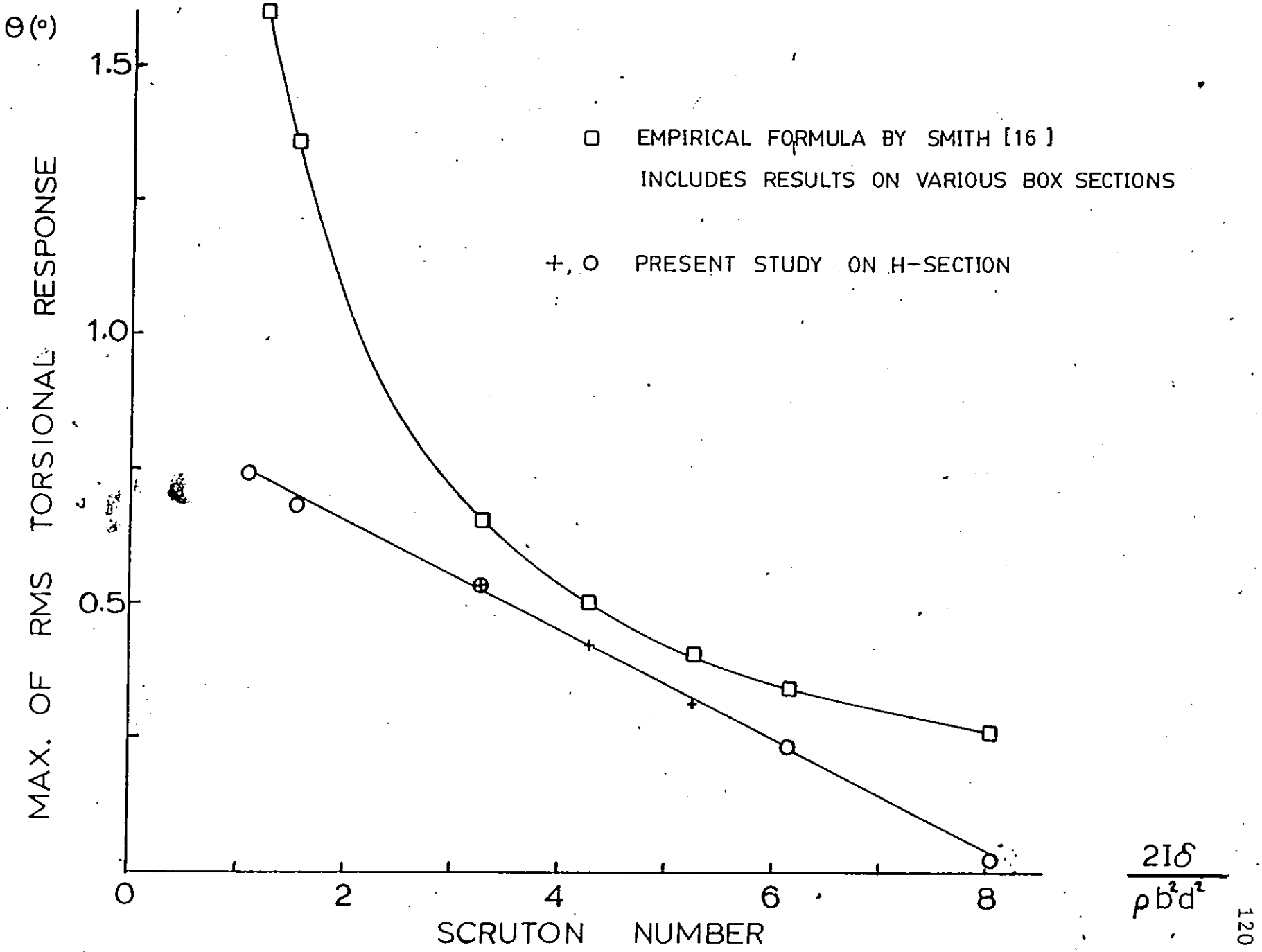

FIG. 16 EFFECT OF SCRUTON NUMBER ON VORTEX INDUCED TORSIONAL RESPONSE

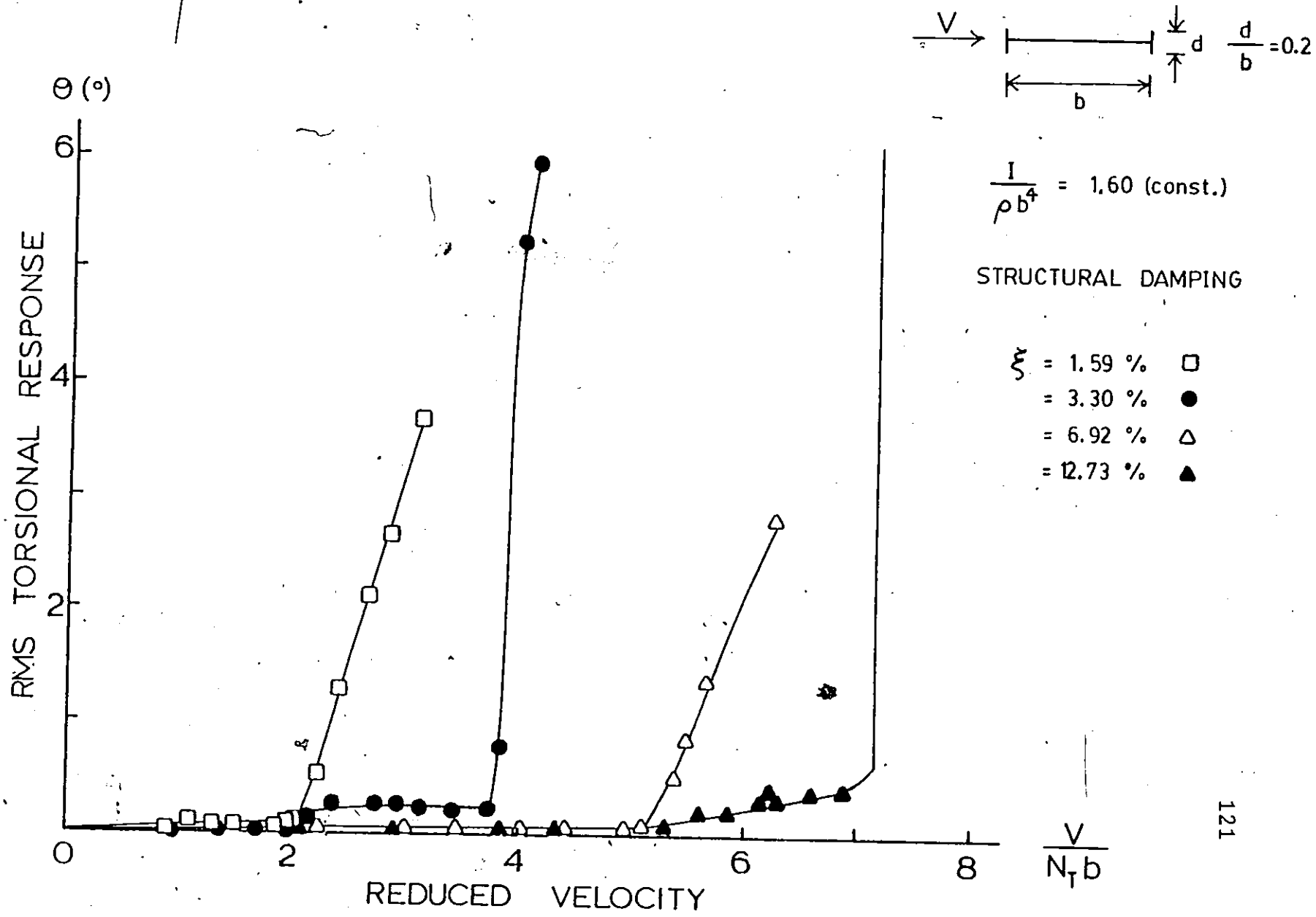

FIG. 17 TORSIONAL INSTABILITY RESPONSE WITH VARIABLE STRUCTURAL DAMPING

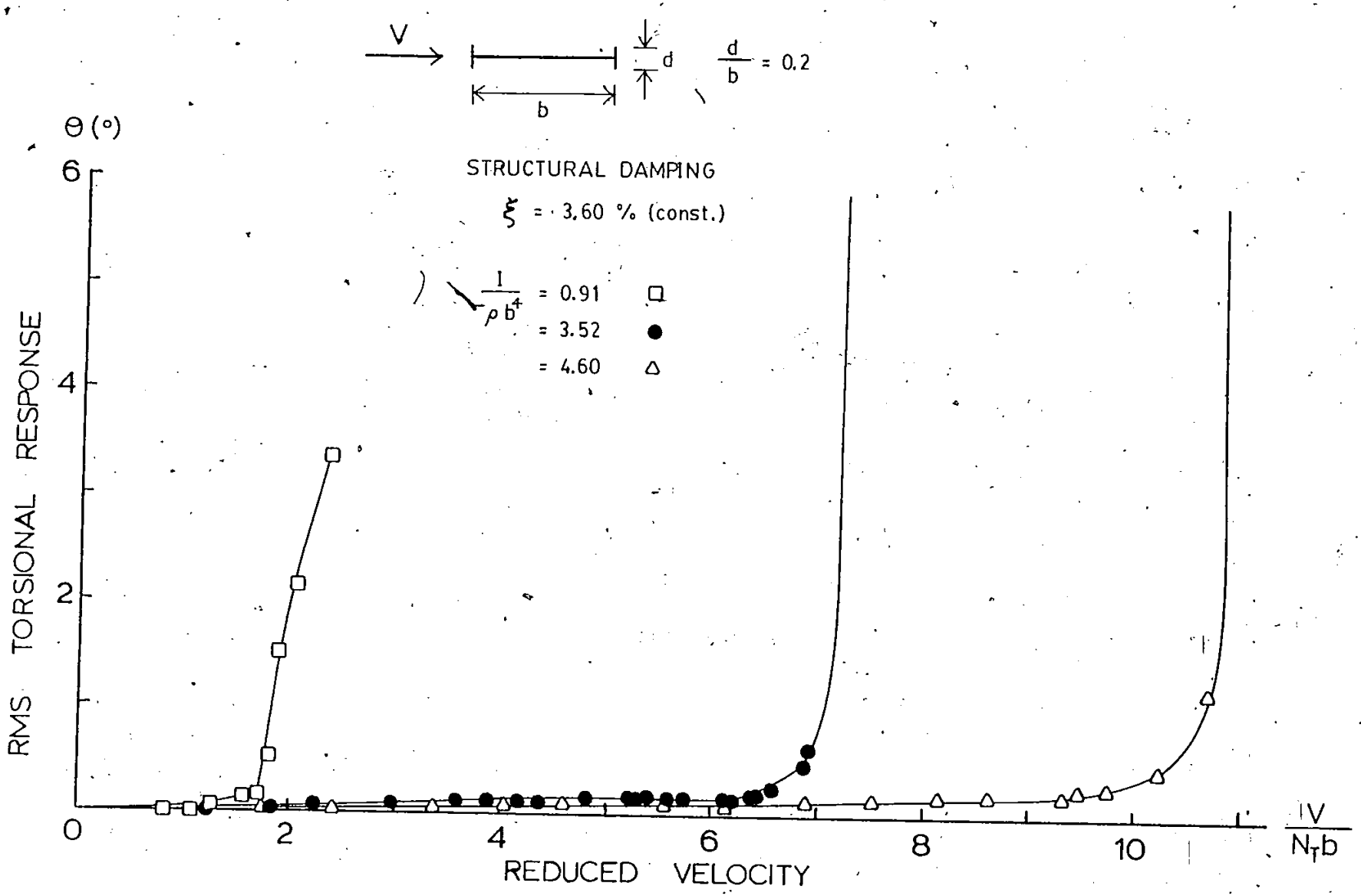

FIG. 18 TORSIONAL INSTABILITY RESPONSE WITH VARIABLE MASS PARAMETER

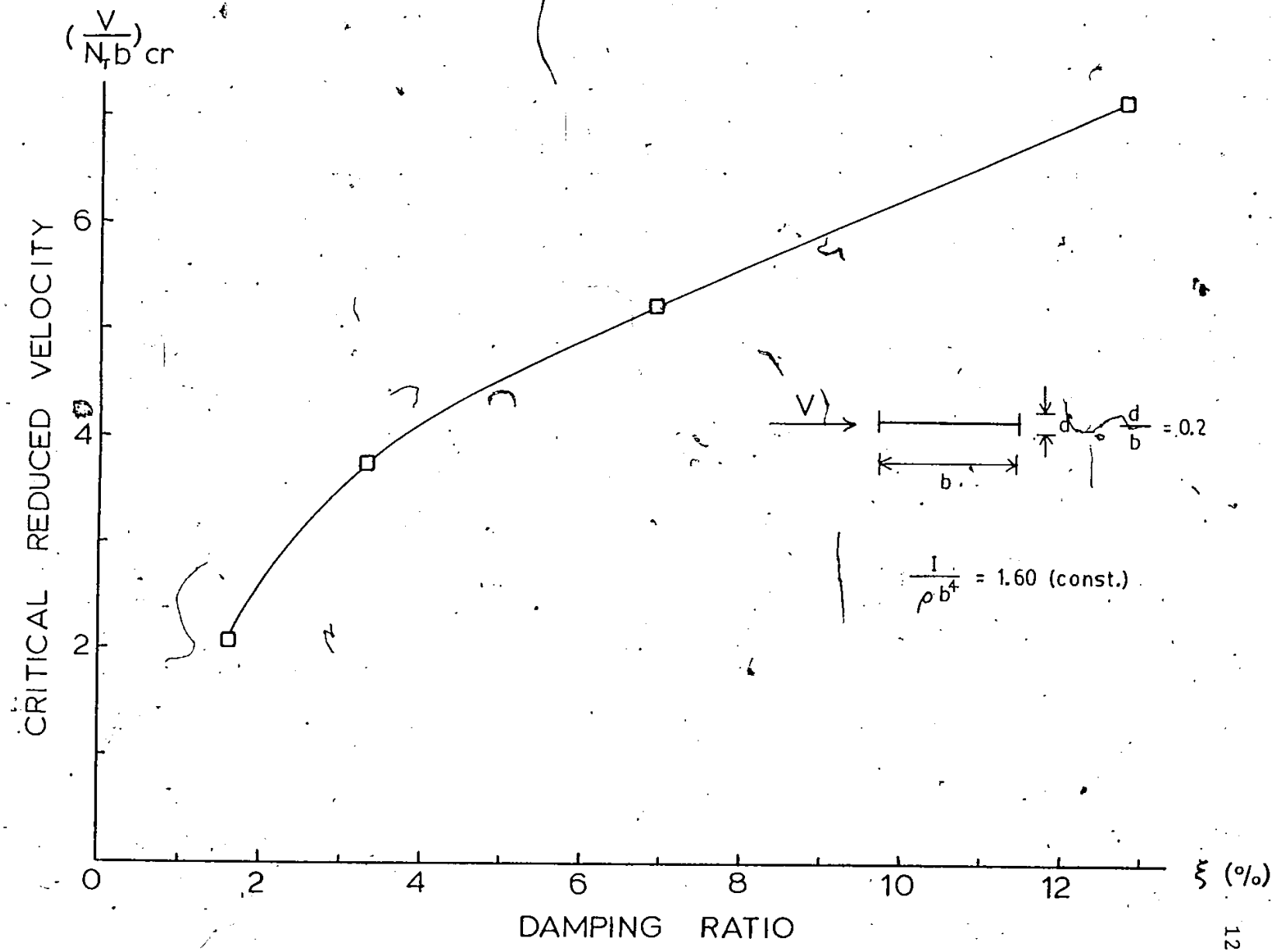

FIG. 19 EFFECT OF STRUCTURAL DAMPING ON CRITICAL SPEED OF TORSIONAL INSTABILITY

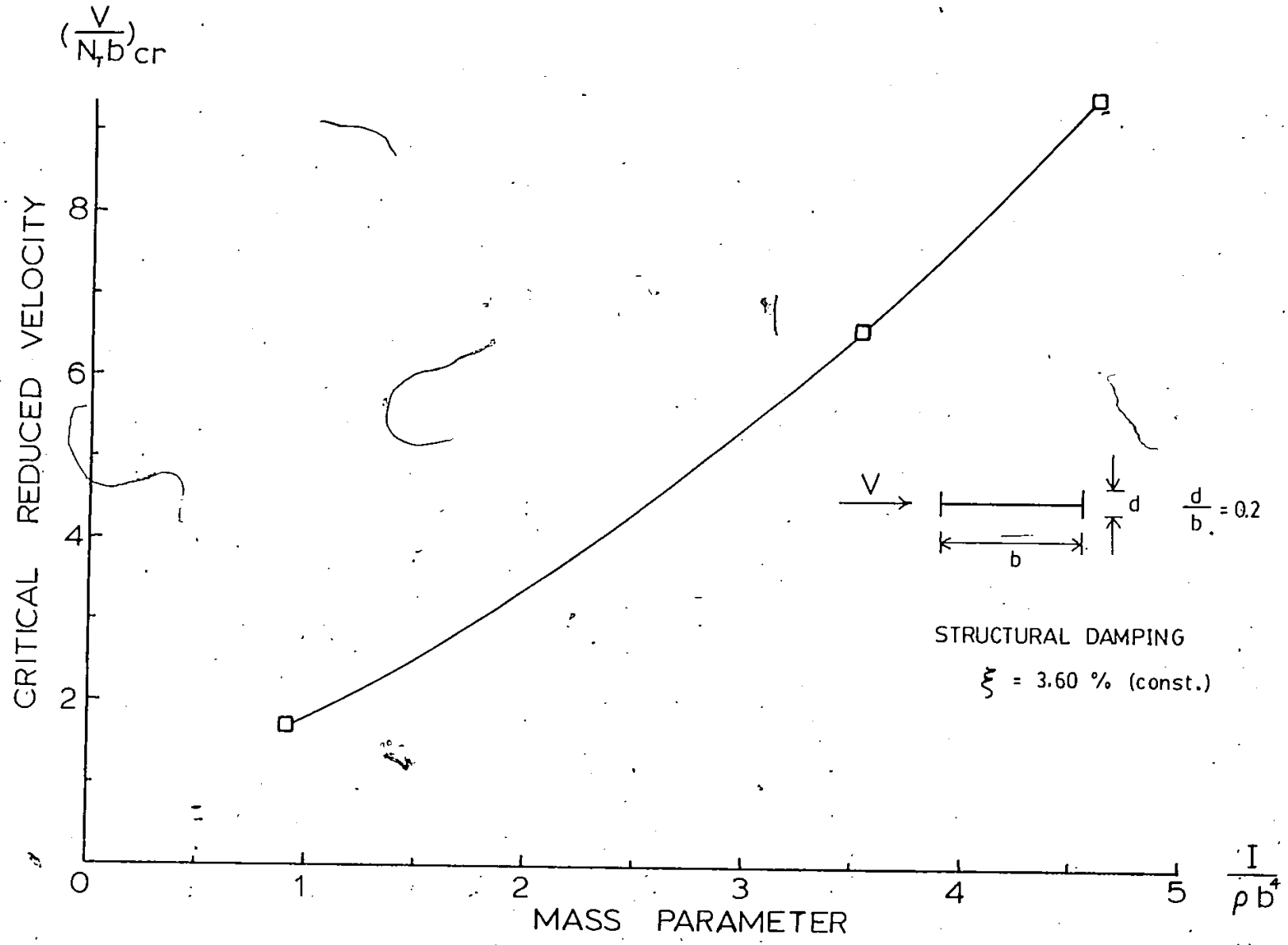

FIG. 20 EFFECT OF MASS PARAMETER ON CRITICAL SPEED OF TORSIONAL INSTABILITY

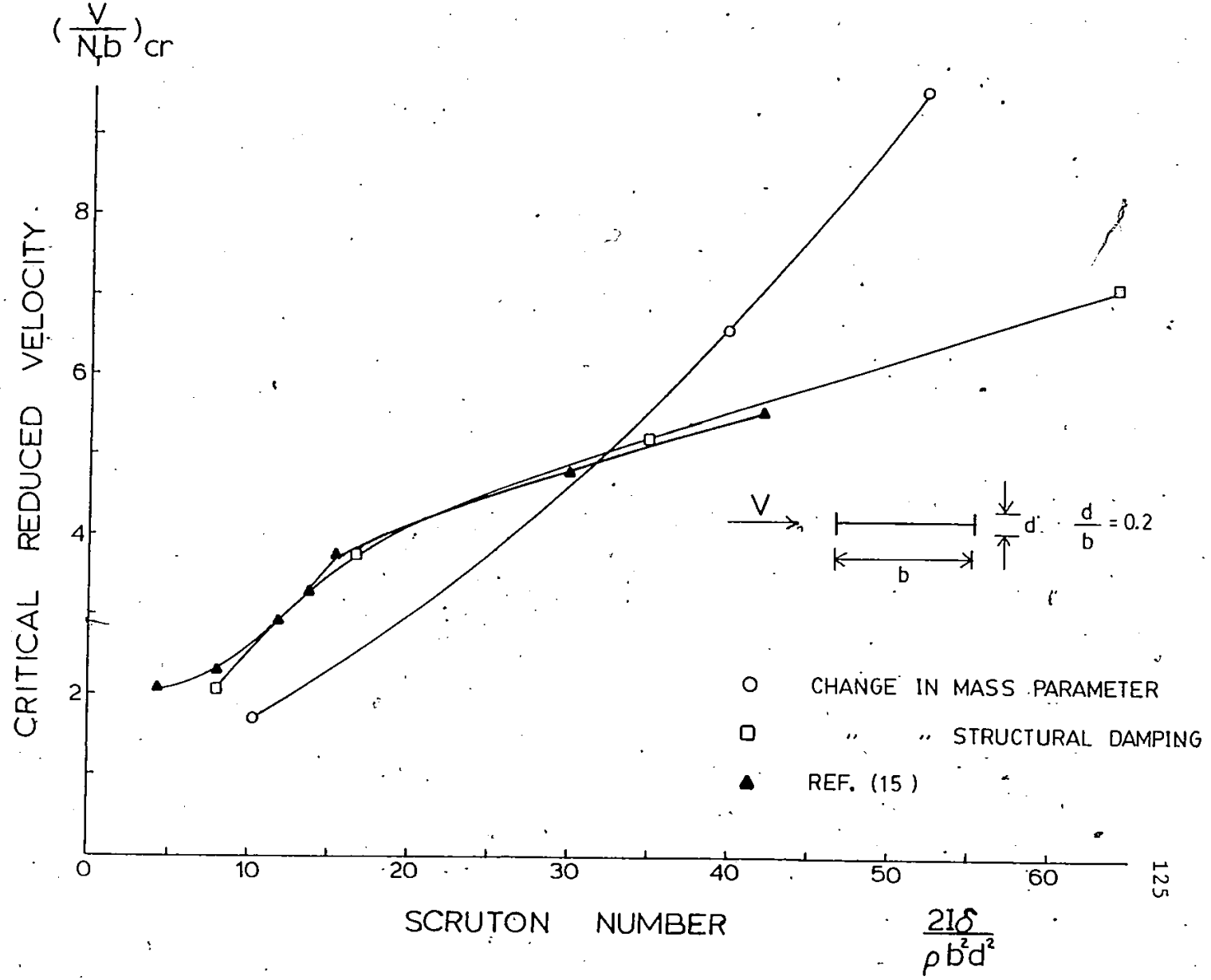

FIG. 21 EFFECT OF SCRUTON NUMBER ON CRITICAL SPEED OF TORSIONAL INSTABILITY

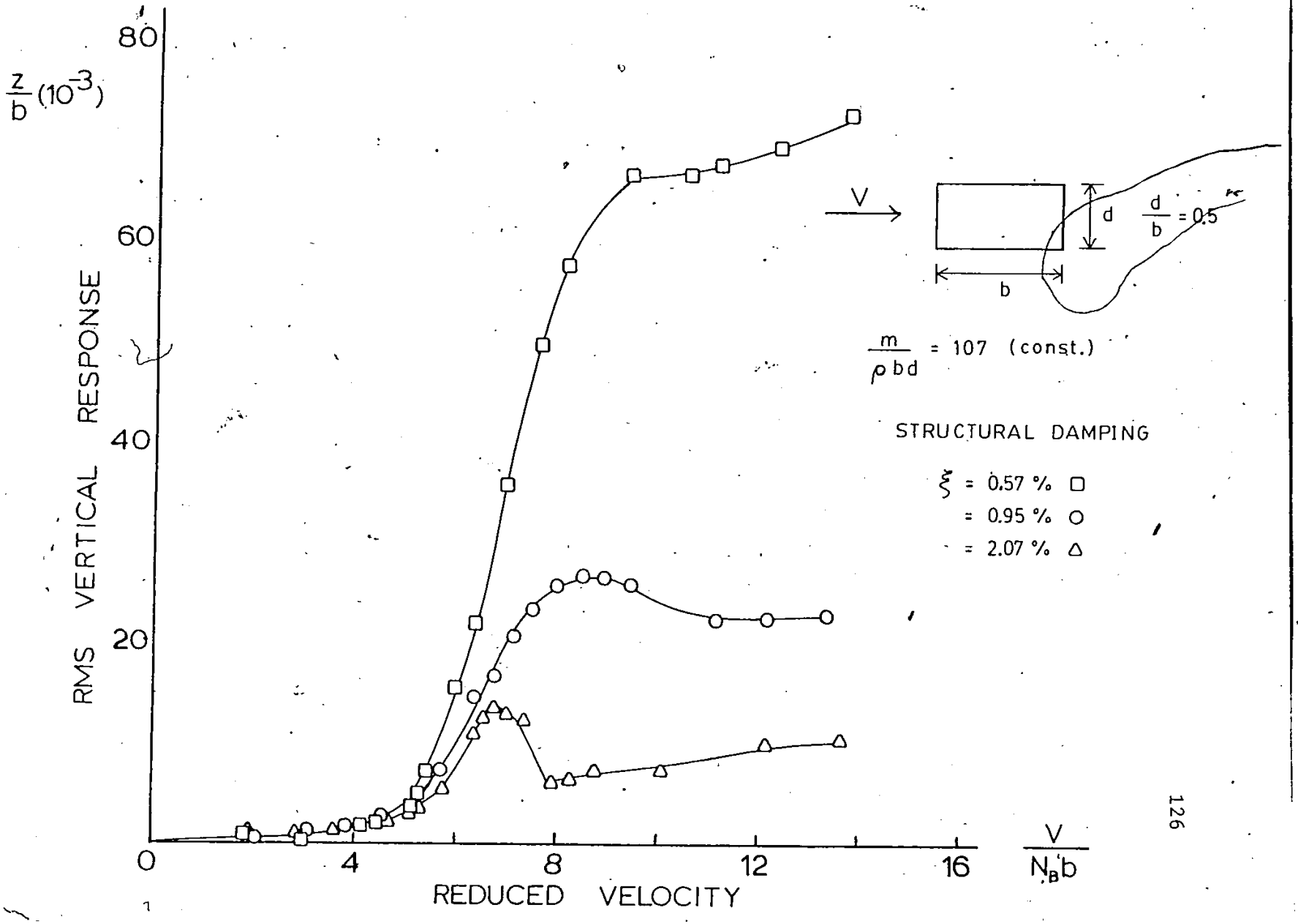

FIG. 22 VERTICAL RESPONSE OF 1:2 RECTANGULAR BOX WITH LIGHT MASS

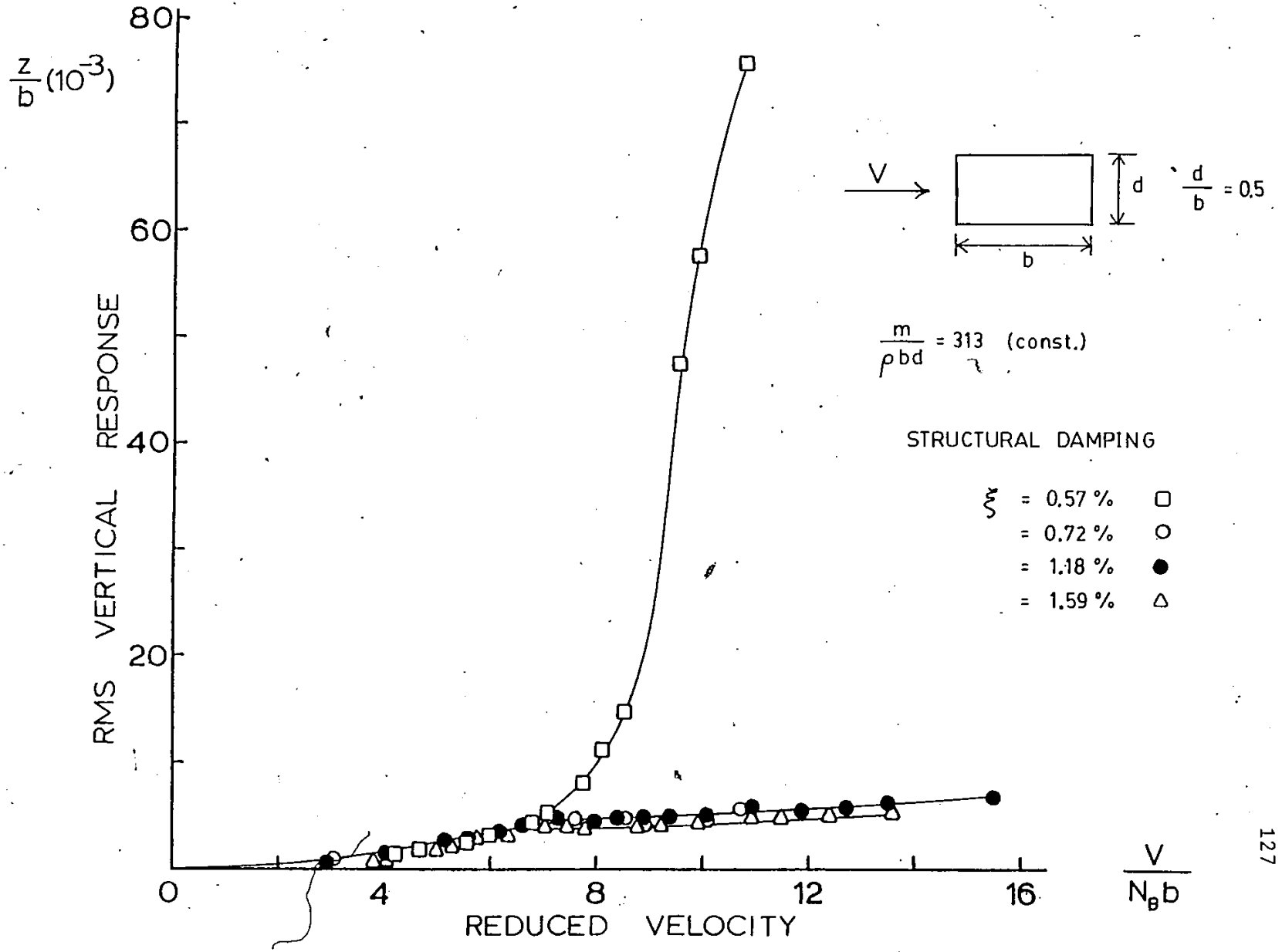

FIG. 23 VERTICAL RESPONSE OF 1:2 RECTANGULAR BOX WITH HEAVY MASS

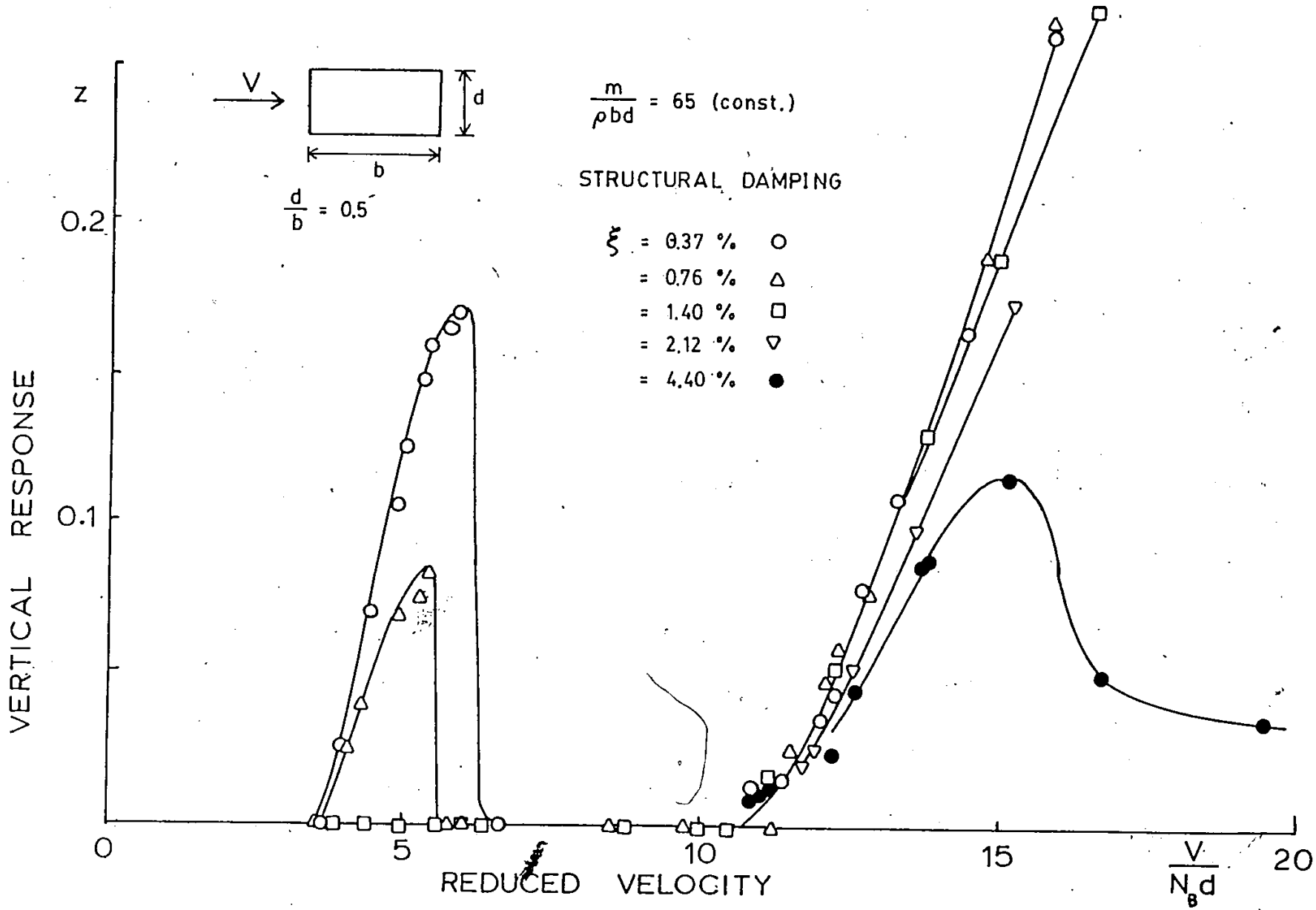

FIG. 24 VERTICAL RESPONSE OF 1:2 RECTANGULAR BOX, AFTER NOVAK [18]

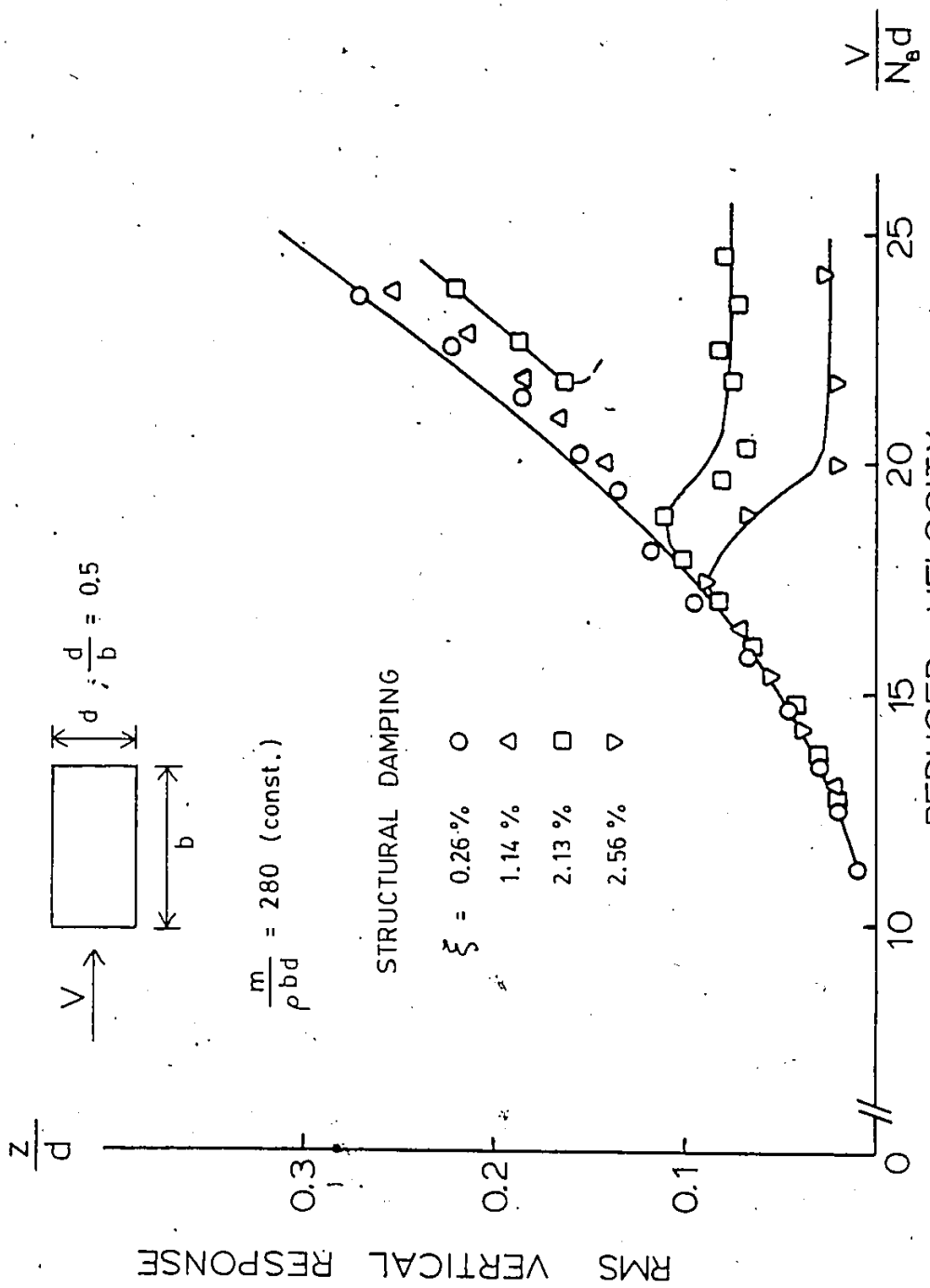

FIG. 25 VERTICAL RESPONSE OF 1:2 RECTANGULAR BOX, AFTER YAMADA [19]

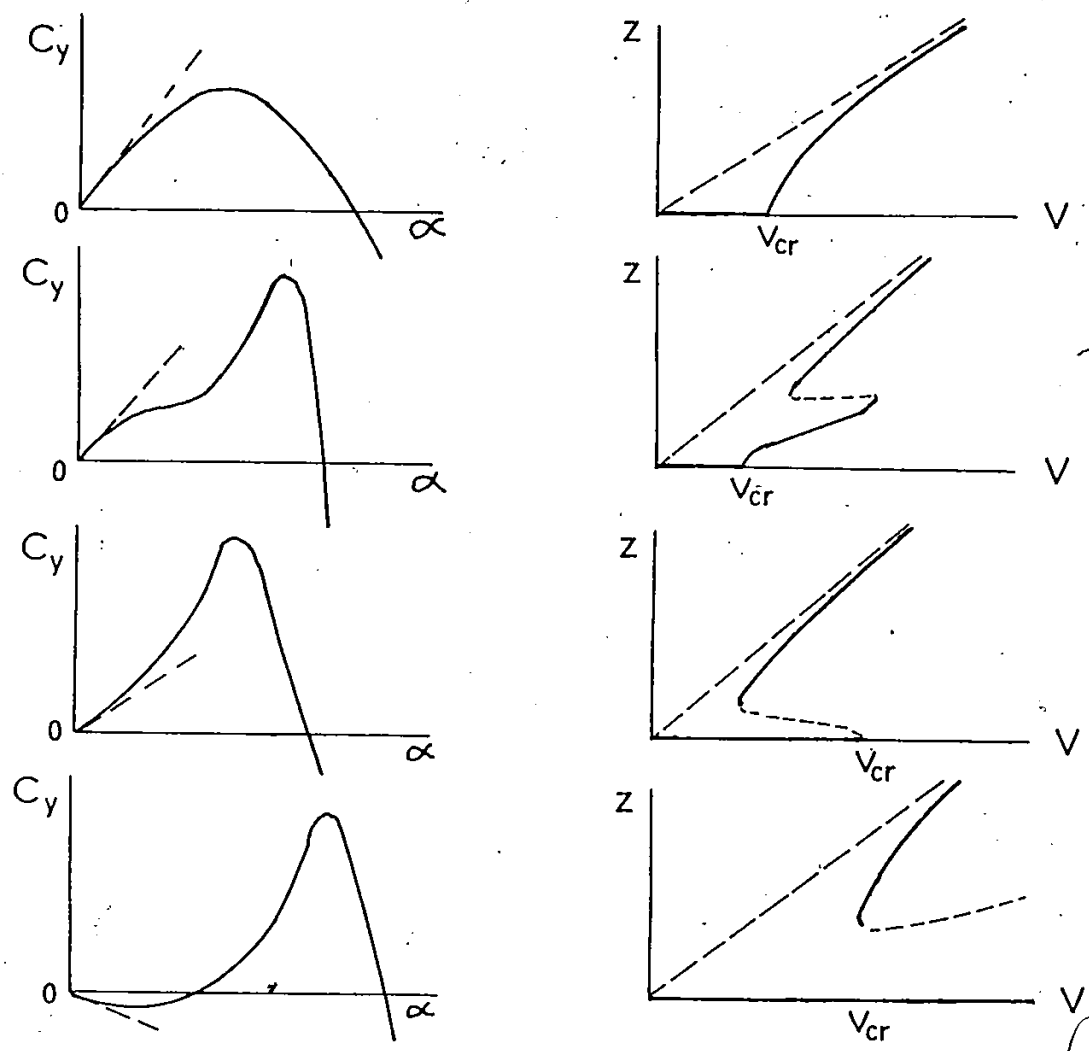

FIG. 26 TYPICAL LATERAL FORCE COEFFICIENTS AND CORRESPONDING TYPES OF GALLOPING RESPONSE, AFTER NOVAK [18]

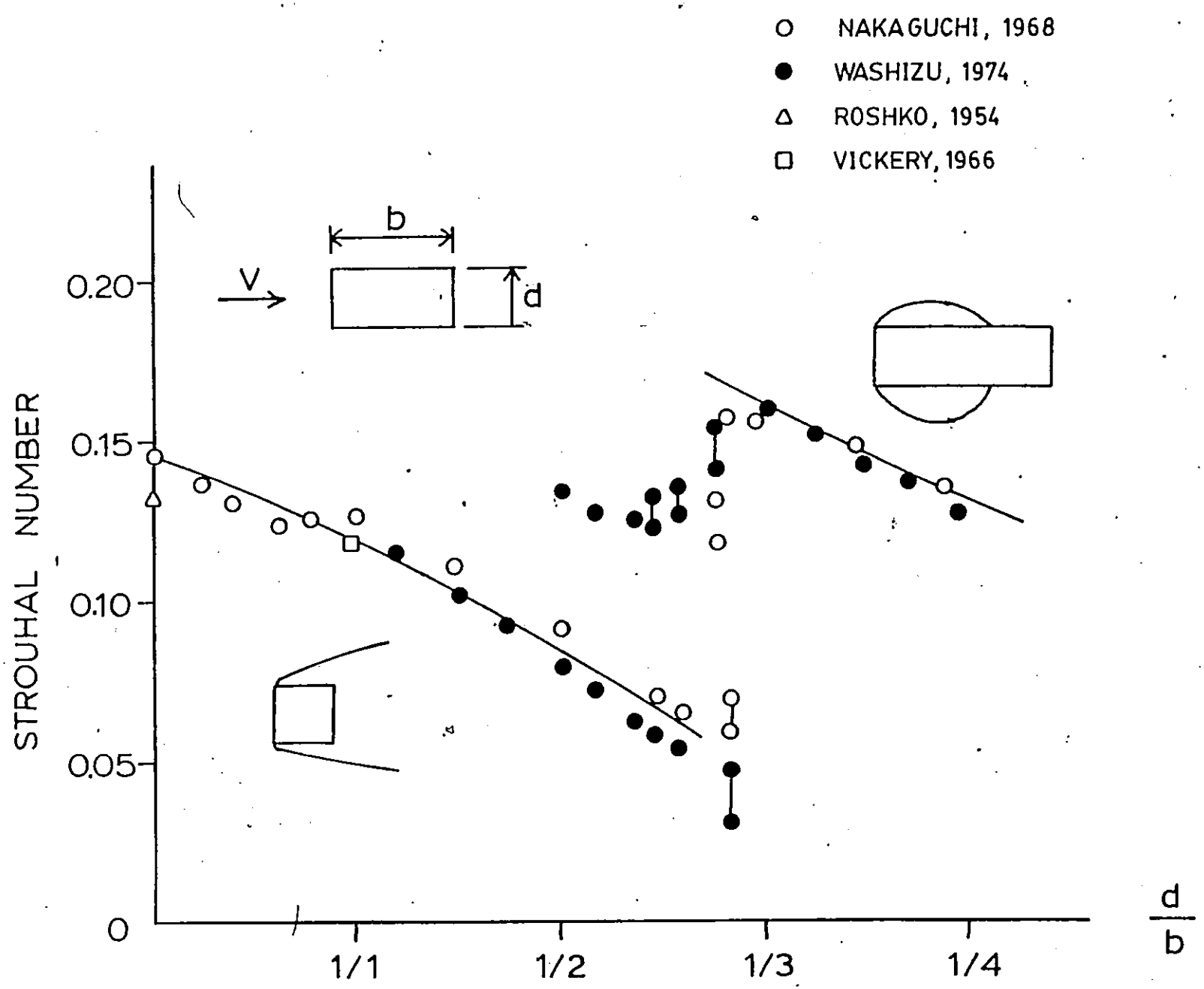

FIG. 27 STROUHAL NUMBER VS. ASPECT RATIO OF RECTANGULAR BOX [19]

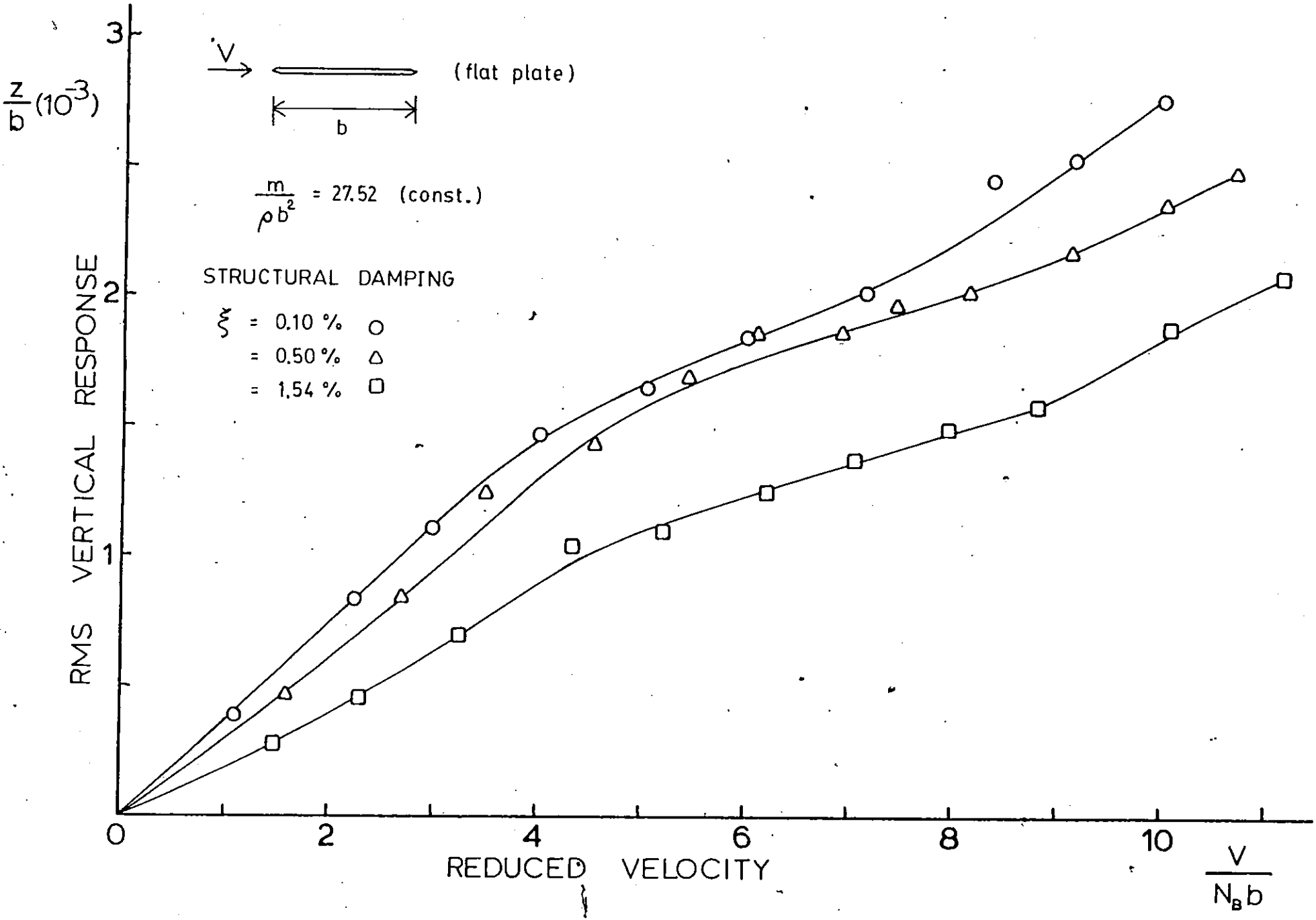

FIG. 28 VERTICAL BUFFETING RESPONSE WITH VARIABLE STRUCTURAL DAMPING

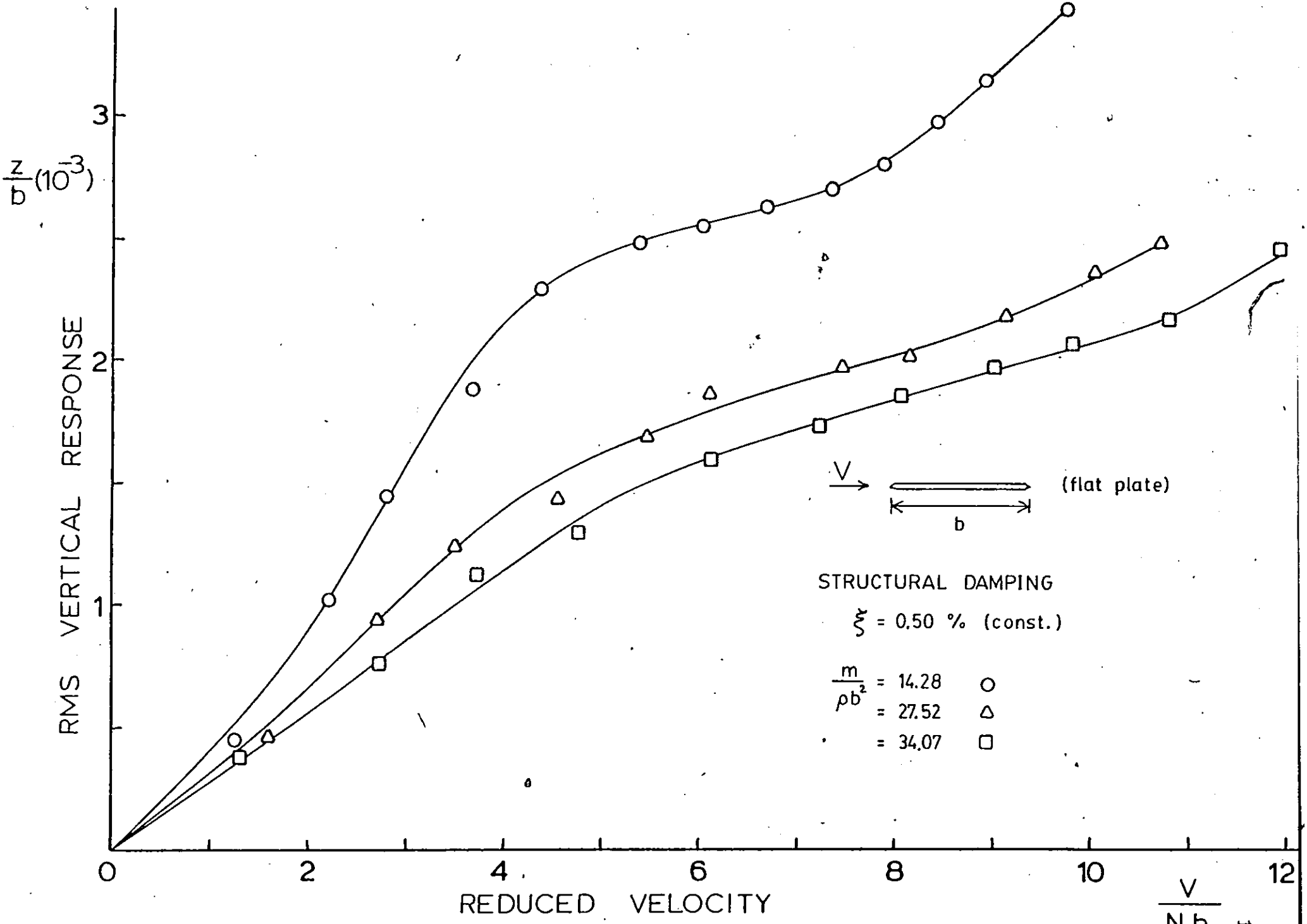

FIG. 29 VERTICAL BUFFETING RESPONSE WITH VARIABLE MASS PARAMETER

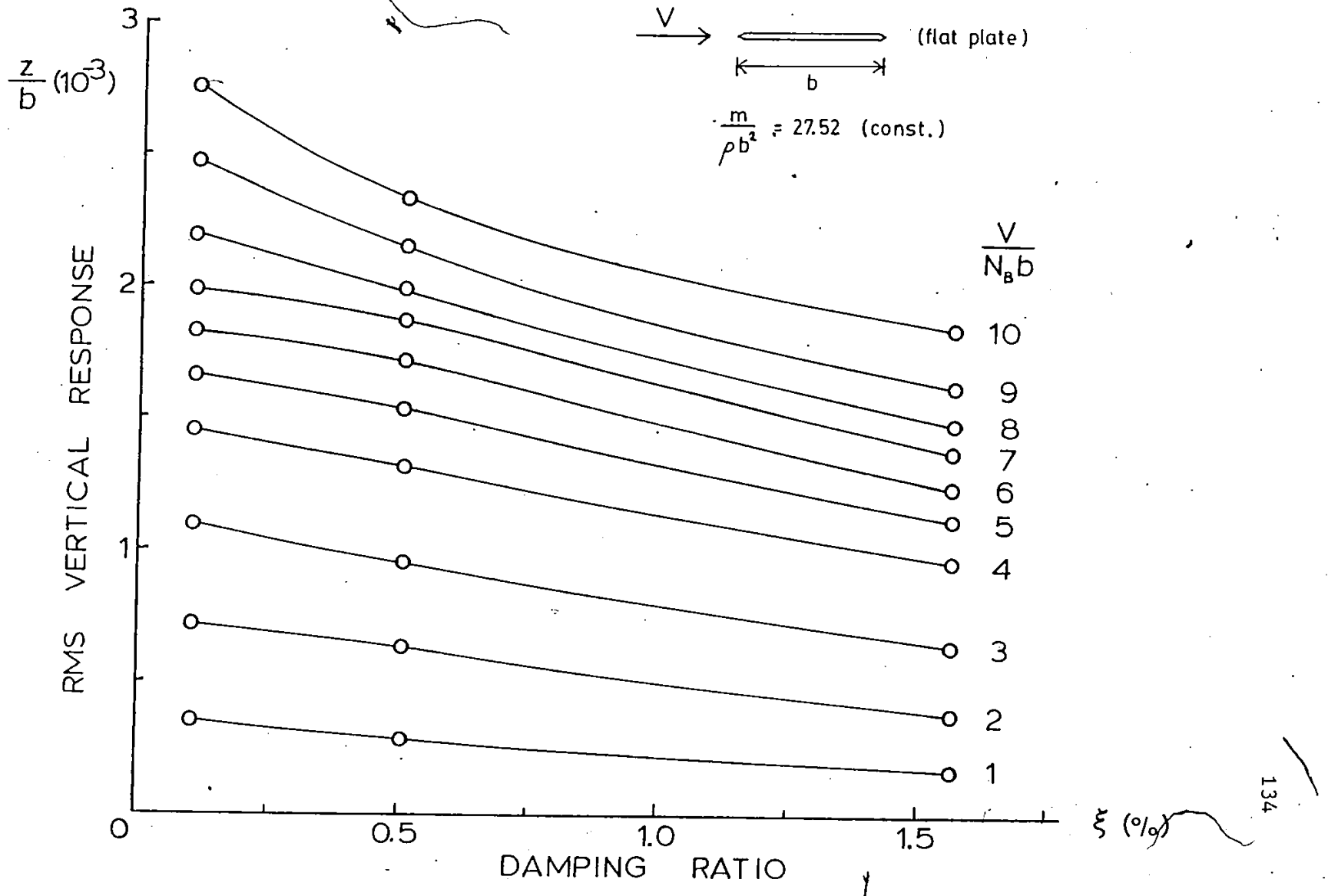

FIG. 30 EFFECT OF STRUCTURAL DAMPING ON VERTICAL BUFFETING RESPONSE

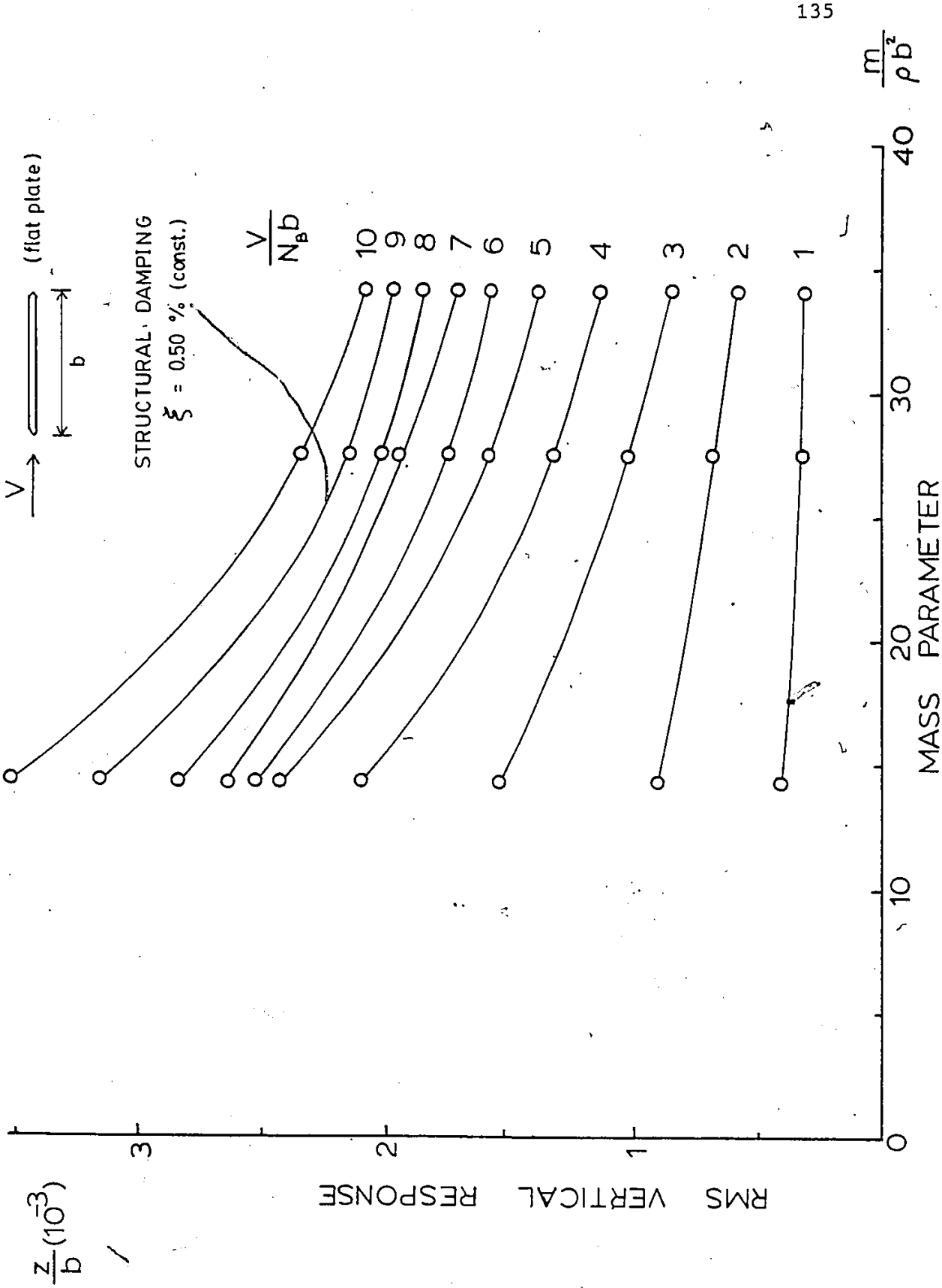

FIG. 31 EFFECT OF MASS PARAMETER ON VERTICAL BUFFETING RESPONSE

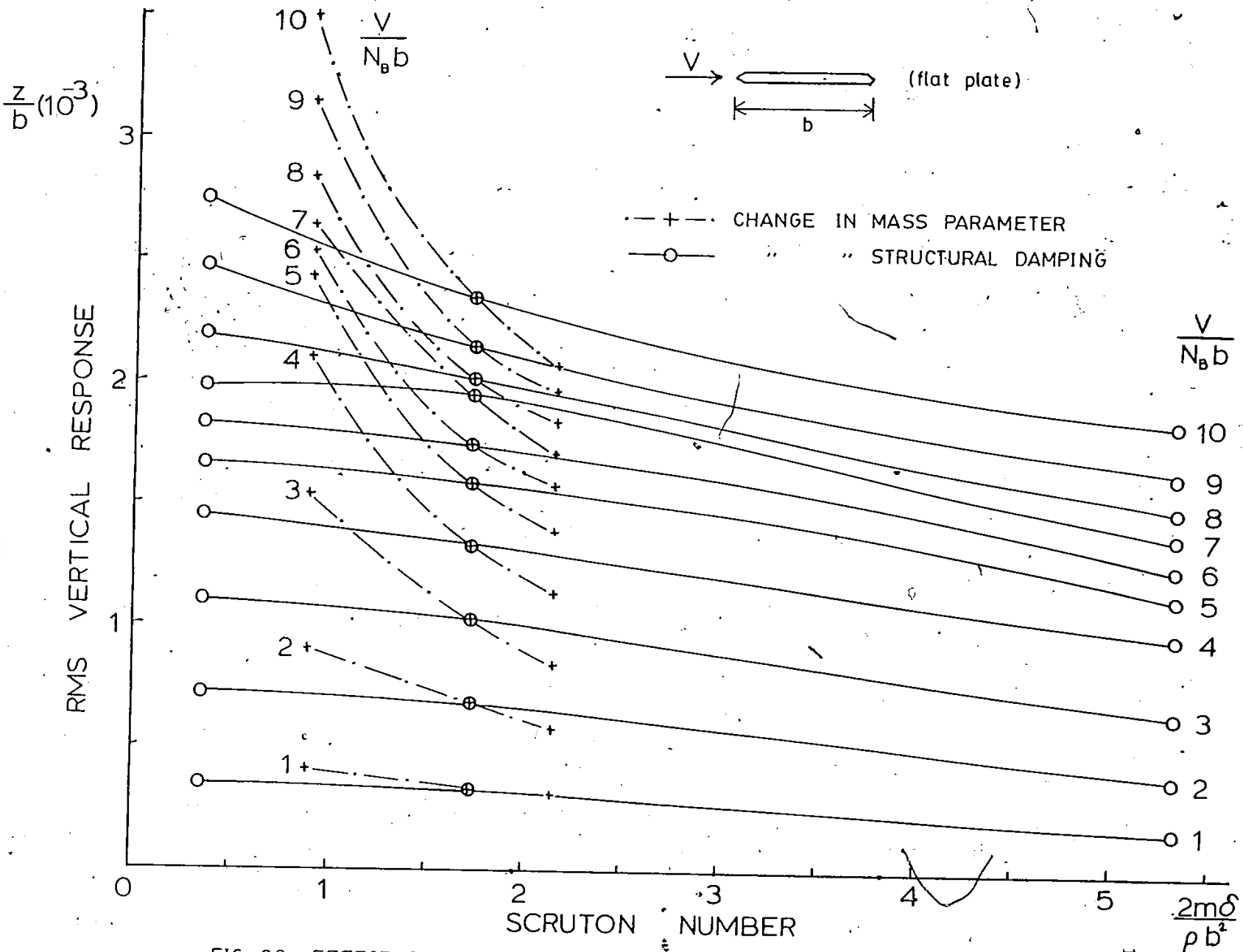

FIG. 32 EFFECT OF SCRUTON NUMBER ON VERTICAL BUFFETING RESPONSE (EXPERIMENTAL RESULTS)

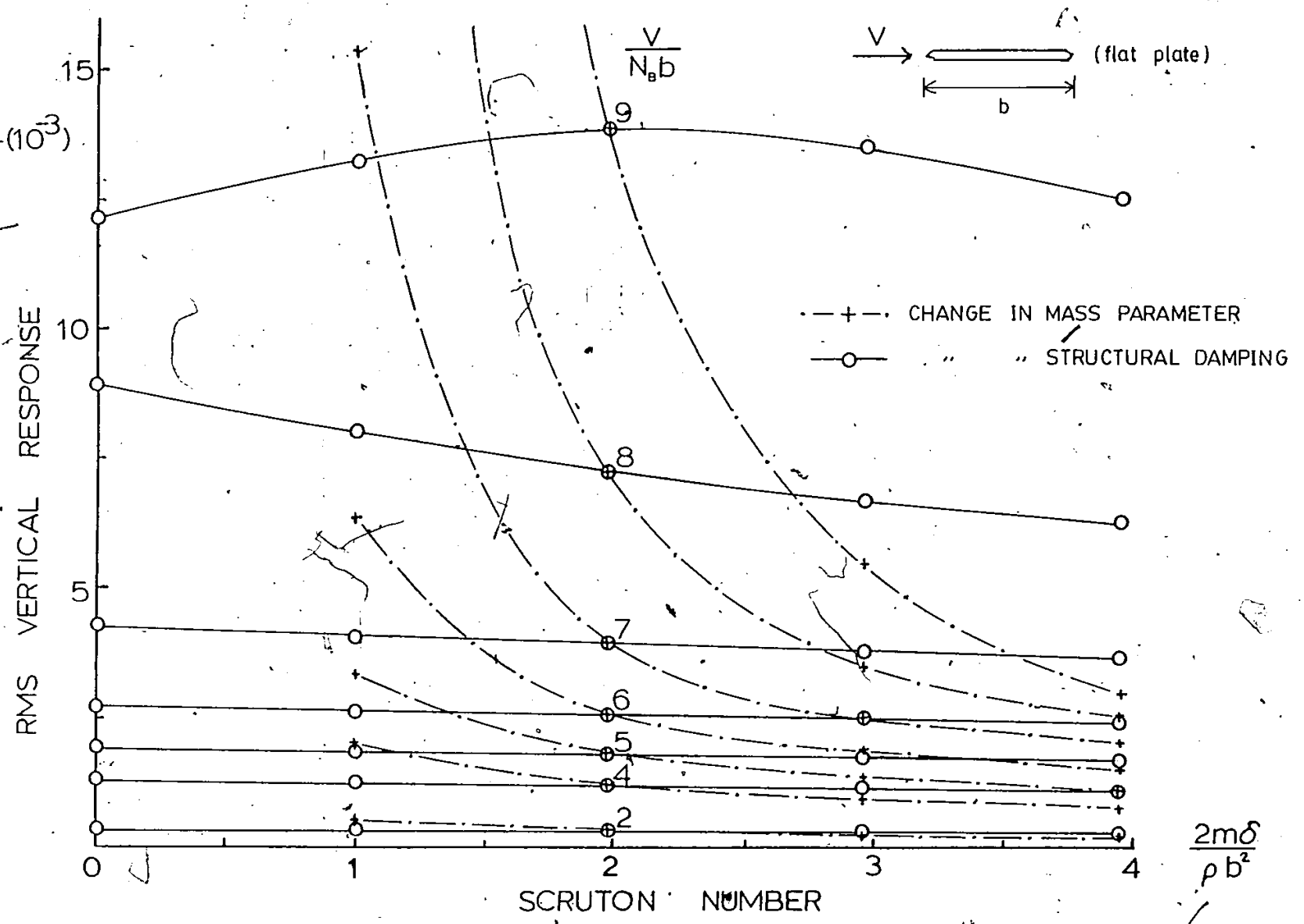

FIG. 33 EFFECT OF SCRUTON NUMBER ON VERTICAL BUFFETING RESPONSE (ANALYTICAL RESULTS)

Appendix C

FORMULATION OF GENERALIZED MASS

When a continuously distributed elastic structure such as a bridge is excited by sinusoidally fluctuating force, it will vibrate in resonance at narrow frequency range around its natural frequencies. Associated with each natural frequency, there is a mode shape defined. A single-degree-of-freedom analysis can be applied to the analysis of multi-degree-of-freedom system using the following concept:

Let $\phi(x)$ be the function describing the mode shape and, as a generalized coordinate, $Y(t)$ describes the displacement of the motion corresponding to a reference point on the structure where $\phi = 1$. The displacement at any point x along the structure is, therefore,

$$y(x,t) = \phi(x).Y(t) \qquad (C1)$$

The kinetic energy, K.E., of the system vibrating in the pattern indicated by eq. C1 is

$$K.E. = \int_{system} \frac{1}{2} m(x)\{\phi(x).\dot{Y}(t)\}^2 \, dx \qquad (C2)$$

Equating this expression for the K.E. of the continuous system to the K.E. of the equivalent single-degree-of-freedom system $1/2\ M\dot{y}(t)^2$ yields

$$M = \int_{system} m(x).\phi^2(x) \, dx \qquad (C3)$$

where M = generalized mass,

and $m(x)$ = true mass per unit length.

Similarly, by equating the work done by the external forces of the two systems, generalized force, F, is obtained.

$$F = \int_{system} f(x,t).\phi(x)\, dx \qquad (C4)$$

where $f(x,t)$ = distributed external force.

Generalized stiffness can be obtained using the expression $\omega = \sqrt{K/M}$, as

$$K = \omega^2 M \qquad (C5)$$

Therefore the response F/K can be expressed by

$$\frac{F}{K} = \frac{\int f(x,t).\phi(x)\, dx}{\omega^2 \int m(x).\ \phi^2(x)\, dx} \qquad (C6)$$

If the external force, $f(x,t)$, is independent of the coordinate x and the distributed mass, $m(x)$, is constant, Eq. C6 becomes

$$\frac{F}{K} = \frac{f(t)}{\omega^2 m} \frac{\int \phi(x)\, dx}{\int \phi^2(x)\, dx} \qquad (C7)$$

Appendix D

MEASUREMENT

D.1 FREE VIBRATION

The model was manually excited in either vertical or torsional mode. Signal traces such as the one shown below were then obtained from the chart recorder. The natural frequency and structural damping could then be calculated.

Sample calculation:

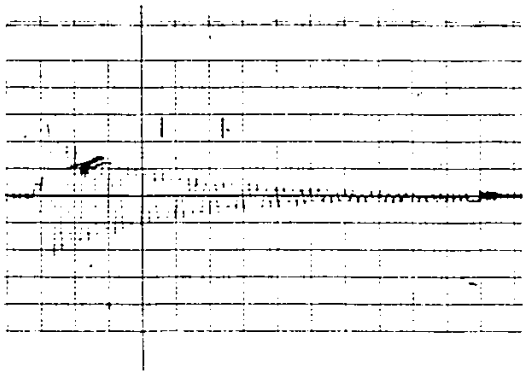

Tracing of the 1x2 box section in vertical mode.

Speed of the moving chart = 5 mm/sec

Length of the trace, L = 9 mm

Number of cycles, n = 7

Natural frequency, $N_B = 7x5/9 = 3.89$ Hz

$A_0 = 7$ mm

$A_8 = 4$ mm

Logarithmic decrement, $\delta = (\ln(7/4))/8 = 0.070$

Damping ratio, $\xi = (\delta/2\pi)x100 = 1.11\%$.

D.2 CALIBRATION FOR MODEL RESPONSES

The model deflection was detected using strain gauges at the leaf springs. These two signals were fed through the sum-and-difference amplifier from which the vertical and torsional responses, respectively, were obtained.

D.2.1 Vertical Response

A dial gauge was placed at the centre of the mid-span point of the model for the calibration. A known magnitude of displacement, say 1 mm, was given and the corresponding voltage displayed on the voltmeter was recorded. The same

process was repeated for several steps. A linear relation was obtained from the plotting of given displacement against voltage output and the calibration factor was decided. The result is listed in Table D1.

D.2.2 Torsional Response

In order to assure the pure torsional displacement, the position of the centre of rotation of the model was fixed by putting a thread at the point where the model was connected to the mechanism which controlled the damping and stiffness of the system (see Fig. 4). Knowing the vertical displacement at the edge of the model, the width of the model, and the corresponding voltage displayed, the calibration factor was determined. Since the calibration factor depends on the distance between the springs, the same procedure was repeated at different spacings between the springs. The results are listed in Table D1.

TABLE D1

Calibration factors

	Calibration factors
Vertical	0.03 mm/mV
Torsional	
Distance between springs	
0.102 m	0.0348 deg./mV
0.152 m	0.0222 deg./mV
0.203 m	0.0174 deg./mV
0.254 m	0.0135 deg./mV
0.305 m	0.0116 deg./mV
0.356 m	0.0102 deg./mV

Appendix E

COMPUTER PROGRAM

```
**********************************
*                                *
*     RESPONSE CALCULATION       *
*                                *
**********************************

      DIMENSION BMU(5),BNU(5),ZZ(6),ZA(6),AFZ(5)
      COMPLEX*16
CMPLX,HO,H1,DEN,CC,ZL,AL,ZM,AM,BZ,BA,AA1,AA2,AA3,AA4
      COMPLEX*16 DEL,CC1,CC2,CC3,CC4,CC5,CC6

************************************************
*                                              *
*  SL    : SLOPE OF LIFT FORCE COEFFICIENT     *
*  SM    : SLOPE OF MOMENT COEFFICIENT         *
*  BET   : FREQUENCY RATIO FA/FZ               *
*  SP    : SPAN LENGTH OF THE BRIDGE           *
*  AMU   : MASS RATIO                          *
*  ANU   : MASS MOMENT OF INERTIA RATIO        *
*  HG    : DECK HEIGHT                         *
*  BB    : LINEAR DIMENSION OF THE BRIDGE DECK *
*  CC    : CORRELATION FACTOR                  *
*  TI    : TURBULENCE INTENSITY                *
*  ZZ    : FLEXURAL DAMPING                    *
*  ZA    : TORSIONAL DAMPING                   *
*  FZ    : FLEXURAL FREQUENCY                  *
*  FA    : TORSIONAL FREQUENCY                 *
```

```
*                                                    *
******************************************************
      READ(5,101) (AFZ(I),I=1,1)
101   FORMAT(5F10.3)
      PI=4.*ATAN(1.)
      READ(5,102) BB,TI,HG
102   FORMAT(3F10.2)
      WRITE(6,50) BB,TI,HG
 50   FORMAT(3F10.2)
      READ(5,103) (ZZ(I),ZA(I),I=1,5)
103   FORMAT(10F6.3)
      WRITE(6,51) (ZZ(I),ZA(I),I=1,5)
 51   FORMAT(10F6.3)
      READ(5,104) (BMU(I),BNU(I),I=1,5)
104   FORMAT(10F6.2)
      WRITE(6,52) (BMU(I),BNU(I),I=1,5)
 52   FORMAT(10F6.2)
      SL=2.*PI
      SM=PI/2
      WRITE(6,11)
 11   FORMAT(1H1////10X,'INPUT DATA - FLAT PLAT'//)
      DO 2 L=1,1
       FZ=AFZ(L)
       SP=0.5969
       FA=0.0
      DO 2 M=1,1
       FA=FA+AFZ(L)
```

```
      DO 2 K=1,5
      DO 2 J=1,5
      BET=FA/FZ
      AMU=BMU(K)
      ANU=BNU(K)
      WRITE(6,12) AMU,ANU
   12 FORMAT(///,10X,'MU =',F5.2,3X,'NU =',F5.2/)
      WRITE(6,13) FZ,FA
   13       FORMAT(10X,'FREQUENCY(HZ)          ---       VERT
  =',F6.3,3X,'TORS=',F6.3/)
      ZZZ=ZZ(J)*100.0
      ZAA=ZA(J)*100.0
      WRITE(6,14) ZZZ,ZAA
   14  FORMAT(10X,'DAMPING(%)   ---   VERT  =',F7.5,3X,'TORS
  =',F7.5/)
      WRITE(6,15) SP
   15 FORMAT(//,10X,'SPAN LENGTH (M) = ',F10.5//)
      DO 1 I=1,10
      VR=FLOAT(I)
C*****************************************************
C*                                                   *
C*  SSZ  =  SQUARE OF RMS OF VERTICAL RESPONSE       *
C*  SSA  =  SQUARE OF RMS OF TORSIONAL RESPONSE      *
C*                                                   *
C*****************************************************
      SSZ=0.0
```

```
      SSA=0.0
      DO 10 IX=1,100
      XI=FLOAT(IX)*0.05
*************************************************************
*                                                           *
*  APPROXIMATION OF THEODERSON'S FUNCTION: F(K) + IG(K)     *
*                                                           *
*************************************************************

      AK=PI*XI/VR
      HO=CMPLX(1.0,-0.0455/AK)
      H1=CMPLX(1.0,-0.30/AK)
      CC=1.0-0.165/HO-0.335/H1
      CC1=-2.0*CC/AK
*************************************************************
*                                                           *
*  USING THEODERSON'S FUNCTION,                             *
*  THE NONLINEAR FORCES CAN BE APPROXIMATE: ZL,AL,ZM,AM     *
*                                                           *
*************************************************************
      ZL=CMPLX(-1.0-AIMAG(CC1),REAL(CC1))
      CC2=CC1/AK
      CC3=(-CC-1.0)/AK
      AL=CMPLX(REAL(CC2)-AIMAG(CC3),AIMAG(CC2)+REAL(CC3))
      CC4=CC/AK
      ZM=CMPLX(-AIMAG(CC4),REAL(CC4))
      CC5=CC4/AK
      CC6=(CC-1.0)/2.0/AK
```

```
      AM=CMPLX(-0.125+REAL(CC5)-AIMAG(CC6),AIMAG(CC5)+REAL(CC6))
*****************************************************
*                                                   *
*  FORM THE FREQUENCY RESPONSE FUNCTIONt A1,A2,A3,A4  *
*  DEL : THE DETERMINANT OF THE FREQUENCY RESPONSE    *
*        FUNCTION                                     *
*                                                   *
*****************************************************
      BZ=CMPLX(1.-XI*XI,2.*XI*ZZ(J))
      BA=CMPLX(BET**2-XI**2,2.*BET*XI*ZA(J))
      AA1=AMU*BZ-ZL*XI**2
      AA2=-AL*XI**2
      AA3=-(ZM*XI**2)
      AA4=ANU*BA-AM*XI**2
      DEL=AA1*AA4-AA2*AA3
      R1=CDABS(AA4/DEL)
      R2=CDABS(AA2/DEL)
      R3=CDABS(AA3/DEL)
      R4=CDABS(AA1/DEL)
*********************************
*                               *
*  FORM THE RESPONSE SPECTRUM   *
*                               *
*********************************
      A=(SL*VR**2/(PI**3))**2
      B=PI**2*2*XI/VR+1
*********************************
```

```
*                                   *
*  FORM THE VELOCITY SPECTURM       *
*                                   *
*************************************
      TT=2.0*PI*0.025/BB/VR
      C=(TI*0.5)**2*TT/PI*(1.0+4.78*TT**2)
      D=(1.0+1.79*TT**2)**(11.0/6.0)
      G=(2.*SM/SL)**2
*************************************
*                                   *
*  THE JOINT ACCEPTANCE FUNCTION    *
*  CC : CORRELATION FACTOR          *
*                                   *
*************************************
      HX=8.*SP*XI/BB/VR
      H=(2./HX)*(1.-(1.-EXP(-HX))/HX)
*********************************************
*                                           *
*  CALCULATE THE CORRESPONDING RMS RESPONSE *
*  TO EACH FREQUENCY                        *
*                                           *
*********************************************
      SZ=(R1**2+G*R2**2)*H*A*C/B/D
      SA=(R3**2+G*R4**2)*H*A*C/B/D
*************************************
*                                   *
*  SUM UP THE SQUARE OF RMS RESPONSE *
```

```
*  FOR EACH FREQUENCY                    *
*                                        *
******************************************
      SSZ=SSZ+SZ*0.05
      SSA=SSA+SA*0.05
 10   CONTINUE
      SSZR=SQRT(SSZ)/2
      SSAR=SQRT(SSA)
      WRITE(6,17) VR,SSZR,SSAR
 17   FORMAT(/10X,'VR=',F7.1,5X,'Z=',F10.5,3X,'A=',F10.5)
  1   CONTINUE
  2   CONTINUE
      STOP
      END
```